NASA Contractor Report 159388

TN-3770218

Final
Report

November 1976

ENTRY DATA ANALYSIS FOR VIKING LANDERS 1 and 2

Martin Marietta Corporation
DENVER DIVISION
P. O. Box 179
Denver, Colorado 80201

FOREWORD

This report is submitted as DRL Line Item N3-C003 under Contract NAS1-9000 to satisfy Phases 2 (DECSET) and 3 (LTARP) of the Entry and Touchdown Analysis Procedure (MDO 1-13).

The principal authors for this report are:

Author	Sections
R. N. Ingoldby	II, III, IV, X
F. C. Michel and T. M. Flaherty	IV, V
M. G. Doty and B. Preston	VII
K. W. Villyard	VIII, XI
R. D. Steele	IX

CONTENTS

Figure

Table

I. INTRODUCTION

This report presents the results of work done to satisfy Phases 2 (Decset) and 3 (LTARP) of the Entry and Touchdown Data Analysis Procedure (MDO 1-13).

In summary, both VL1 and VL2 descents from deorbit to touchdown went smoothly with few anomalies. Those that did exist did not significantly affect the final result: a safe and normal touchdown on the surface. The anomalies that did exist that affected lander operation were: (1) attitude rates somewhat higher than planned during deorbit; (2) somewhat higher L/D and angle of attack than nominal; (3) higher RA return signal strength, thereby minimizing RA terrain bias; and (4) the TDLR sensing "dust" velocity during the last half second of descent, causing some engine throttling. The anomalies were but small departures from nominal predictions of performance. They did not affect the safe landings in any significant way. After reading this report, the reader will realize just how nominal each lander was in meeting all its flight constraints.

II. DEORBIT BURN PERFORMANCE

Each lander performed its deorbit burn in a nominal and quite accurate manner, as indicated in the following sections. In fact, the accuracy of the burn suggests that some IRU and/or initial orbiter alignment accuracy numbers may have been too conservative.

A. TIME OF DEORBIT BURN CUTOFF

The time of deorbit burn cutoff was very close to the predicted time of 1757 sec for both VL1 and VL2. For VL1 it was 1759.8 sec, and for VL2 it was 1757.1 sec, for a difference of 2.8 and 0.1 sec, respectively.

A difference up to 6 sec is acceptable. This difference is primarily the result of normal control-system error dead-band operation in achieving and detecting the end of the burn.

B. VELOCITY TO BE GAINED VERSUS TIME

The three velocity-to-be-gained components in the body frame indicate how well the control system was able to follow the required velocity polynomial and whether there were significant thrust misalignments or cg offsets. In analog/hybrid simulations with no thrust misalignment, cg offsets, or engines out, the control system was able to hold the velocity-to-be-gained components to:

$\bar{V}_{gx} < \pm 2$ sec

$V_{gy} < \pm 1$ sec

$V_{gz} < \pm 1$ sec

The following maximum values for velocity to be gained were obtained for each lander:

	VL1	VL2
V_{gx}	1.309	1.445
V_{gy}	-0.199	-0.199
V_{gz}	0.398	0.414

C. VELOCITY AND POSITION AT DEORBIT BURN END AND ENTRY TIME

The velocity and position at the end of the deorbit burn were not obtained due to the inability of the FPAG to integrate the body accelerations output by DECSET. There was an excessive number of bit hits and noise on the telemetry data that prohibited obtaining an accurate integral.

It is possible to assess the accuracy of the deorbit burn (including the accuracy of orbit determination and the accuracy of determining the thermal pulsing ΔV imparted) by looking at the estimate of the entry conditions obtained from the trajectory reconstruction program (LTARP) by the FPAG. Targeted conditions and the estimate of the actual results are given in the following table:

Entry Velocity Conditions

	VL1			VL2		
	Target	LTARP Estimate	Error	Target	LTARP Estimate	Error
Inertial Vel (fps)	15127.3	15126.6	1.4σ	15138.8	15138.8	≈o
Inertial Flight Path Angle (deg)	-16.87	-16.97	0.9σ	-17.005	-17.027	0.5σ
Latitude-Aerographic (deg)	12.81	12.53	0.7σ	36.89	36.78	0.4σ
Longitude-West (deg)	61.96	62.11	1.4σ	243.04	243.11	0.6σ

What these numbers suggest is that the accuracy of the deorbit burn was quite good for both landers.

Based on the lander trajectory reconstruction, the deorbit execution errors were estimated to be as given in the table below for both landers.

Estimated Deorbit Errors

	Pointing	Magnitude	Touchdown Error
VLC1	-0.18° (0.51σ)	0.22% (1.4σ)	30 km
VLC2	0.24° (0.82σ)	0.055% (0.35σ)	10 km

The current deorbit execution error has the following primary error contributors:

Assumed Value (3σ), μg	Error (3σ) Pointing, deg	Error (3σ) Magnitude, %
Accel Bias, μg		
X 50	--	0.467
Y 50	0.274	--
Z 75	0.403	--
Gyro Bias, deg/hr		
X 0.3	--	--
Y 0.3	0.074	--
Z 0.3	0.062	--
Initial Alignment (Orbiter Uncertainty), deg		
X 0.769	0.516	--
Y 0.636	0.484	--
Z 0.636	0.623	--
RSS	1.066	0.467

Reduction of Deorbit Execution Errors - As noted in the table above, the two primary error sources are accelerometer bias and orbiter initial alignment uncertainty.

1) With additional testing and statistical analysis of the accelerometer biases, the accelerometer bias uncertainity can probably be reduced to 40 μg in all axes. (Tip-off rates at separation are probably low enough so that the Z axis accelerometer bias calibration will not be affected.)

2) Initial Alignment (Orbiter Uncertainity) - The initial alignment pointing error that results from orbiter uncertainity is listed below:

Error Source	Analysis Value (3σ), deg Roll	Pitch/Yaw
Celestial Sensor Alignment Bias, Offset	0.24	0.34
VO Celestial Sensor Limit Cycle	0.476	0.476
VO Roll Prediction	0.466	--
Roll Gyro Limit Cycle	0.163	--
VL Mechanical	0.250	0.250
RSS 3σ	0.769	0.636

There are some known biases and offsets in the sun sensors and star tracker data that can be removed, thereby reducing initial alignment errors. The VL mechanical error could be reduced to $\approx 0.1°$. With these reductions, the initial alignment pointing error that results from the orbiter uncertainity is as follows:

Error Source	Value (3σ), deg Roll	Pitch/yaw
Celestial Sensor Alignment Bias, Offset	0.090	0.029
VO Celestial Sensor Limit Cycle	0.476	0.476
VO Roll Prediction	0.466	--
Roll Gyro Limit Cycle	0.163	--
UL Mechanical	0.100	0.100
RSS 3σ	0.698	0.487

Even with these reductions the initial alignment pointing error is still the largest contributor to the ΔV pointing error. If further reduction is required, the limit cycle and commencement of the roll inertial mode should be examined.

The VO error sources are listed in Viking Flight Team Memo OGCPAG-14917-MHH.

D. ORBIT DISTURBANCE DURING VIKING 2 DEORBIT

The orbiter position relative to the lander after separation was such that, during the VL2 attitude maneuver for deorbit, the roll jets caused disturbing moments on the orbiter. This orientation (with the orbiter in the lander Y-Z plane) occurred 296 sec after separation and coincided with RCS roll pulses associated with termination of the roll portion of the attitude manuever at 294 sec. (The pitch/yaw portion of the attitude maneuver was completed at 305 sec.) The magnitude of the disturbance was aggravated by the selected roll orientation of the lander for deorbit, which put the orbiter in the lander X-Z plane and close to the direction of the roll thrusters. The VL1 deorbit roll orientation put the orbiter in the lander X-Y plane, and, with the larger tip-off rate of VL1 (Table II-1), the orbiter was behind the lander before initiation of attitude control at 240 sec (Fig. II-1). The relative size and position of the orbiter, lander, and lander roll thrusters at 300 sec is shown in Figure II-2. The activity of the RCS system during this period is given in Table II-2.

Table II-1 Separation Conditions

Separation Rate, fps	VL1	VL2
Lander V_x	-0.254	-0.328
V_y	-0.004	-0.004
V_z	-0.027	-0.016
Orbiter V_x	+0.203	+0.262
(Est) V_y	+0.003	+0.003
V_z	+0.022	+0.013
Tip-Off Rates, deg/sec		
$\dot{\theta}_x$	+0.007	0.040
$\dot{\theta}_y$	-0.337	-0.135
$\dot{\theta}_z$	-0.357	-0.049

Note: Lander attitude at separation is inertial reference

Lander X (roll) = Orbiter -Z (-roll)
Lander Y (pitch) = Orbiter -X (-pitch)
Lander Z (yaw) = Orbiter Y (yaw)

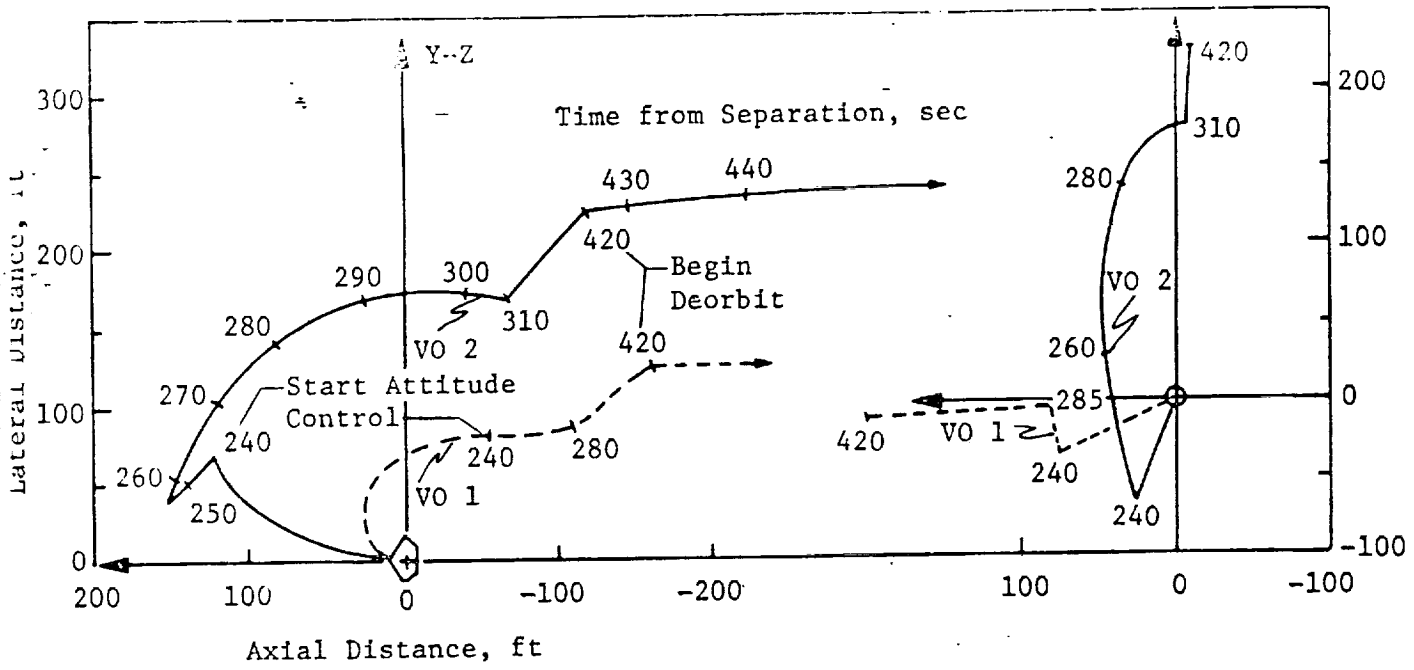

Figure II-1 Orbiter Position Relative to Lander

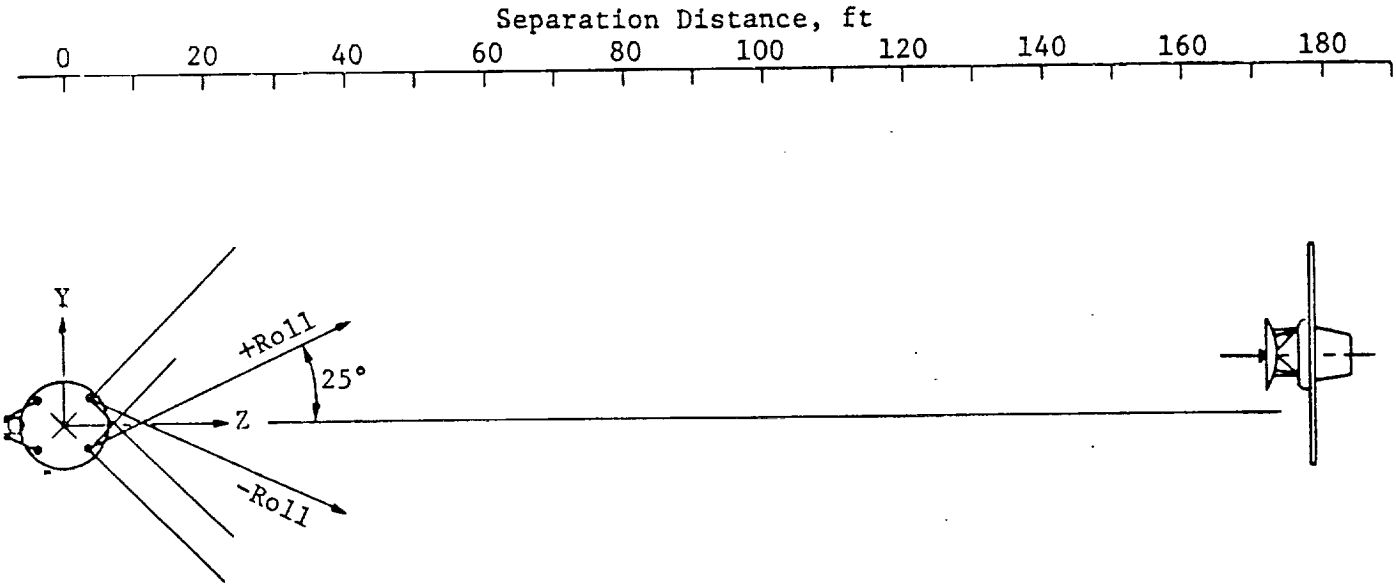

Figure II-2 Orbiter Lander Separation Geometry Viking 2, T Sep + 300 sec

Table II-2 VL2 RCS Activity

Time Interval	Pitch/Yaw	Roll	Comment
0 to 240	0	0	Accelerometer Calibration
240.02	16	+4, -4	Warmup (All ON)
241	24	+1, -17	Start Attitude Control Control
259-292	11	-3, +0	Normal Maneuver
294	0	+15	Stop Roll Rate
296-297	2	0	Normal Limit Cycle
299	0	+17	Resume High Rate
300	0	-17	Stop Roll Rate
303-305	43		Stop Pitch/Yaw
307-420	1 pulse/2 sec avg	1 pulse/3 sec avg	Low-Rate Limit Cycle
421-1750	$\approx$ 175/sec		Deorbit

Note: Each pulse is 0.02 sec, thrust level is 8 lb, each pitch/yaw pulse actuates two jets axial (-X direction), each roll pulse actuates two jets opposed.

III. ATTITUDE CONTROL SYSTEM (ACS) PERFORMANCE

A. LIMIT CYCLE PERFORMANCE

Attitude rates observed on both VLC1 and VLC2 in pitch and yaw exceeded the predicted maximum rates by a factor of 2 after maneuvers and before 0.05 g. These maximum rates were observed during deorbit burn and are listed below:

	VLC1 deg/sec	VLC2 deg/sec	Predicted Maximum deg/sec
ω_r	0.41	0.39	1.69
ω_p	-1.81	-2.08	-0.85
ω_y	-1.09	-2.07	0.85

Discussion - Attitude rates during deorbit burn are affected by the following:

1) Yaw cg offset, which can be as much as 0.25 in.;

2) Deorbit engine thrust mismatch, which can be as much as +5 to -10%;

3) Thrust vector misalignment, which can be as much as 1° per engine;

4) Roll engine thrust mismatch, which can also be as much as +5 to -10%.

The predicted rate of 0.85 deg/sec for pitch and yaw was based on a nominal hybrid simulation with no yaw cg offset, no engine thrust mismatch, and no engine thrust vector misalignment. The output of this run is shown in Figure III-1. The yaw rate is very small, and the pitch rate does not exceed 0.81 deg/sec.

A number of analog hybrid runs were made with various parameters changed to determine their effect on pitch and yaw rates during deorbit to determine if the observed rates could be reasonably explained. Figure III-2 is a run with only the yaw cg offset by a small amount (0.1 in.). There was no apparent effect on the pitch or yaw rate during the run.

Figure III-3 shows a case in which engine thrust was misaligned by 3° along with a yaw CG offset as in Figure III-2. The yaw rate increased drastically while the pitch rate only increased slightly.

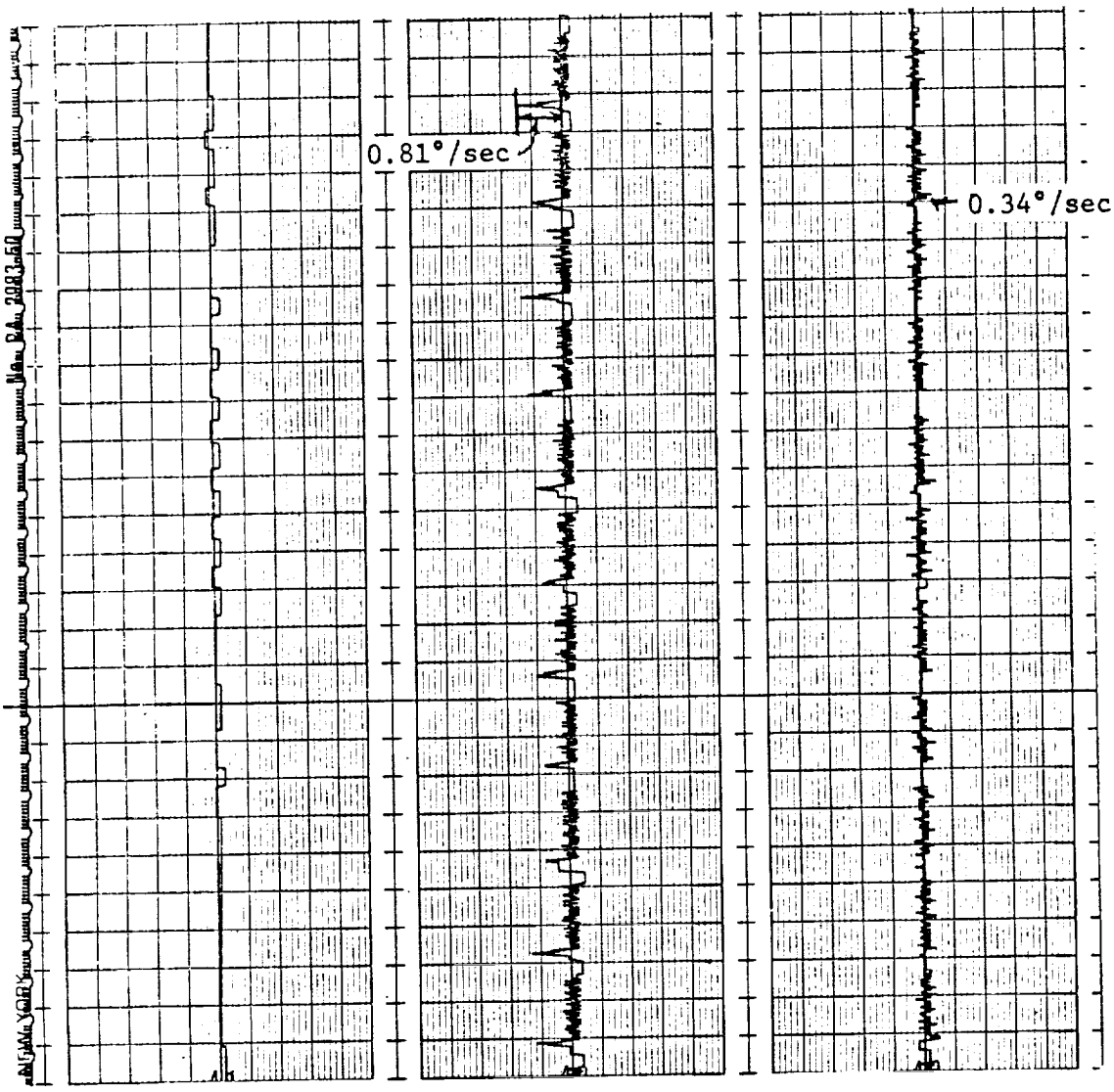

No yaw cg offset
No thrust mismatch
No thrust vector misalignment

Figure III-1 Nominal Deorbit Run (Predicted)

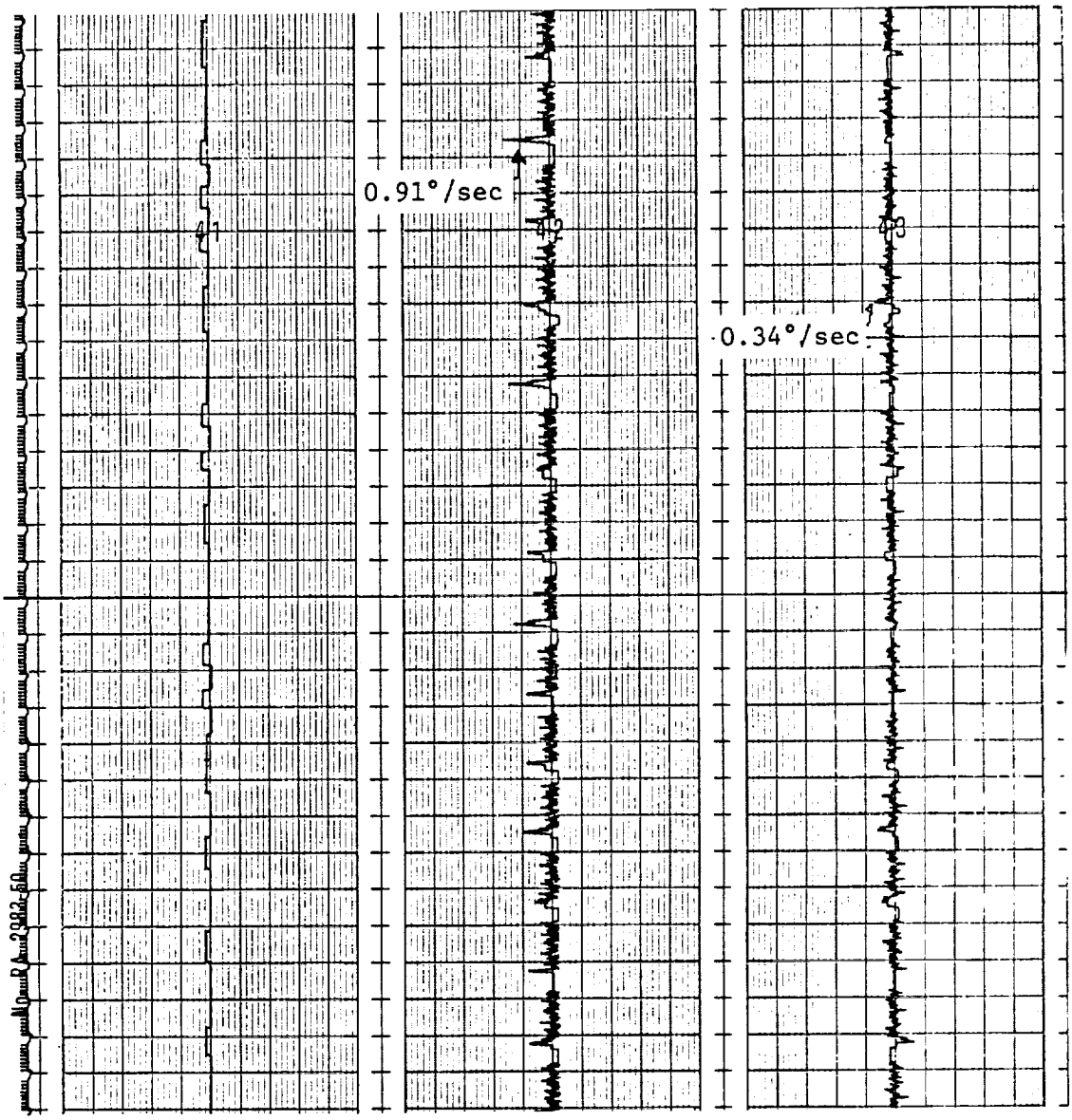

Yaw cg offset = 0.1 in.

Figure III-2 Deorbit Run with Offsets

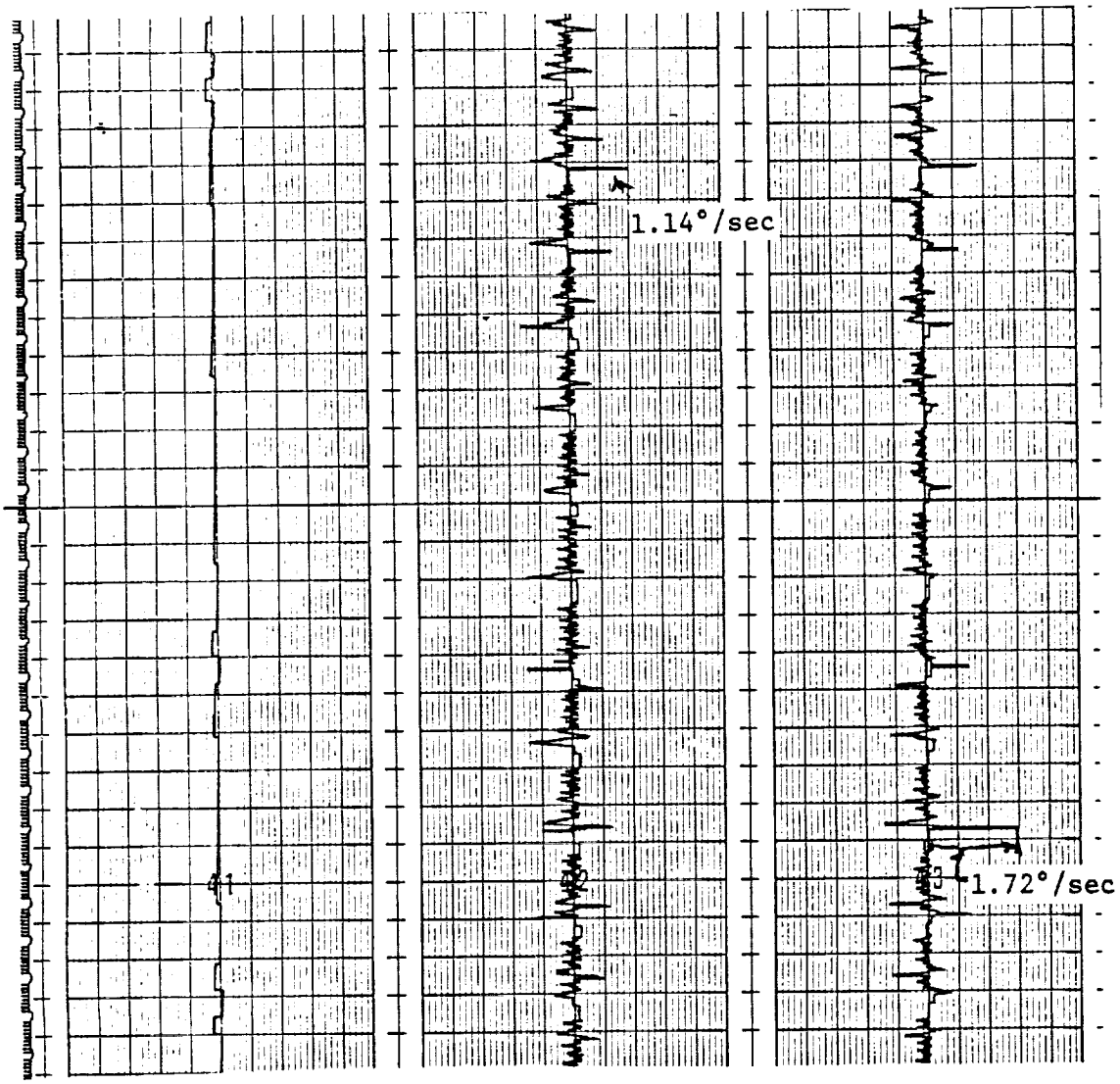

Thrust misalignment = 3°
Yaw cg offset = 0.1 in.

Figure III-3 Deorbit Run with Offets

In Figure III-4 the thrust misalignment was increased to 4° with the yaw cg offset being 0.1 in. The peak yaw rate increased to 1.89 deg/sec, and the peak pitch rate went to 1.08 deg/sec. The overall rate limit cycle increased on both axes.

In Figure III-5, all parameters were offset as shown. The peak rates were not as high as in Figure III-4. However, the overall limit cycling was much larger.

Conclusion - Based on simulations run, it is concluded that the maximum rates observed on both landers were most likely due to some combination of cg offset, engine thrust mismatch, and thrust vector misalignment.

It is recommended that in future programs of this type the predicted limits be based on a simulation that includes expected offsets or, if possible, actual measured offsets for that vehicle.

The attitude errors observed after maneuvers and before 0.05 g were within the predicted limits of 0.354° everywhere except in coast, where the limit is 7.07°. No attitude errors during coast exceeded the predicted limit of 7.07°.

Maximum Attitude Errors

Deorbit

	VLC1 deg	VLC2 deg
θ_r	0.254	0.258
θ_p	0.343	0.312
θ_y	0.349	0.331

Coast

	VLC1 deg	VLC2 deg
θ_r	-4.99	4.93
θ_p	6.82	7.04
θ_y	6.61	6.75

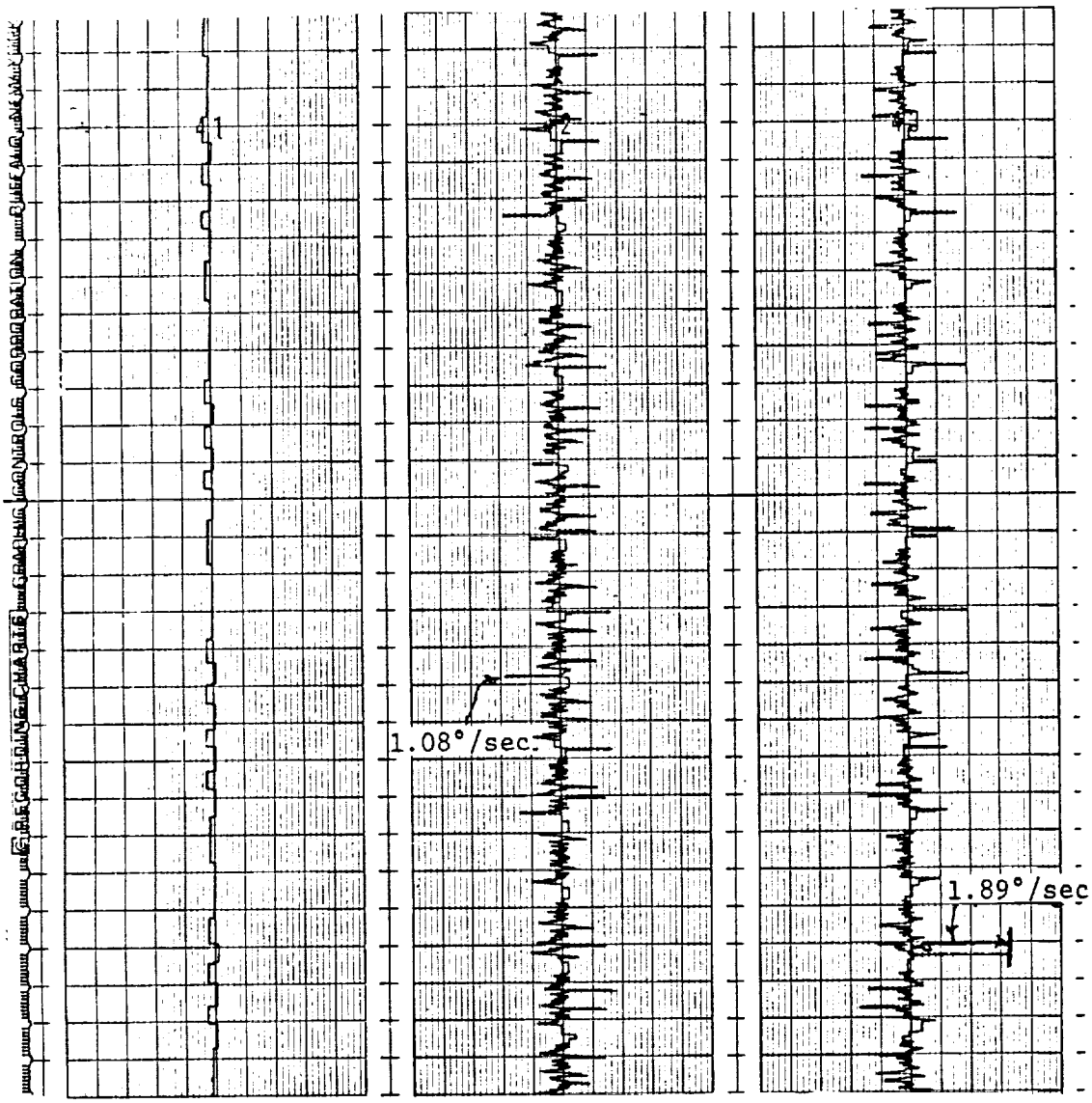

Roll Rate
0.002 rad/sec/line

Pitch Rate
0.002 rad/sec/line

Yaw Rate
0.002 rad/sec/line

Thrust misalignment = 4°
Yaw cg offset = 0.1 in.

Figure III-4 Deorbit Run with Offsets

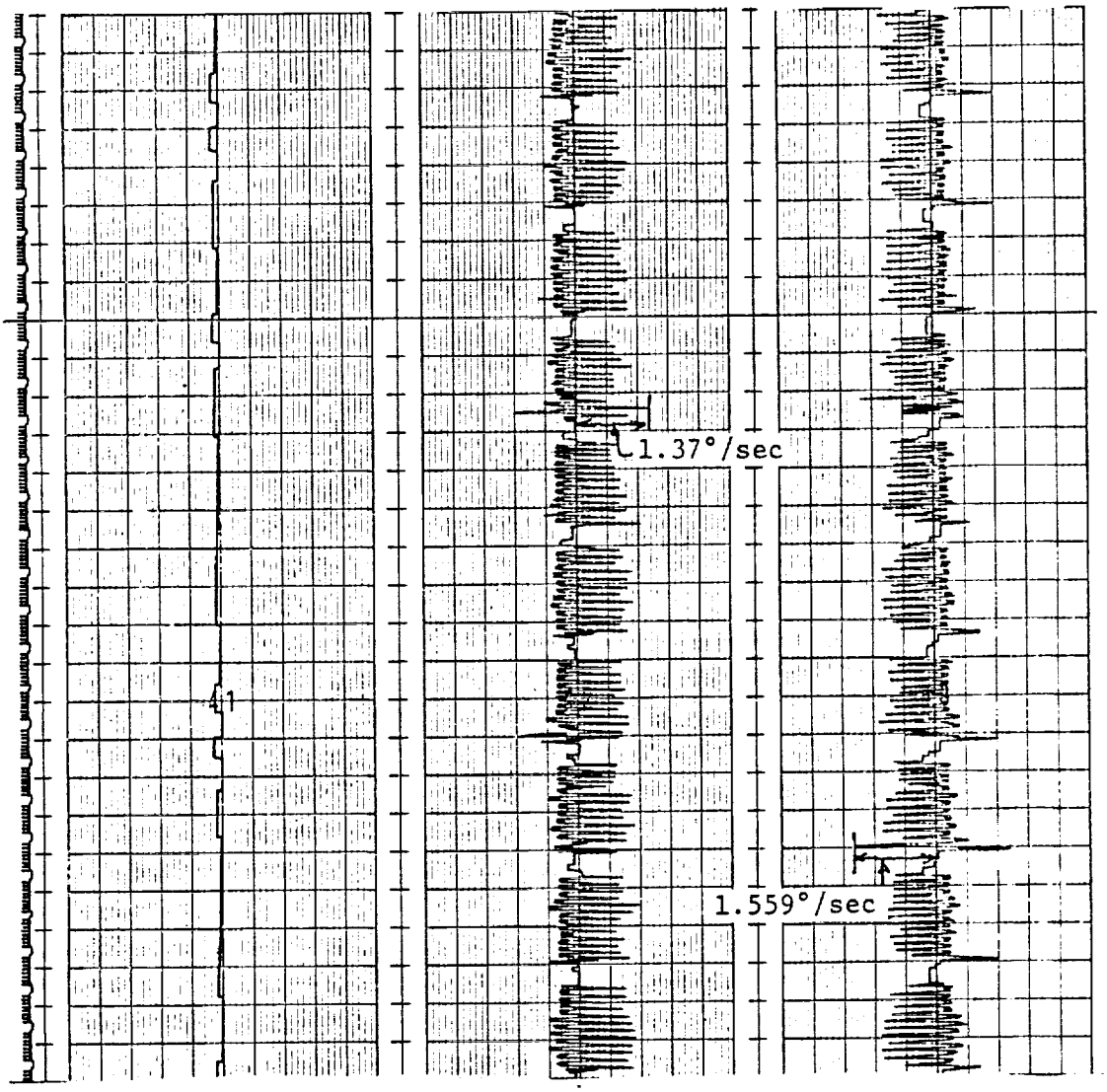

Roll Rate
0.002 rad/sec/line

Pitch Rate
0.002 rad/sec/line

Yaw Rate
0.002 rad/sec/line

Yaw cg offset = 0.1 in.
Thrust mismatch:
Deorbit Engines 8, 9, 11, 12 = -10%
Deorbit Engines 2, 3, 5, 6 = +10%
Roll Engine 1 = -5%
Roll Engine 7 = +5%
Thrust misalignment = 2°

Figure III-5 Deorbit Run with Offsets

B. MANEUVER CONVERGENCE

Maneuver convergence is verified by observing that the attitude errors are within the limit cycle range within 180 sec after initiation of a maneuver. The attitude error on both landers converged within the limit cycle range within the required 180 sec. The attitude rates during the maneuvers were less than 2.0 deg/sec for both landers. The following is a list of attitude errors observed 180 sec after initiation of each maneuver:

Deorbit

	VLC1, deg	VLC2, deg	Limit Cycle Range, ±deg
θ_r	-0.1142	-0.0220	0.250
θ_p	-0.1904	-0.1104	0.354
θ_y	-0.1272	-0.0112	0.354

Coast

	VLC1, deg	VLC2, deg	Limit Cycle Range, ±deg
θ_r	0.1611	0.5578	5.0
θ_p	1.675	0.2131	7.07
θ_y	1.839	4.1055	7.07

180° Roll

	VLC1, deg	VLC2, deg	Limit Cycle Range, ±deg
θ_r	2.391	1.410	5.0
θ_p	1.015	4.952	7.07
θ_y	2.391	1.581	7.07

Preentry

	VLC1, deg	VLC2, deg	Limit Cycle Range, ±deg
θ_r	0.1660	-0.2126	0.250
θ_p	0.1272	-0.1565	0.354
θ_y	0.1892	-0.0876	0.354

C. RATE DAMPING CONTROL

Pitch, yaw, and roll attitude rates were all below the expected value of 2.0 deg/sec during entry after 0.05 g, except during the parachute phase of the mission. Maximum rates observed during this phase are listed below.

	VLC1, deg/sec	VLC2, deg/sec
ω_r	1.44	-1.38
ω_p	-1.28	1.36
ω_y	1.64	1.67

Oscillation increased during Phase 9 entry about 30 sec before mortar fire, which is normal.

IV. ENTRY AERODYNAMIC PERFORMANCE

The aerodynamic performance of the entry vehicle was completely satisfactory. Both vehicles trimmed at higher negative angles of attack than expected and thus had higher L/D than planned. Base-cover heating exceeded expectations but was acceptable. Real gas effects caused several parameters to vary from predictions based on wind tunnel tests using air, but these variations did not have a significant effect on the missions.

A. DYNAMIC PRESSURE

From on-board measurement of stagnation pressure, it was possible to derive the dynamic pressure. The method is outlined in Ref 1 and treats the Mars atmosphere as 100% CO_2 in thermochemical equilibrium. Velocity relative to the atmosphere and atmospheric temperature are required in the method and were obtained from LTARP. However, the results are largely independent of LTARP despite the use of these two parameters.

Dynamic pressures derived from flight-measured stagnation pressures differ significantly from those derived and used in LTARP. The LTARP values are based on accelerations measured in flight and aerodynamic characteristics, particularly the axial force coefficient (C_A), determined from wind-tunnel tests using air.

Ratios of the pressure-derived values to the LTARP values are shown in Figures IV-1 and IV-2. Data points were taken at 5-sec intervals. The altitudes at which maximum dynamic pressure and parachute mortar fire occurred are given in the figures for reference.

Figures IV-1 and IV-2 also show a solid line, which indicates the calculated effect on stagnation pressure, and thus on dynamic pressure, of a pure CO_2 atmosphere with disassociation effects. The LTARP results are based on air behaving as a perfect gas. The solid lines in the figure therefore represent the difference expected between the stagnation pressure based and the LTARP dynamic pressures due to the difference between the real Mars atmospheric gas and the wind-tunnel test medium. A further difference in C_A and thus in dynamic pressure is caused by differences between the trim angle-of-attack variation with Mach number as obtained from the wind-tunnel tests and used in LTARP and the actual flight trim alphas.

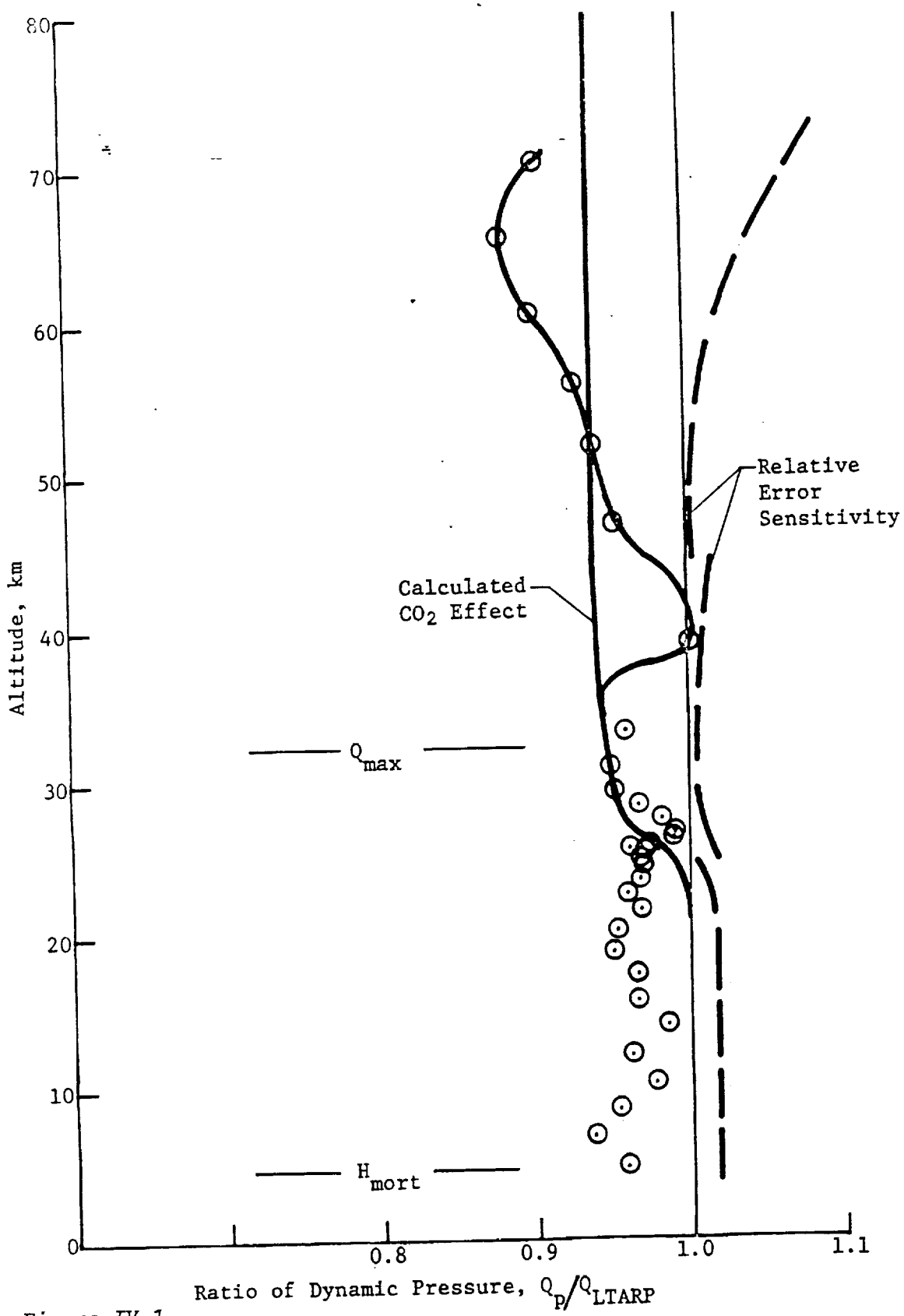

Figure IV-1
Effect of Basing Dynamic Pressure on Stagnation Pressure, VL1

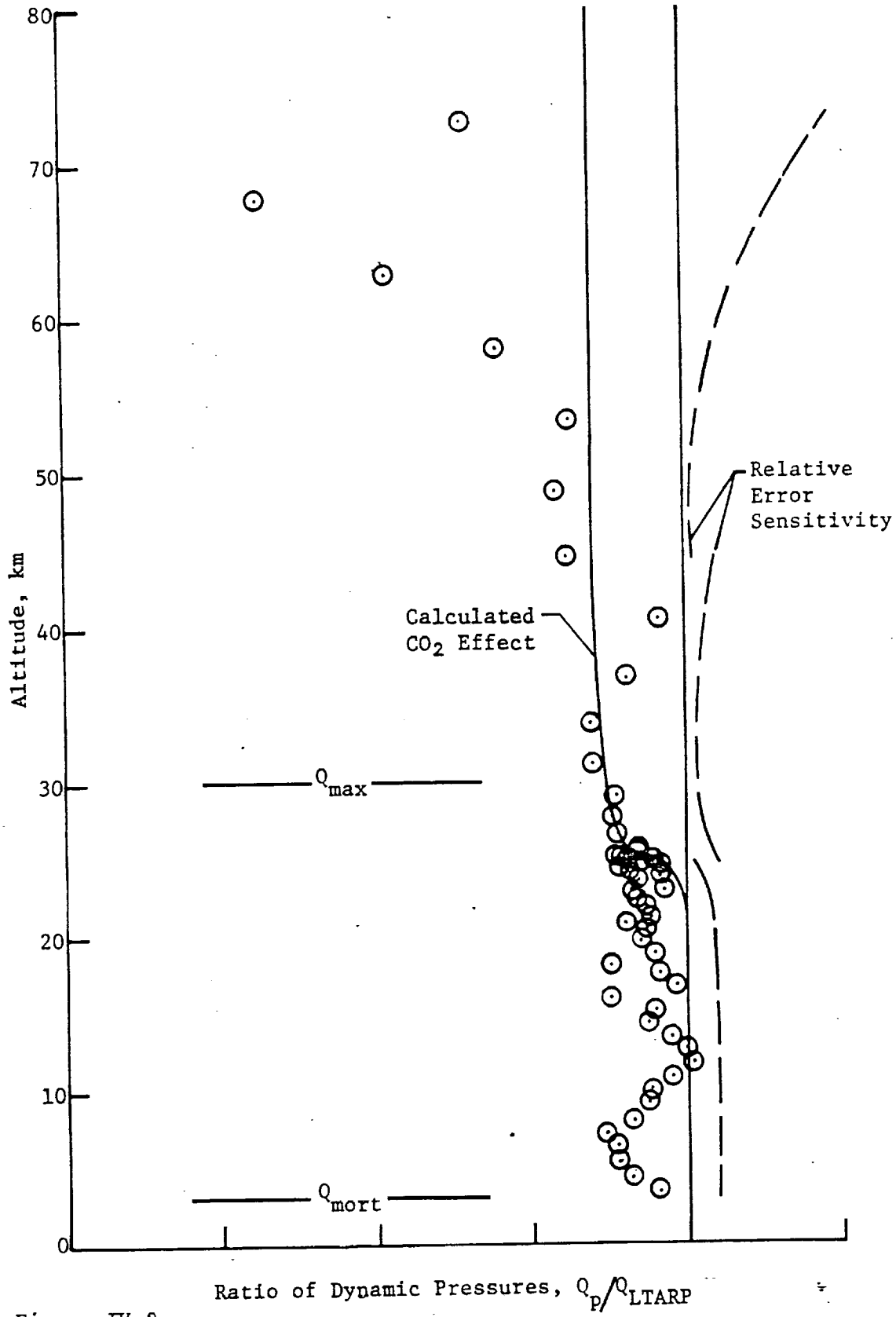

Figure IV-2
Effect of Basing Dynamic Pressure on Stagnation Pressure, VL2

Flight data points show sizeable percentage errors at the higher and lower extremes of the altitude range. However, absolute magnitudes of both the dynamic pressures and the discrepancies between them are low at these altitudes. The stagnation pressure instrument also has a high and low range. It is in the low range area of operation that the unexpected discrepancy occurs. The effect of a single data bit error in the areas of high- and low-range instrument operation is also shown in the figure.

Although there is considerable scatter in the dynamic pressure data and various explanations for it, it seems evident that the real gas effect given by the solid line in the figures should be taken into consideration. This does have a noteworthy effect on the atmosphere derived by LTARP.

A reduction of dynamic pressures by 6% above about 25 km will not affect the LTARP trajectory or velocity time histories if the aerodynamic coefficients such as C_A undergo a corresponding increase over the wind-tunnel test values. However, the atmospheric density variation above this altitude will be reduced by the same percentage. Because the pressure at an altitude is found by integrating the densities at all the higher altitudes, a reduction in pressure will be apparent down to about 10 km. The temperature variation with altitude is derived from the density and pressure using the gas law. At altitudes above 45 km, the temperature is unchanged because both density and pressure are 6% low. Temperature is reduced at altitudes between 10 and 30 km and especially around 22 km. In the region between 20 and 25 km, the change in temperature is as great as 7°K. This change would largely eliminate the pronounced bump that appears in both the VL1 and VL2 reconstructed temperature profile. Revising the temperatures would have some effect on the trajectory reconstruction because of the effect of temperature on Mach number. The whole LTARP calculation cycle would have to be repeated to fully evaluate the effects. The LTARP-derived density and pressure curves would also be smoothed and straightened if the flight stagnation pressures were used to derive the dynamic pressure.

B. ANGLES OF ATTACK AND SIDESLIP

Four pressure ports are located on the surface of the aeroshell cone at a radius of 50 in. The two ports in the vertical plane indicate angle of attack while the two in the lateral plane indicate sideslip angle. Figures IV-3 and IV-4 show the angles of attack and sideslip for Viking 1 and 2 as derived from the pressure ports and LTARP. Because of the poor agreement, an independent check was made by using data from the on-board

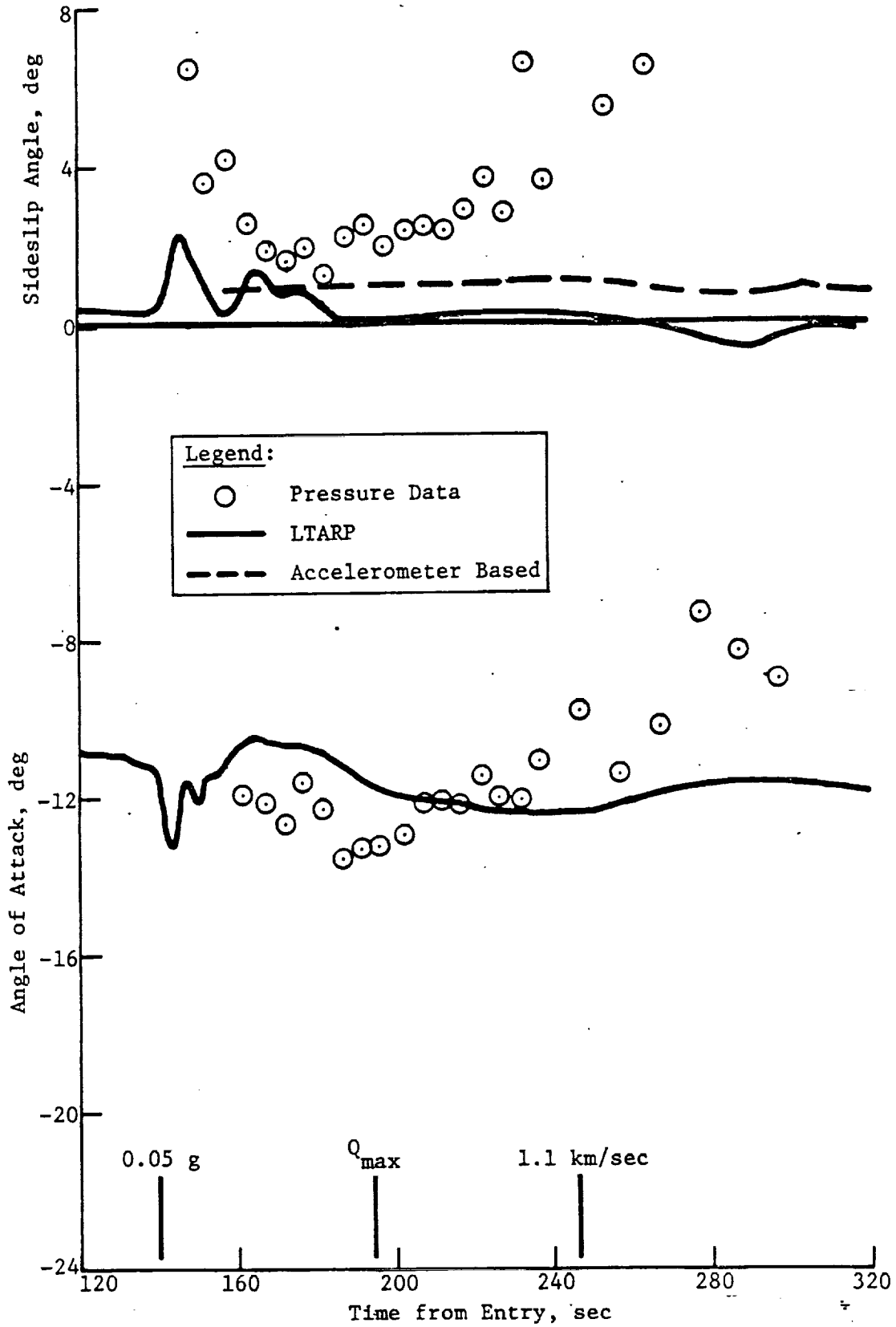

Figure IV-3 Angles of Attack and Sideslip, VL1

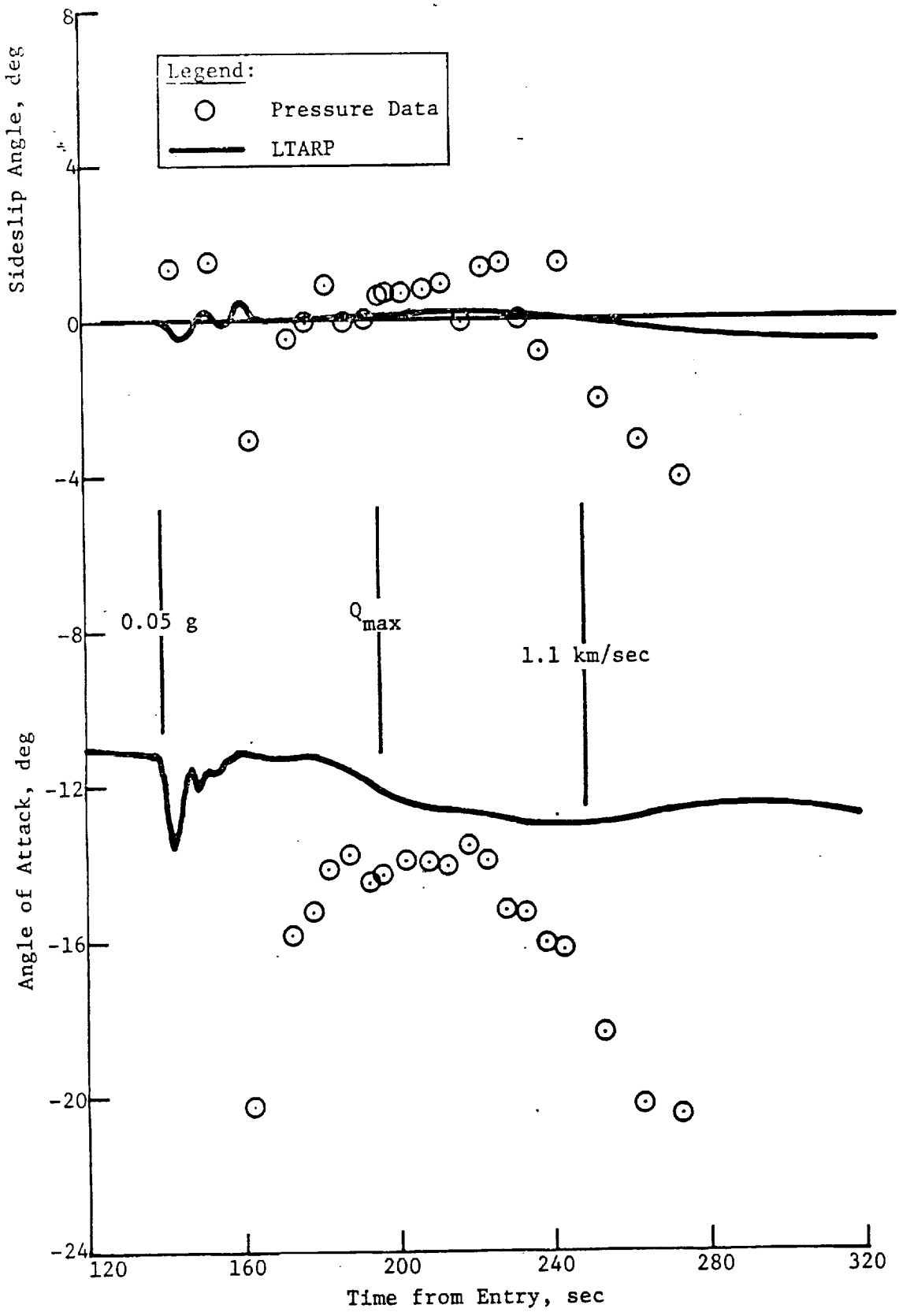

Figure IV-4 Angles of Attack and Sideslip, VL2

accelerometers to determine the resultant acceleration angle. This angle varies nearly linearly with the angle of attack. The variation of this angle with time was much more nearly proportionate to the LTARP data. Thus, angles of attack and sideslip derived from the four pressure ports are not considered dependable data. Possible causes of the inconsistency of the data, besides instrumentation and data recording tolerances, include variations in the pressures at the opposing ports due to the flow not being in thermochemical equilibrium at the higher speeds. Newtonian flow effects could also be a factor at the higher speeds. At lower speeds, near and after the time for maximum heating, both outgassing and local surface changes due to ablation could be responsible for degrading the data.

The angles of attack derived by LTARP from VL1 and VL2 are from 0 to 3° more negative than the trim angles of attack predicted from the air wind-tunnel tests. (see Fig. IV-5). Lift-to-drag ratios are correspondingly higher, as would be expected. The limited real gas data available before the flights did not indicate that higher trim angles should be expected with real gas. Accordingly, other possible causes of the high angles of attack were investigated.

Figures IV-3 and IV-4 show angles of sideslip near zero for both VL1 and VL2 from LTARP. However, on VL1 the accelerometer data indicates an essentially constant sideslip angle of 1°, as shown in Figure IV-3. This anomaly was not evident on VL2. In addition, the VL1 reaction control system roll jets were activated much more often to overcome a roll moment and maintain the desired roll angle. This confirms the existence of some unsymmetrical effect on VL1.

A possible cause of off-nominal angles of attack and sideslip is displacement of the cg. Accordingly, the cg tolerances and possible bias sources were reviewed. Plus or minus tolerances were found to originate from variations in physical dimensions and the temperature effect on the RCS/deorbit tanks. Another factor is that the fuel in both the RCS/deorbit and the terminal descent tanks aligns with the acceleration vector, thereby creating a cg bias. This is partially balanced by the effect of greater ablator loss on the windward ray. Another type of bias is caused by the linear and angular misalignment of the aerodynamic axis of symmetry with the vehicle reference system. The following table summarizes the estimate cg effects.

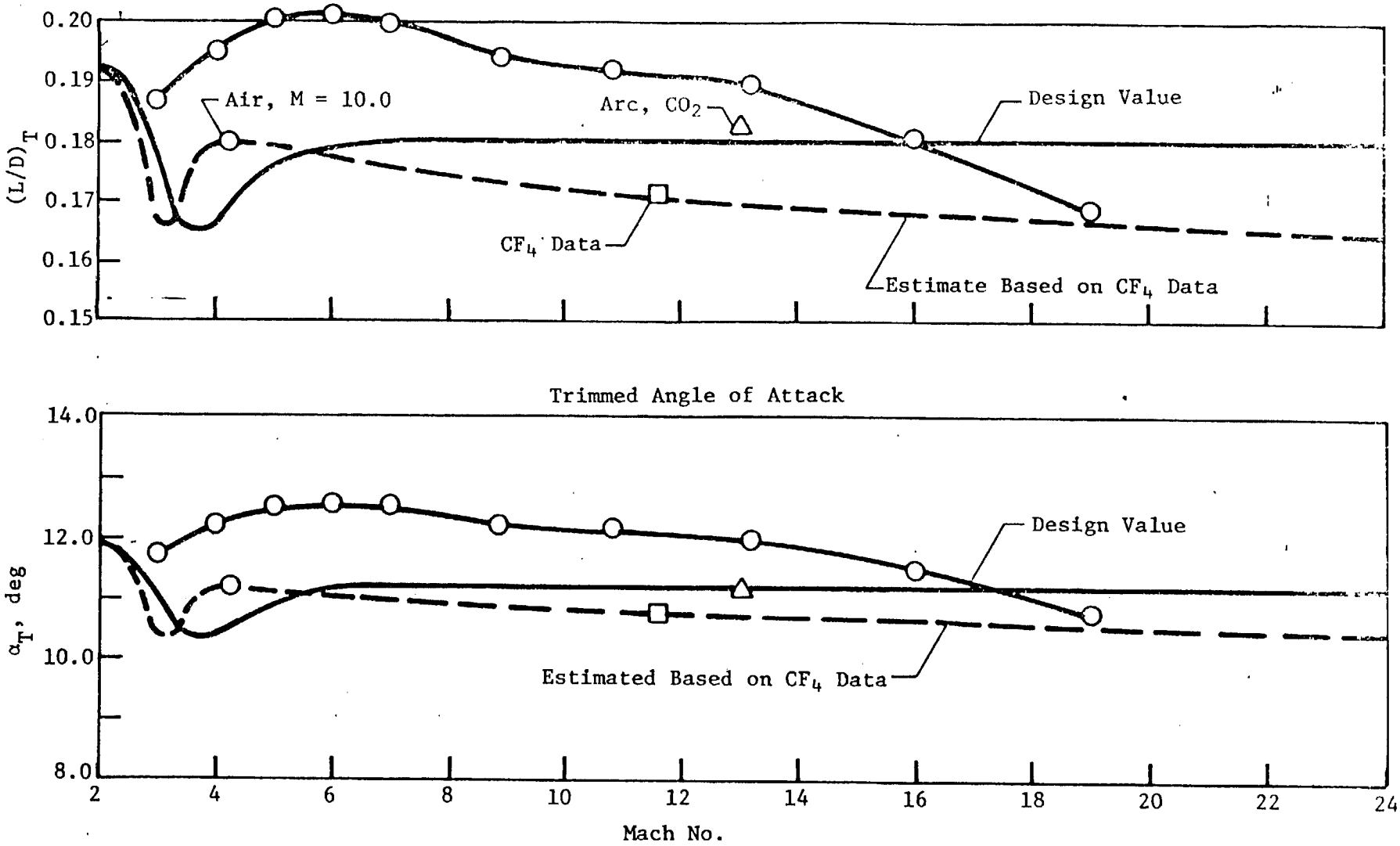

Figure IV-5 Viking Trimmed L/D

Table IV-1 Entry Vehicle cg Displacements

	Vertical, in.	Lateral, in.
Physical Dimension Tolerances (RSS)	±0.058	±0.025
Acceleration and Ablation Bias	-0.023	0
Aeroshell Axis Offset (VL1)	+0.003	+0.005

The sensitivity of trim angle of attack to cg position in the hypersonic regime is 5.64 deg/in., based on wind-tunnel tests in air. Thus, vertical cg bias plus tolerance could only account for a change in trim angle of attack of from +0.21 to -0.44°.

The effect of outgassing and loss of ablator material on the entry vehicle aerodynamics and trim alpha is unknown. It has been estimated that the ablator would give up 8 lb of material in a severe entry. An appreciable amount of heat is removed from the boundary-layer gas in the process. This obviously occurs in the period near the peak heating rate. The gas mixture flowing around the upper perimeter of the vehicle and becoming entrained in the wake will experience changes in density, molecular weight, and temperature. These could cause a net increase in the pressure on the upper base cover and thus a nose-down trim change. The discontinuity in the base pressure history, as shown in a subsequent section of this report, tends to confirm the existence of some unusual effects associated with the peak stagnation heating.

In summary, the angles of attack and lift-to-drag ratios for both VL1 and VL2 were greater than predictions based on wind-tunnel tests and nominal cg positions. VL2 trim angles of attack were about 1° more negative than those for VL1. Although not indicated by LTARP, the accelerometer data on VL1 only indicates as essentially constant 1° sideslip angle. The causes of higher trim angles of attack on both vehicles cannot be positively identified but are believed to be some combination of off-nomianl cg position and outgassing/ablation effects. The sideslip angle on VL1 and its accompanying roll moment are probably due to a lateral cg offset or a small configuration asymmetry.

C. ENTRY AERODYNAMIC FORCES

Figure IV-6 shows the axial force coefficients (C_A) for VL1 and VL2 as determined from on-board accelerometer data. The dynamic pressure used in these calculations was based on the flight stagnation pressure measurements, as discussed in a preceding section.

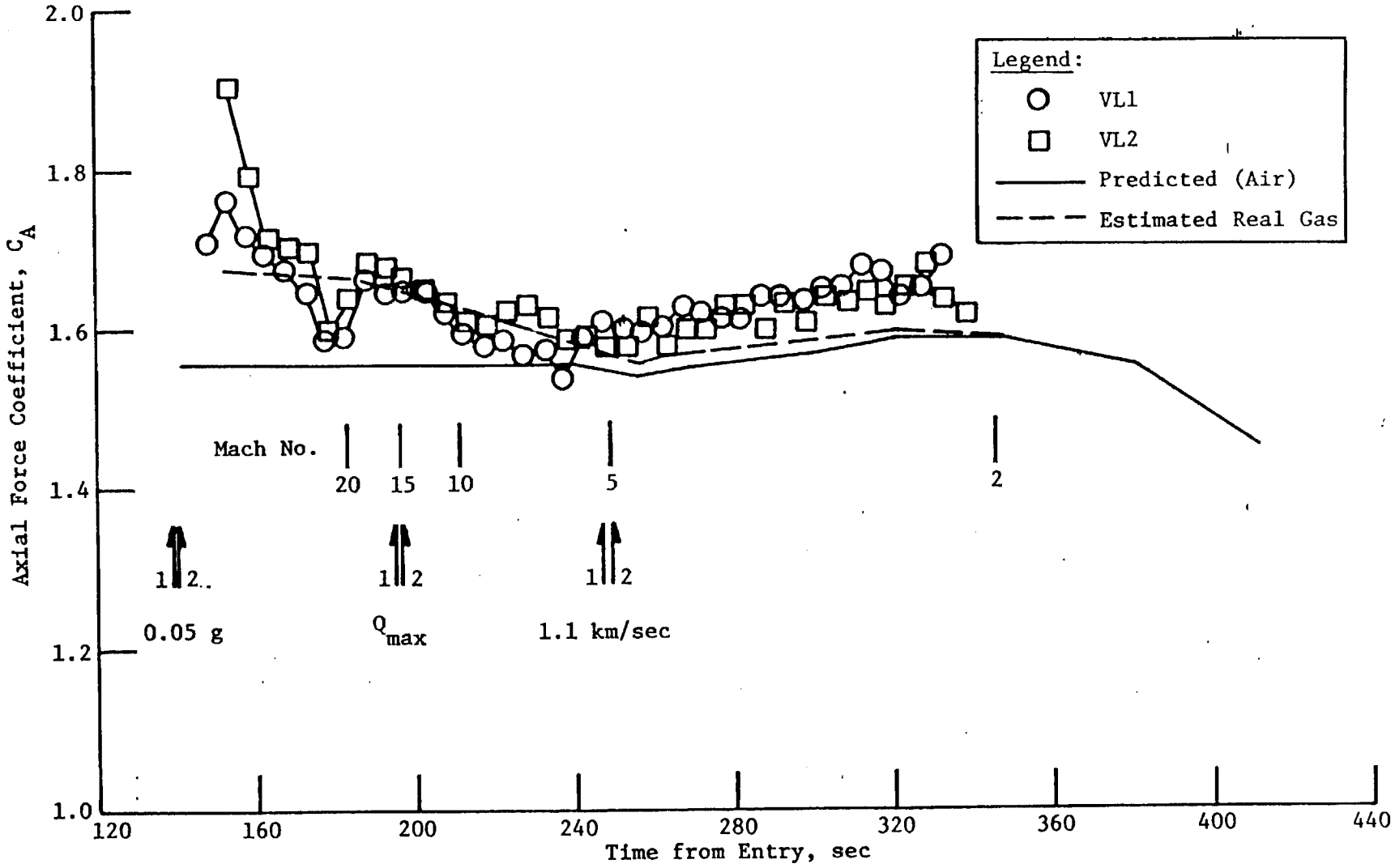

Figure IV-6 Axial Force Coefficient, VL1 and VL2

Predicted values of C_A at the trim angles of attack derived from wind-tunnel tests in air are also shown. Because flight trim angles were higher, a slight reduction in C_A would be expected. However, the figure shows that flight axial force coefficients were significantly higher. This was particularly true early in the entry when the Mach number was greater than 10. To help explain this difference, the real gas C_A was estimated by comparing the stagnation pressure coefficient for CO_2 in thermochemical equilibrium to the perfect gas values for air. The resulting variation is shown in the figure. It can be seen that the real gas effect largely explains the C_A variation experienced on VL1 and VL2. Very early in the entry near the 0.05-g point, accelerations are very small and the accuracy of the force coefficient calculation is poor. No obvious explanation is available for the high C_A values later in the entry between Mach 2 and 5.

Figure IV-7 shows the inclination of the total acceleration vector component in the X-Z plane. This angle is derived from flight data and is independent of the dynamic pressure whether derived from the stagnation pressure or by the LTARP method with its wind estimates and perfect gas aerodynamics. This angle is proportional to the angle of attack and lift-to-drag ratio. It can be shown that this vector inclination angle plus arc tan L/D equals the angle of attack.

As shown in Figure IV-7, acceleration vector inclinations for both VL1 and VL2 were significantly higher than predictions based on wind-tunnel tests in air. This is because VL1 and particularly VL2 trimmed at higher angles of attack than predicted. In addition, the variation of the inclination angle with angle of attack is steeper for real gas than for air.

D. STATIC STABILITY

The static stability derivatives $\left(C_{m_\alpha} \text{ and } C_{n_\beta}\right)$ were determined by considering oscillation frequencies recorded during VL1 and VL2 entries to be undamped natural frequencies. The results, shown in Figure IV-8, indicate that, during the early high-speed portion of the entry, the pitch stability was about 50% greater than the prediction derived from the air wind-tunnel tests. This is a real gas effect and was expected and discussed in Ref 2.

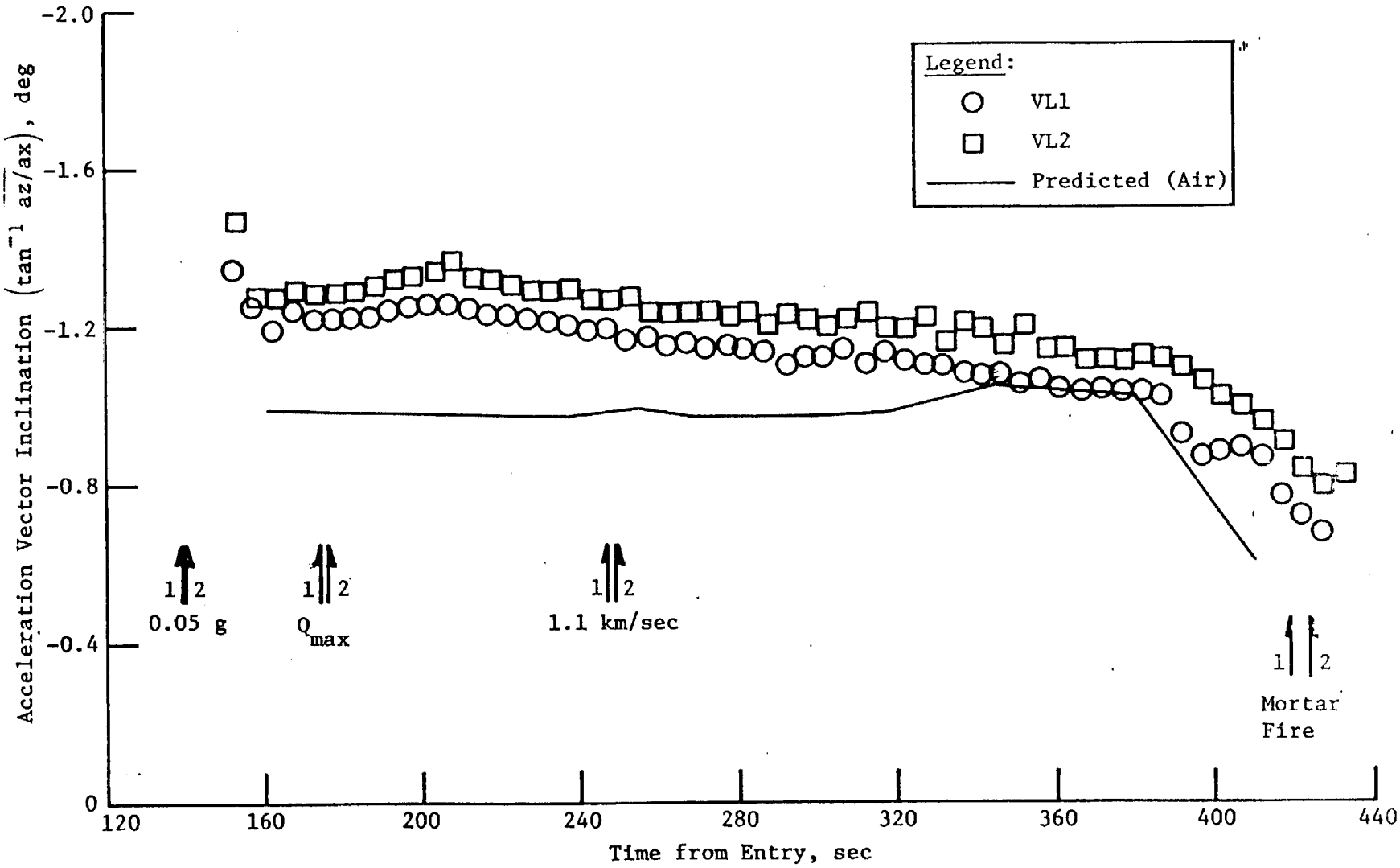

Figure IV-7 Acceleration Vector Inclination, VL1 and VL2

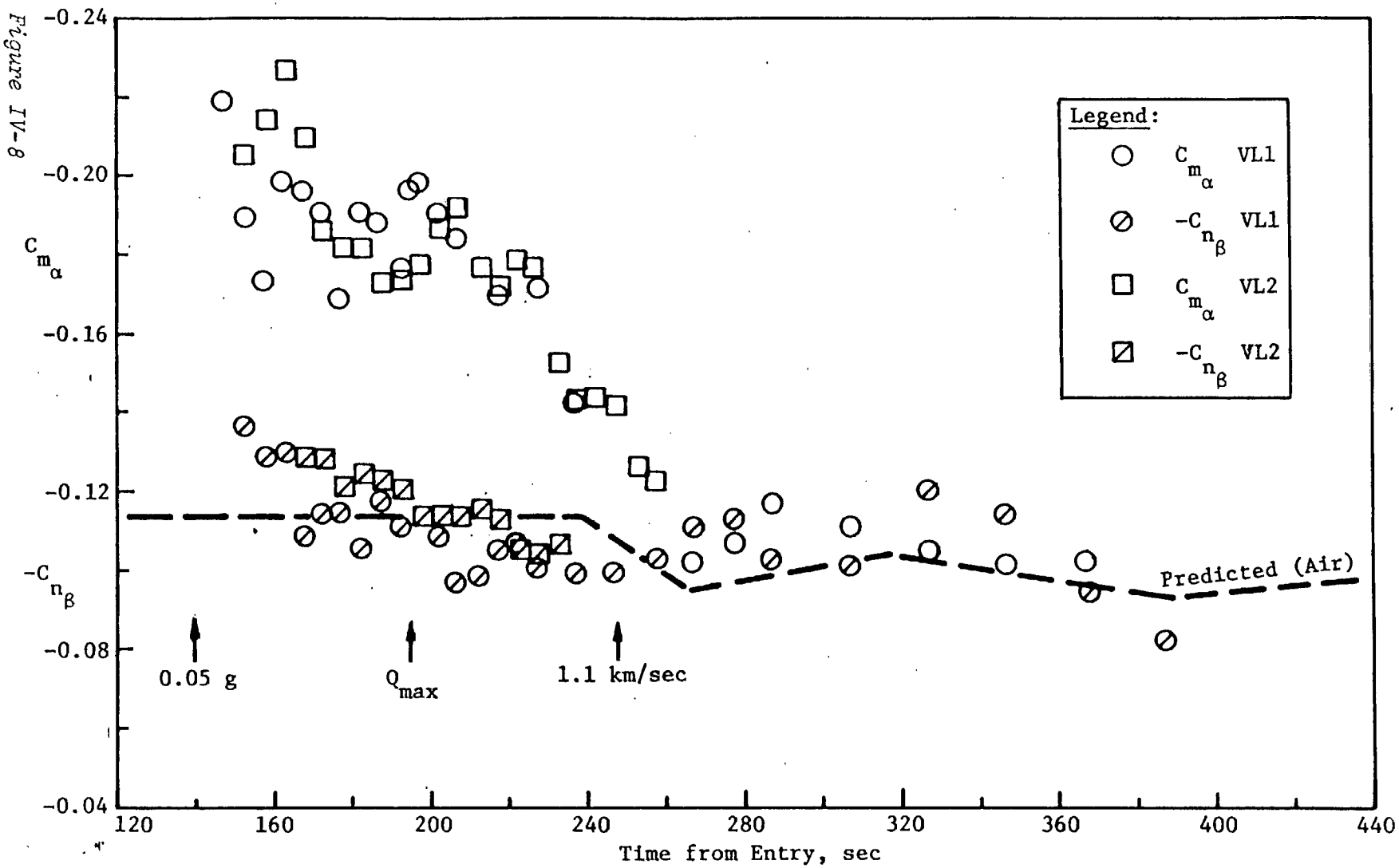

Figure IV-8 Static Stability Derivatives

The static directional stability data shown in Figure IV-8 does not exhibit the increase found in the pitch data. This is believed due to the fact that the yaw oscillations occur near zero sideslip angle while the pitch oscillations were about the trim angle of attack. Reference 2 shows that the real gas pitching moment versus angle-of-attach curve to be rather flat near zero and much steeper in the 10 to 15° angle-of-attack region. The uncoupling of the pitch and yaw oscillations as evidenced by their different frequencies was not anticipated.

E. BASE PRESSURE

Figure IV-9 shows the time history of the base pressure for VL1 and VL2. It can be seen that there was an interruption or discontinuity in the buildup of the pressure on both vehicles. The existence of this anomaly was verified by examining the vehicle internal pressure indicated by the pressure indicator mounted on the lander. This Kiel probe gage is used to obtain ambient pressure after separation of the aeroshell and base cover. The internal pressure in the aeroshell/base cover closely follows the external base pressure because of the vent through the base cover.

The discontinuity in the base pressure history cannot be readily explained, but it is strongly suspected that it is associated with changes in the wake composition following the peak heating period and its associated outgassing and ablation.

Figure IV-10 shows the ratio of base to stagnation pressure throughout the entry. It can be seen that there is relatively low scatter in the data and the trend with Mach number is very consistent.

Figure IV-11 shows venting system performance for VL1. The base cover design pressures were 1.44 mb collapsing and 6.76 mb bursting. The fact that the actual differential pressures were less than a tenth of these values indicates that the base cover vent performed effectively.

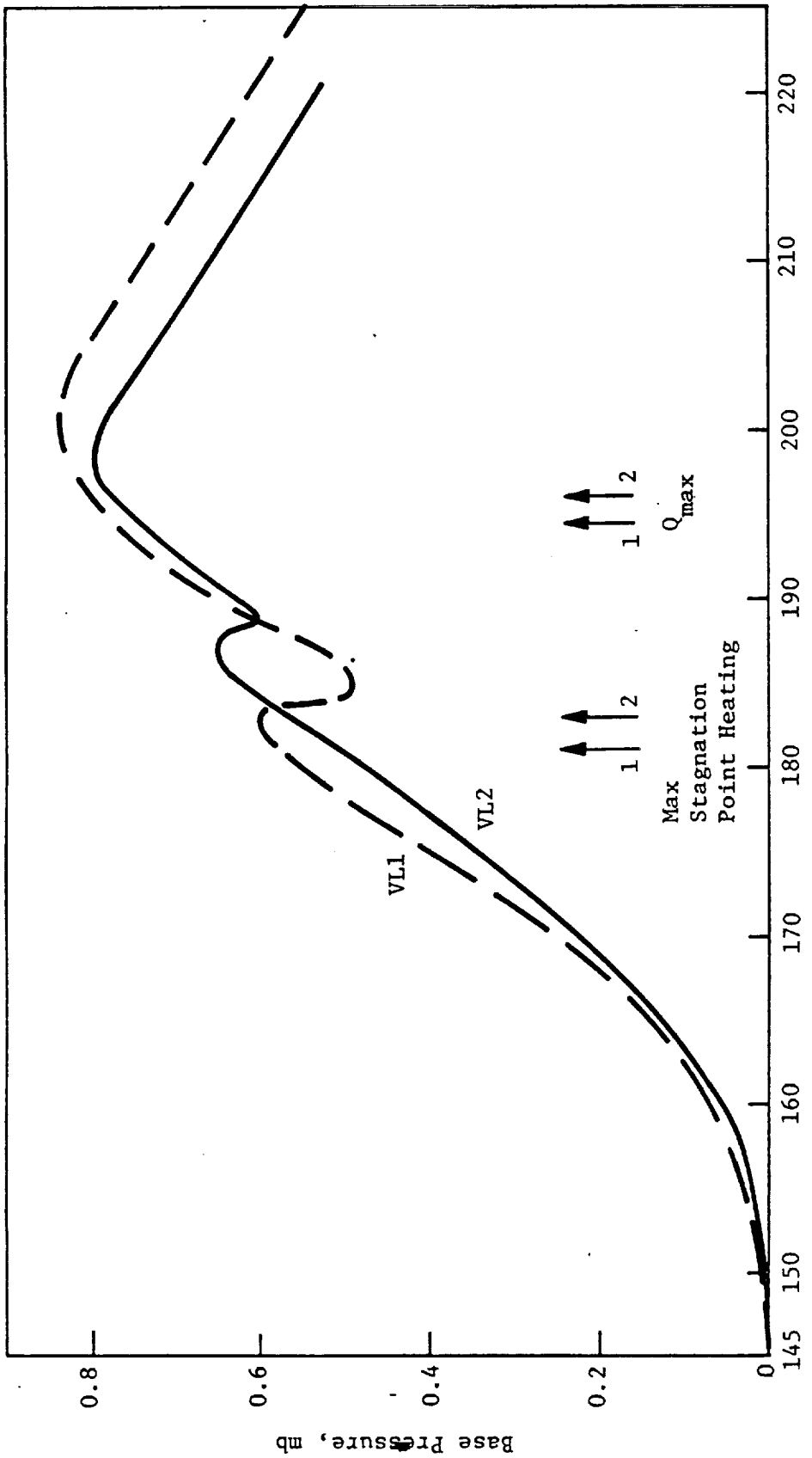

Figure IV-9 Base Pressure History, VL1 and VL2

Figure IV-9

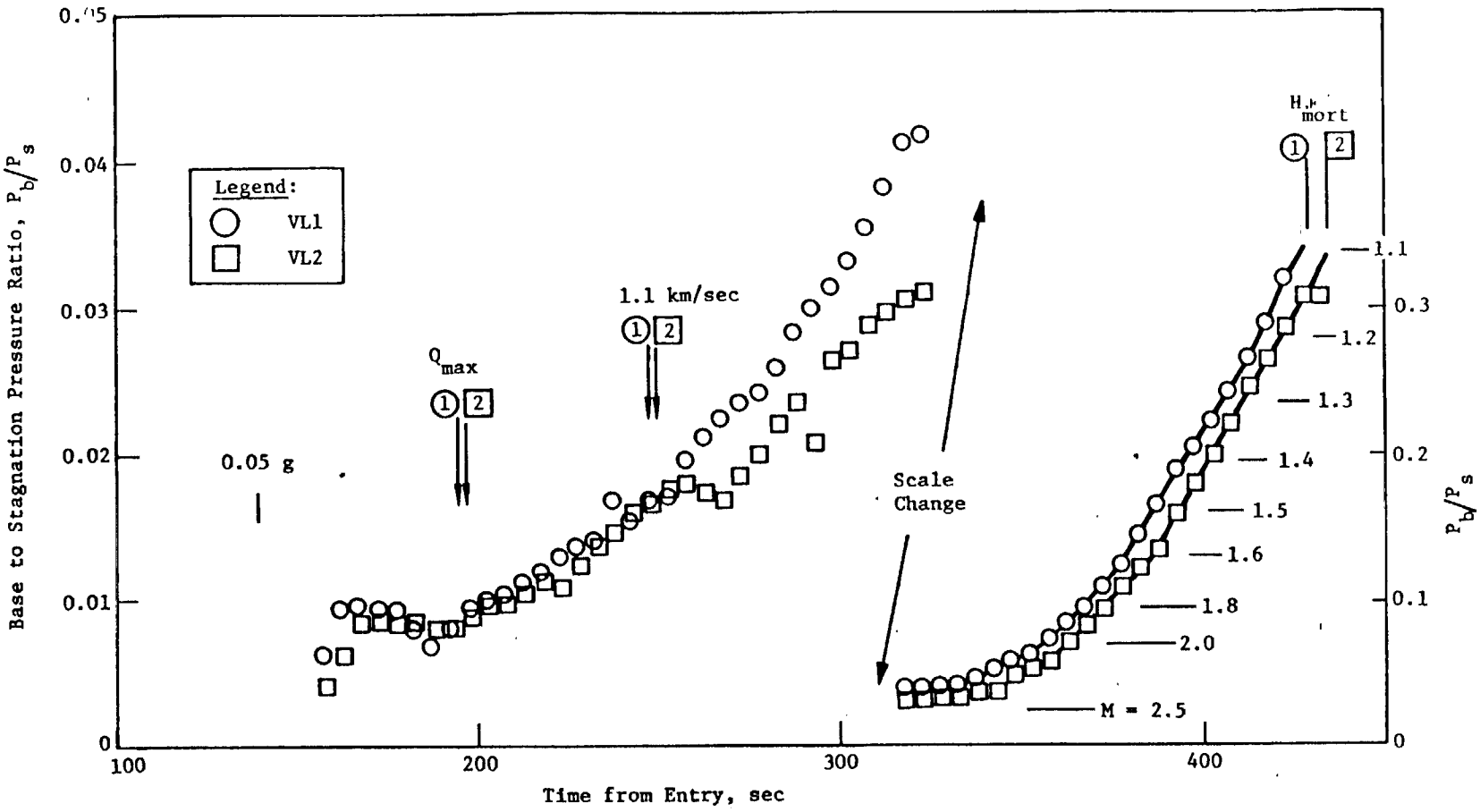

Figure IV-10 Base to Stagnation Pressure Ratio, VL1 and VL2

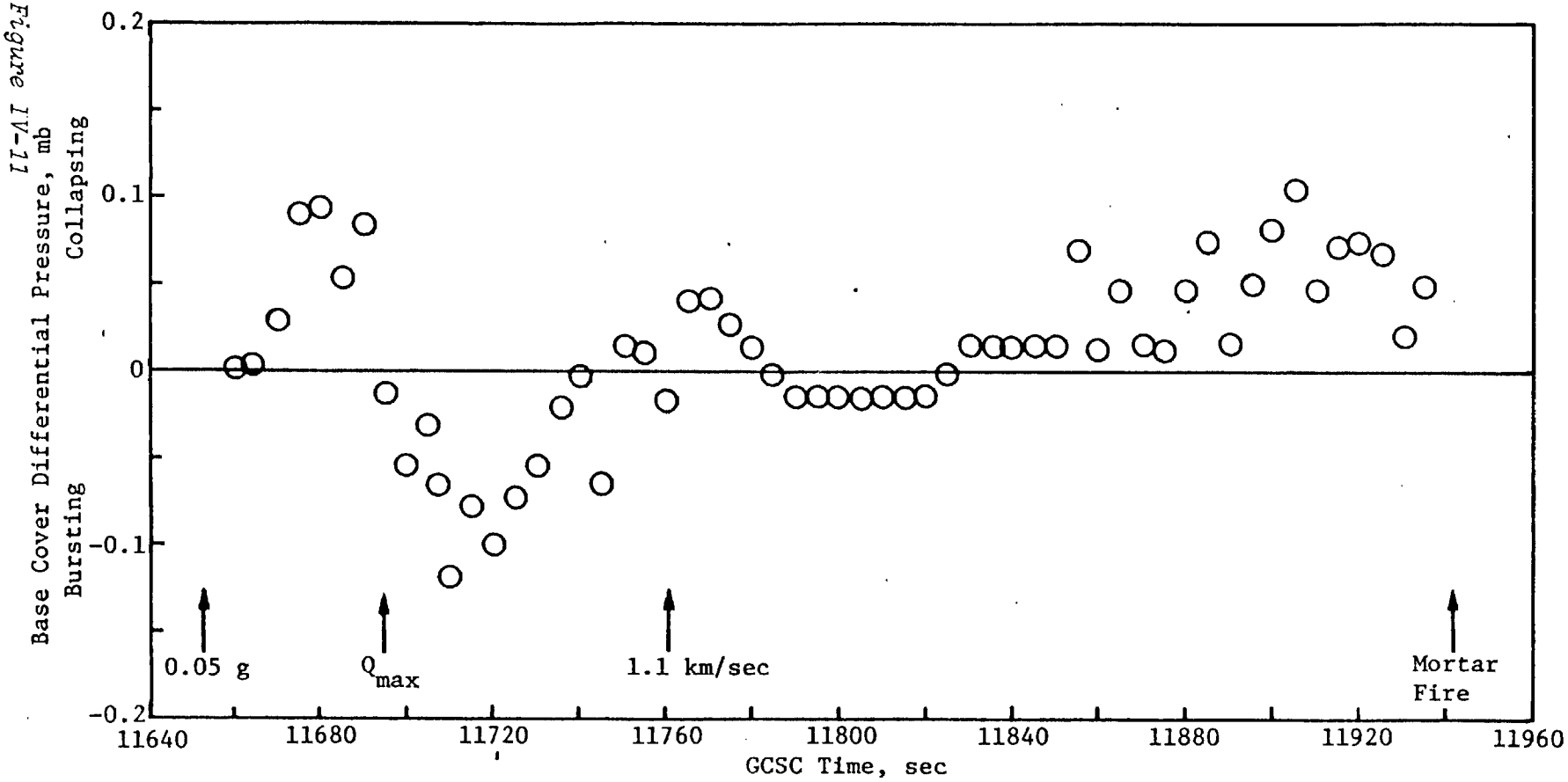

Figure IV-11 Entry Vehicle Venting Performance, VL1

F. AEROSHELL HEATING

Figures IV-12 and IV-13 show the stagnation point heating rate and accumulated heat load as estimated from the flight and LTARP data for VL1 and VL2. The maximum expected heating rate of 26 $Btu/ft^2/sec$ and the total heating load limit of 1375 Btu/ft^2 were not approached in either landing.

The effectiveness of the aeroshell as a heat shield may be evaluated by means of temperature sensors mounted on the backface of the aeroshell and on the bases of components that penetrate partly through the aeroshell. These components are the radar antenna, stagnation pressure indicator, and recovery temperature sensor. Higher temperatures result from higher total heat loads. Predicted temperatures for two severe cases with different total heat loads are given in Table IV-2 along with the flight results. The table shows that actual flight temperatures were far below predictions. The difference is much more than can be attributed to the low total heat loads experienced in flight. It is therefore obvious that the prediction methods are quite conservative and the total load limit of 1375 Btu/ft^2 established before flight can be exceeded as far as the aeroshell heat shield is concerned.

Table IV-2
Predicted and Flight Heat Shield Backface Temperatures

	Prediction		Flight	
			Viking I	Viking II
Entry Angle, α_E, deg	-14.5	-16.25	-17.8	-17.6
Total Heat, Q_T, Btu/ft^2	1548	1280	1035	1046
Locations	Peak Temperatures, °F			
Aeroshell Cone, Inboard	535	440	156	153
Aeroshell Cone, Outboard	640	530	201	189
Aeroshell Antenna	565	475	123	88
Stag. Pressure XDCR	515	410	N.A.	N.A.
Recovery Temp XDCR (Before Deployment)	565	475	233	N.A.

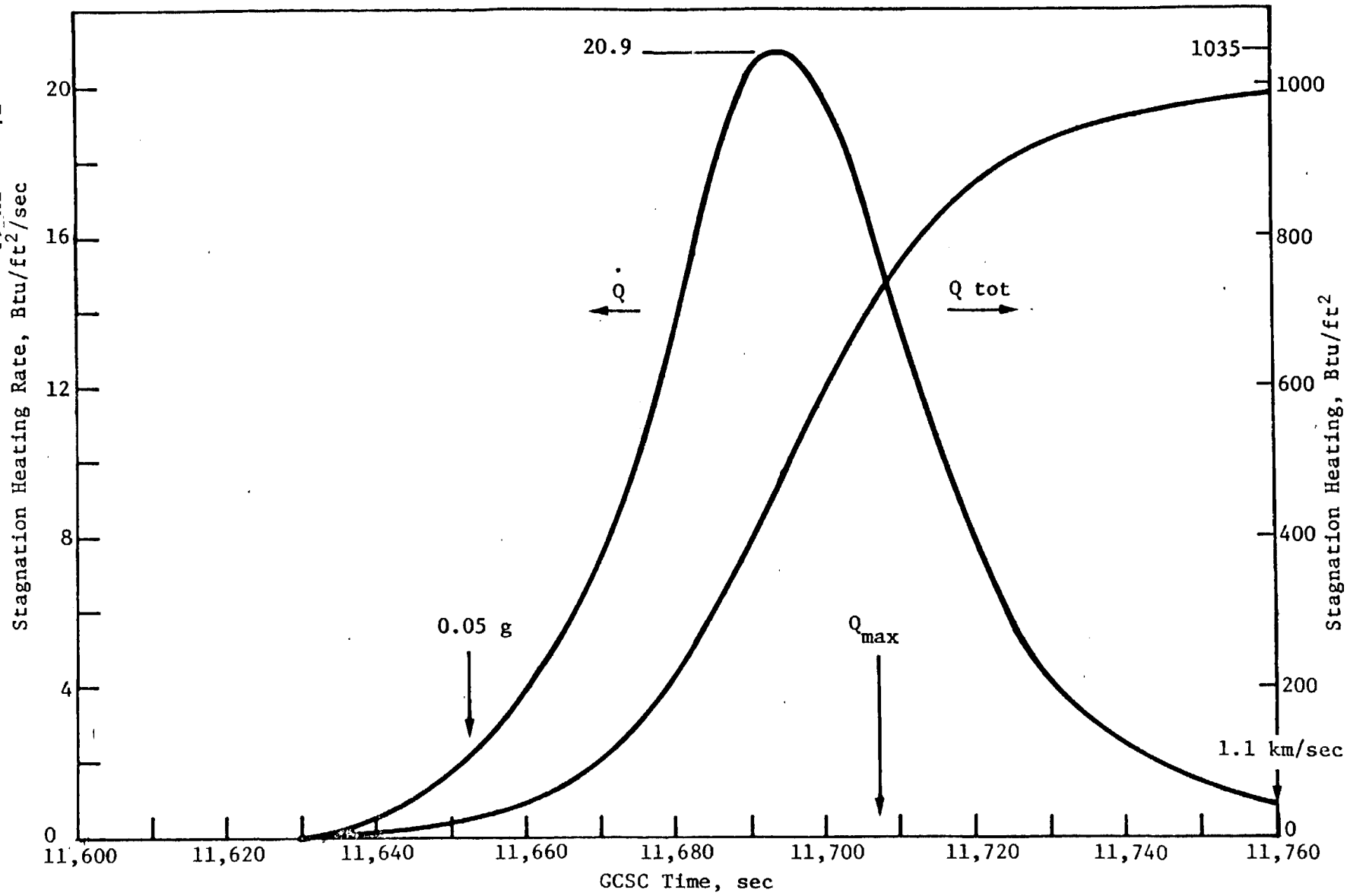

Figure IV-12 Viking 1 Stagnation Point Heating, VL1

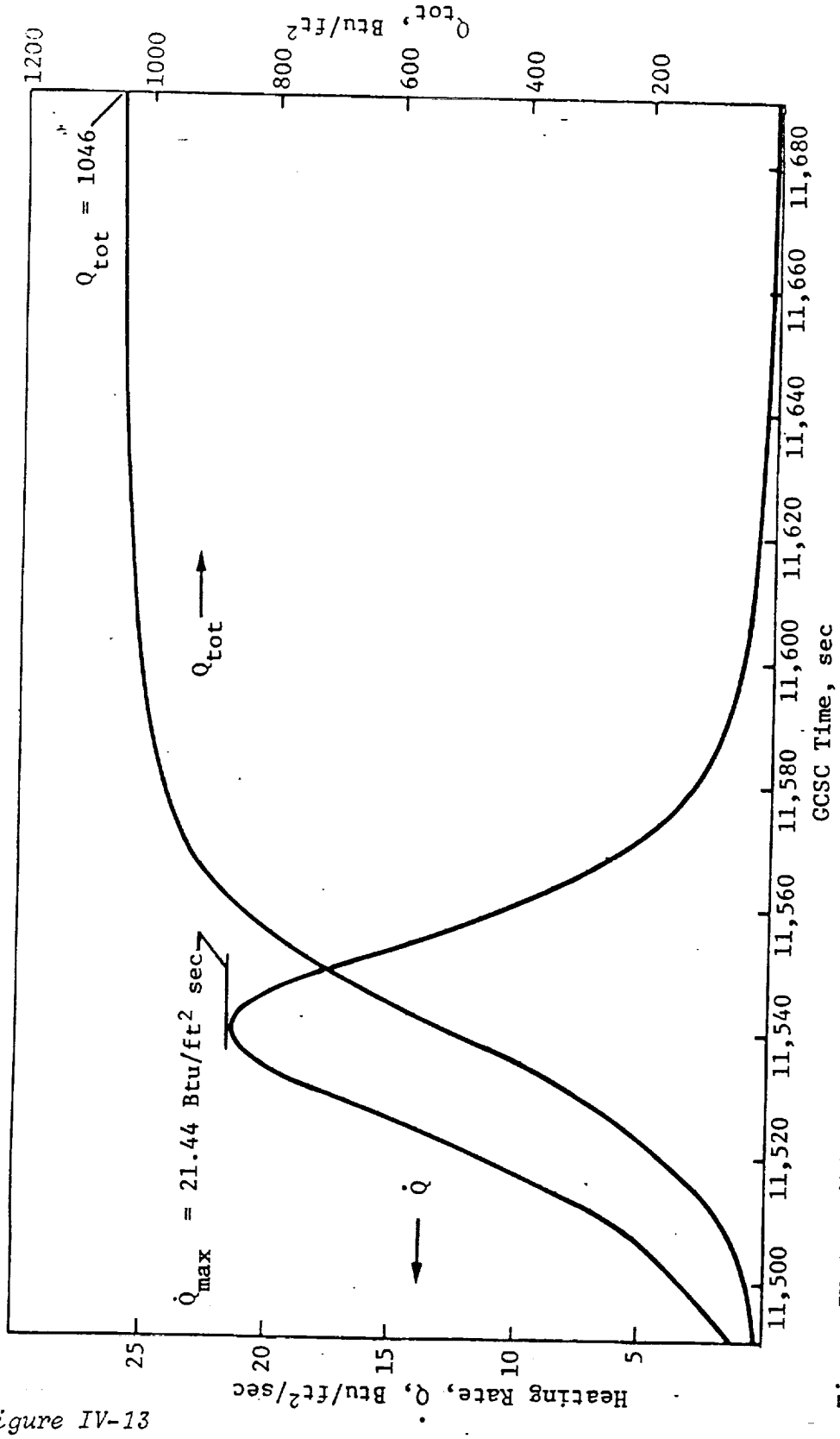

Figure IV-13 Viking 2 Stagnation Point Heating

Figure IV-13

G. BASE COVER HEATING

Preflight base cover heating predictions were based on a heating rate of 2% of the nose stagnation-point heating rate. An uncertainty factor of 1.5 was applied to this value, making the effective rate 3%. Data from the entry of the first capsule showed a peak temperature on the fiberglass inner cone that exceeded expectations. Furthermore, the temperature sensor on the aluminum outer cone failed well before it attained its peak value. Accordingly, a study was made to estimate what temperature would have been indicated by the sensor on the aluminum if it had worked properly. In addition, worst-case predictions were made for Viking 2. Both were based on an apparent base heating rate of 4.2%, which was derived from the Viking 1 fiberglass data. The actual Viking 2 entry was not a severe case but closely resembled the first entry. On Viking 2, the aluminum temperature sensor functioned properly and the results confirm the prediction based on the 4.2% heating rate. The following table summarizes these base cover temperature predictions and flight data. The actual data for the temperatures on the aluminum outer cone is shown in Figure IV-14.

Table IV-3 Peak Base Cover Temperatures

	ASTN Inner Cone Fiberglass, °F	ASTE Outer Cone Aluminum, °F
Expected for Viking 1 at Flight Stagnation Point Heating Rate	369	416
Actual Viking 1 Flight Data	406	Sensor Failed
Estimated* Viking 1 Flight Value	--	492
Actual Viking 2 Flight Data	394	498
Estimated* Worst Case	447	542

*Estimates made in Ref 3.

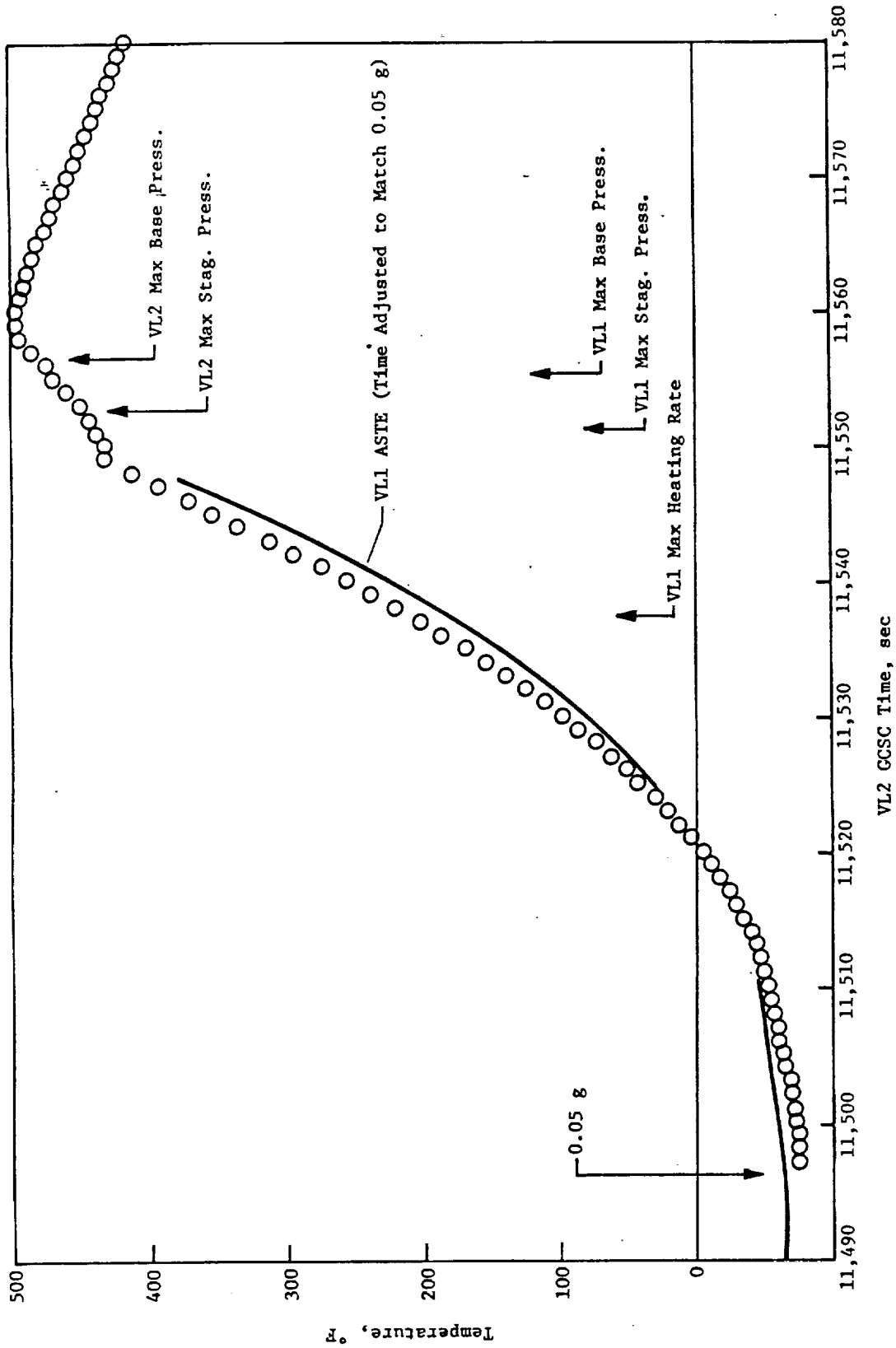

Figure IV-14 Base Cover over Cone (ASTC) Temperature

Figure IV-14

H. AEROSHELL SEPARATION

Figure IV-15 shows the aeroshell separation conditions for VL1 and VL2 as calculated by LTARP. The conditions are close to predictions and clearly within the range proven satisfactory in the BLDT tests. Examination of lander attitude data for the period immediately following aeroshell separation shows that the requirement for tip-off rates of less than 30 deg/sec was easily met in both vehicles. Any tip-off transient is masked by the dynamic motion of the parachute/lander combination.

I. REFERENCES

1. TR-3720003 *Viking Aerophysics Data Book,* Revision J., Martin Marietta, April 1975.

2. TR-3709014 *Viking Aerodynamics Data Book,* Revision G., Martin Marietta, June 1975.

3. Viking Flight Team Memorandum LSO-17290-TMF of 5 August 1976, "Viking 1 Entry Heating of Basecover and Aeroshell, Results and Prediction for Viking 2."

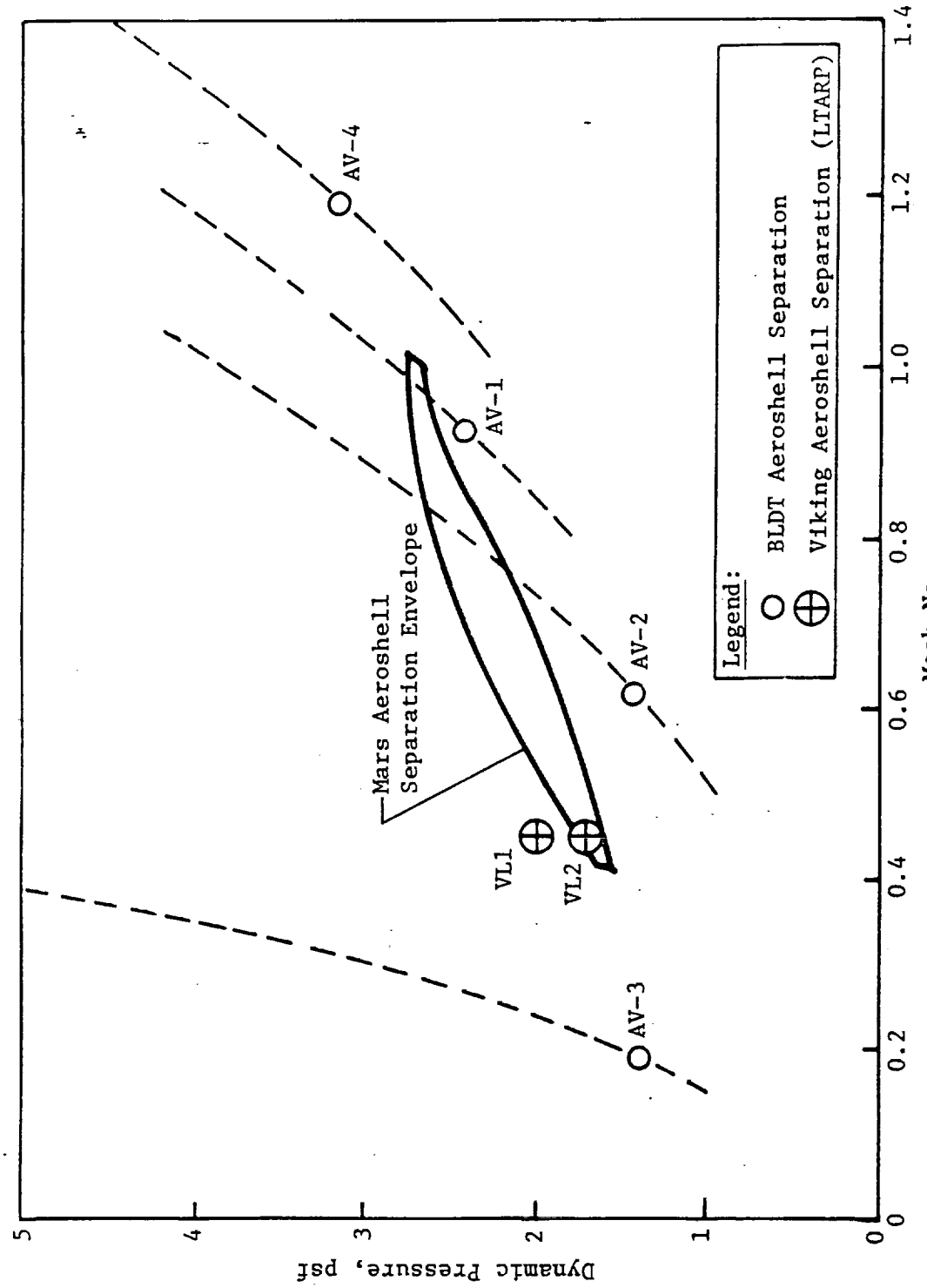

Figure IV-15 Aeroshell Separation Conditions

Figure IV-15

V. PARACHUTE PERFORMANCE

The parachutes on VL1 and VL2 both performed in a completely satisfactory manner and quite close to expectations.

A. PARACHUTE DEPLOYMENT CONDITIONS

The flight conditions at mortar fire of both Viking landers were well within the envelope of acceptable conditions as shown in Figure V-1. The reaction of the lander to the mortar impulse was evident on the axial accelerometer where velocity increments of 4.6 and 5.05 fps respectively for VL1 and VL2 were indicated. These values compare favorably with the nominal expected of 5.04 fps for a 105-fps mortar velocity. The 1-sec time to line stretch is also nominal for these conditions.

B. PEAK LOADS, PITCH/YAW DISTURBANCE

The parachute inflation occurred quite rapidly and resolution of the time is limited. However, the axial accelerometer data (Fig. V-2) shows that the deployment dynamics are surprisingly similar for the two flights and the inflation time between line stretch and peak load was somewhat less than predicted (Fig. V-3). The magnitude of the peak loads was close to the predictions for the deployment conditions and well below the design peak load of 17,500 lb (Fig. V-4). The pitch rates, which are telemetered, are the averages over 0.1 sec. The peak rates caused by the parachute deployment were therefore estimated using the observed frequency. The peak rates obtained in this manner were within the torquing capabilities of the gyro and as expected for the load, as shown in Figure V-5.

C. PARACHUTE STABILITY

The disturbance to the vehicle caused by parachute deployment damped with time so that, at aeroshell separation, the peak rates were within the 30-deg/sec allowable.

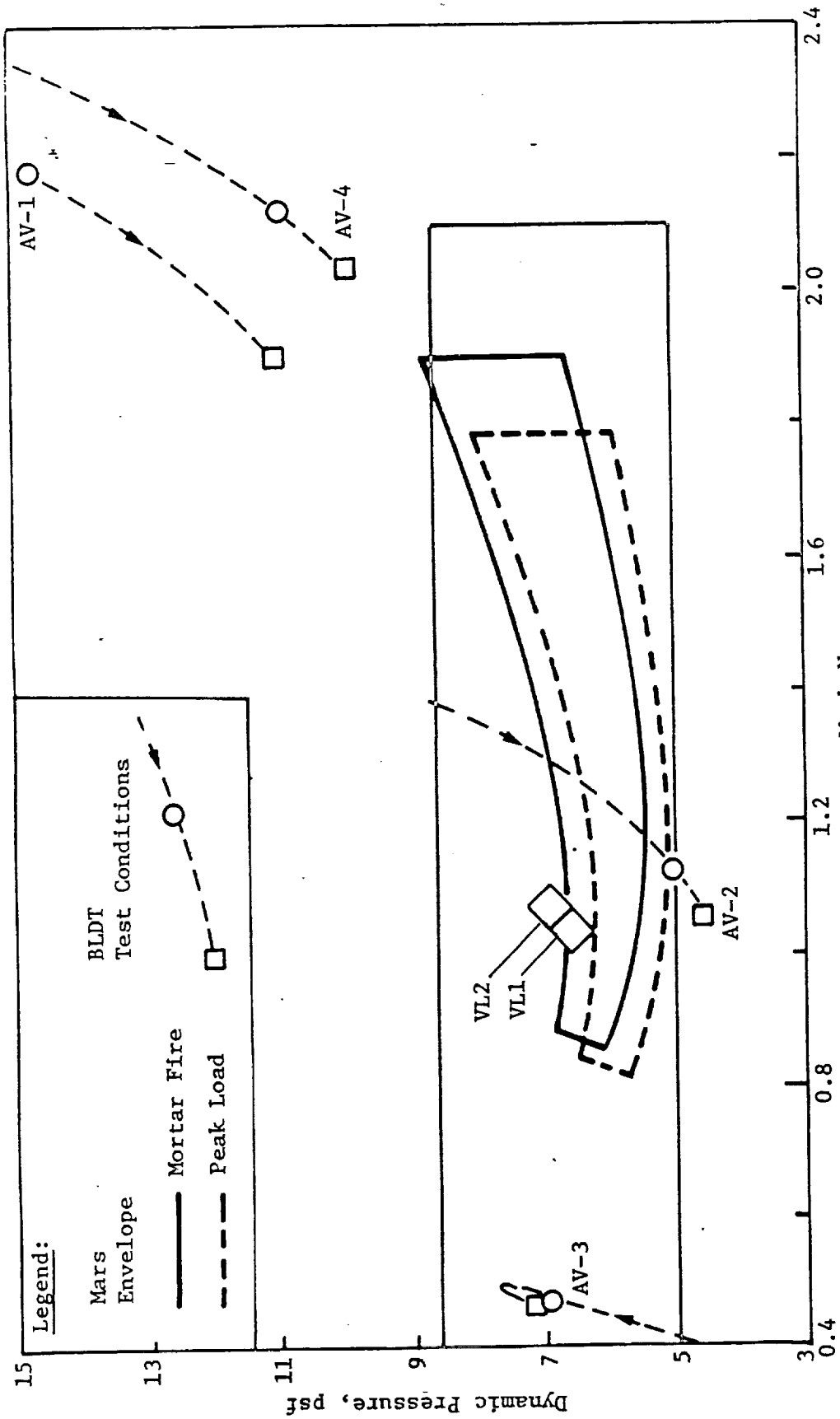

Figure V-1 Mars Envelope and Test Conditions

Figure V-1

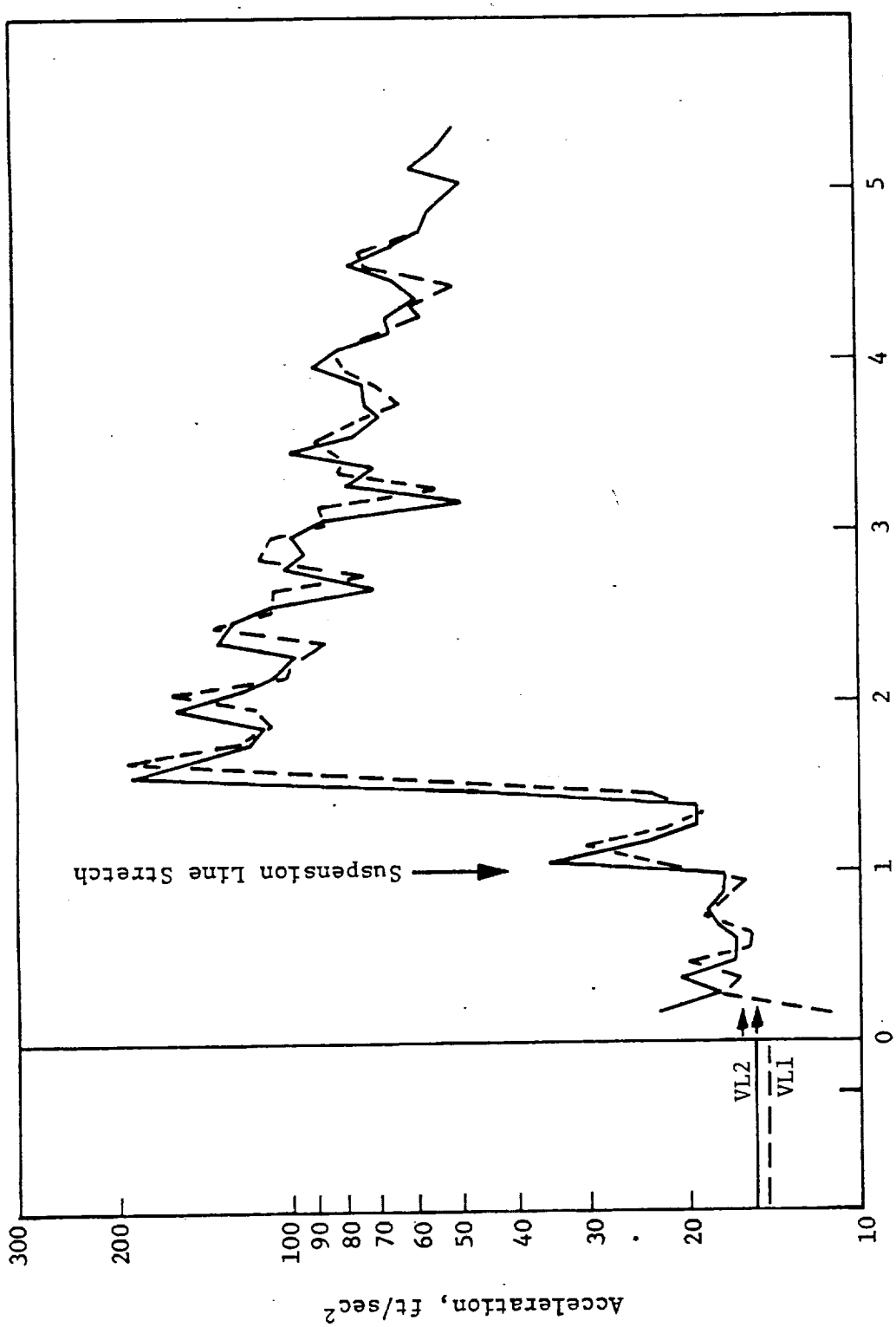

Figure V-2 Axial Acceleration during Parachute Deployment

Figure V-2

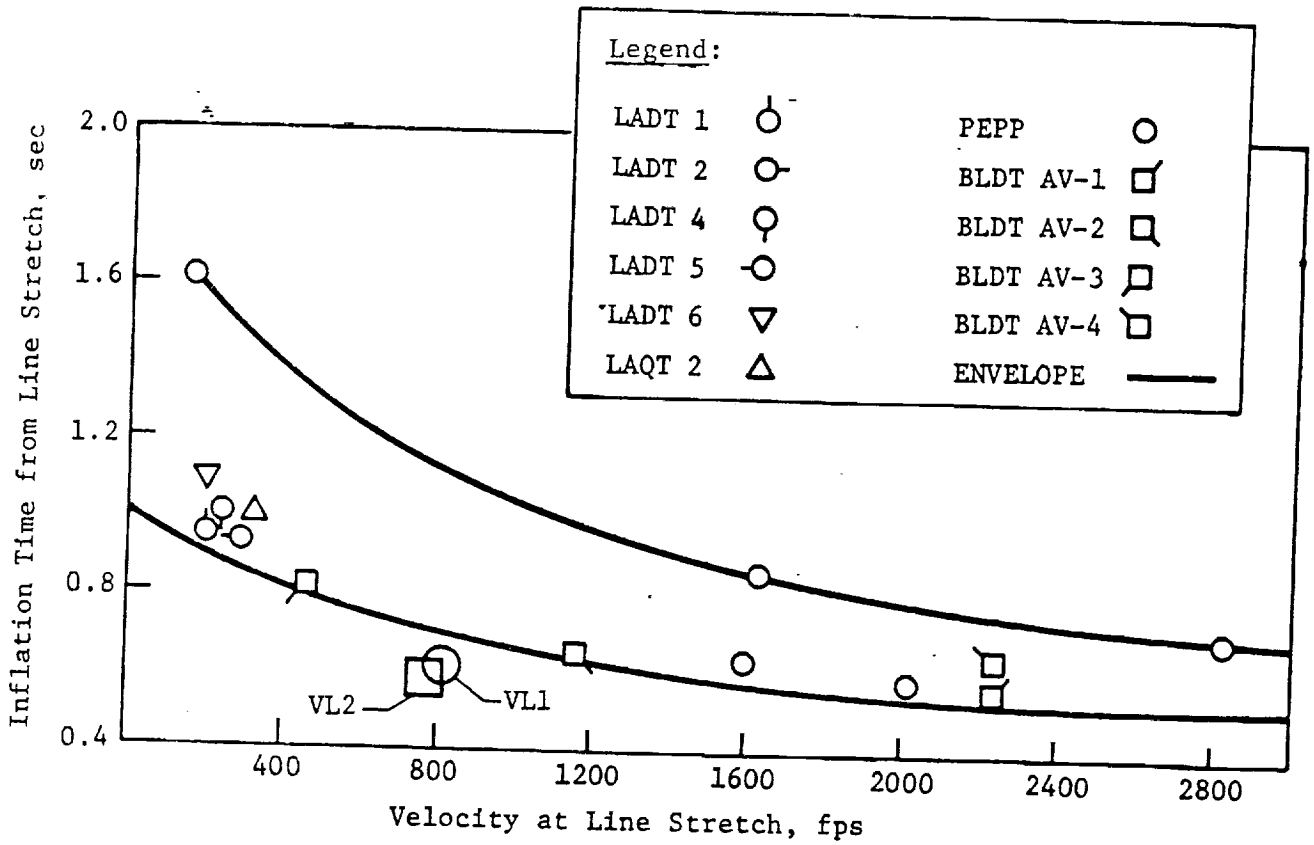

Figure V-3 Parachute Filling Time Data

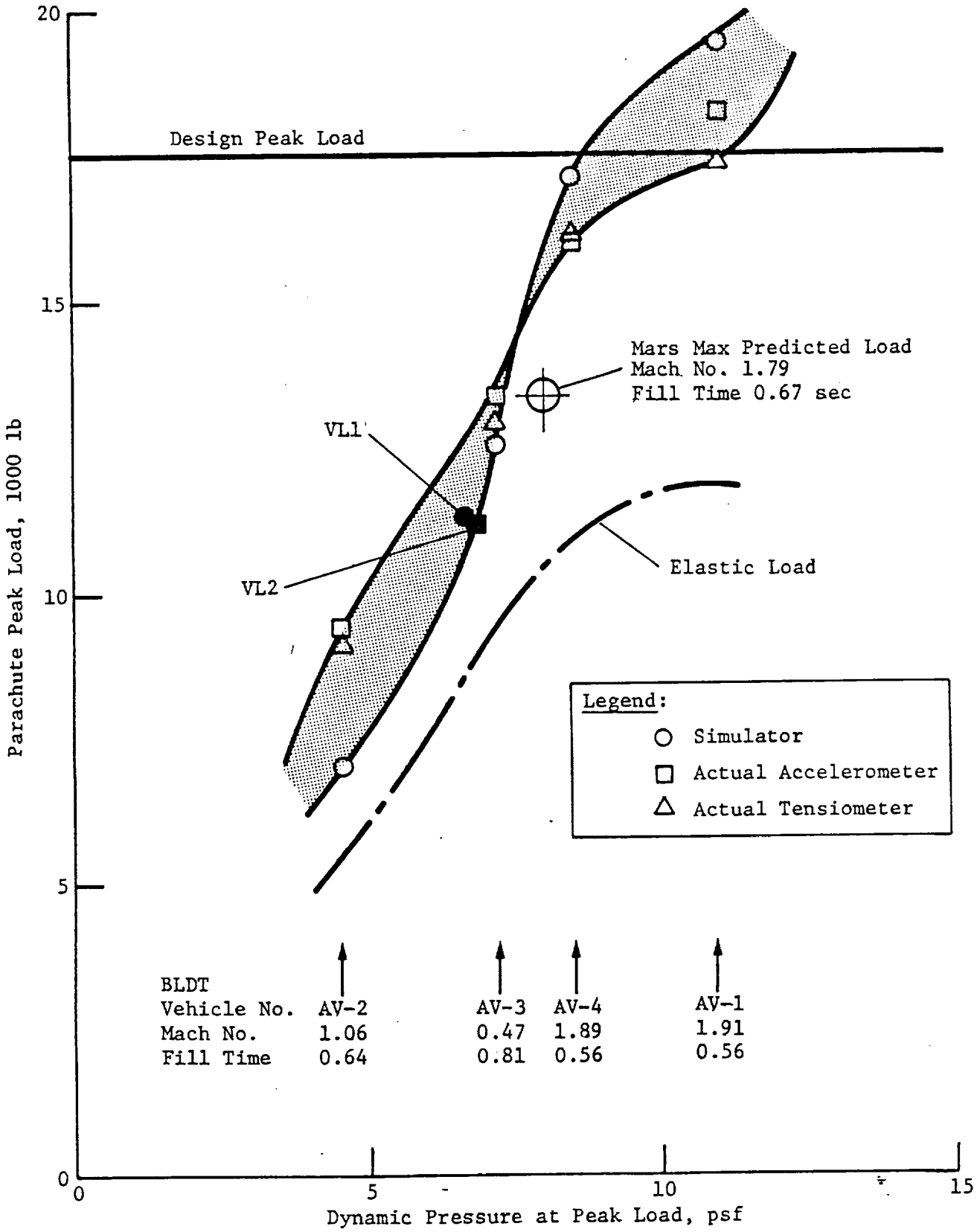

Figure V-4 Predicted versus Actual Load

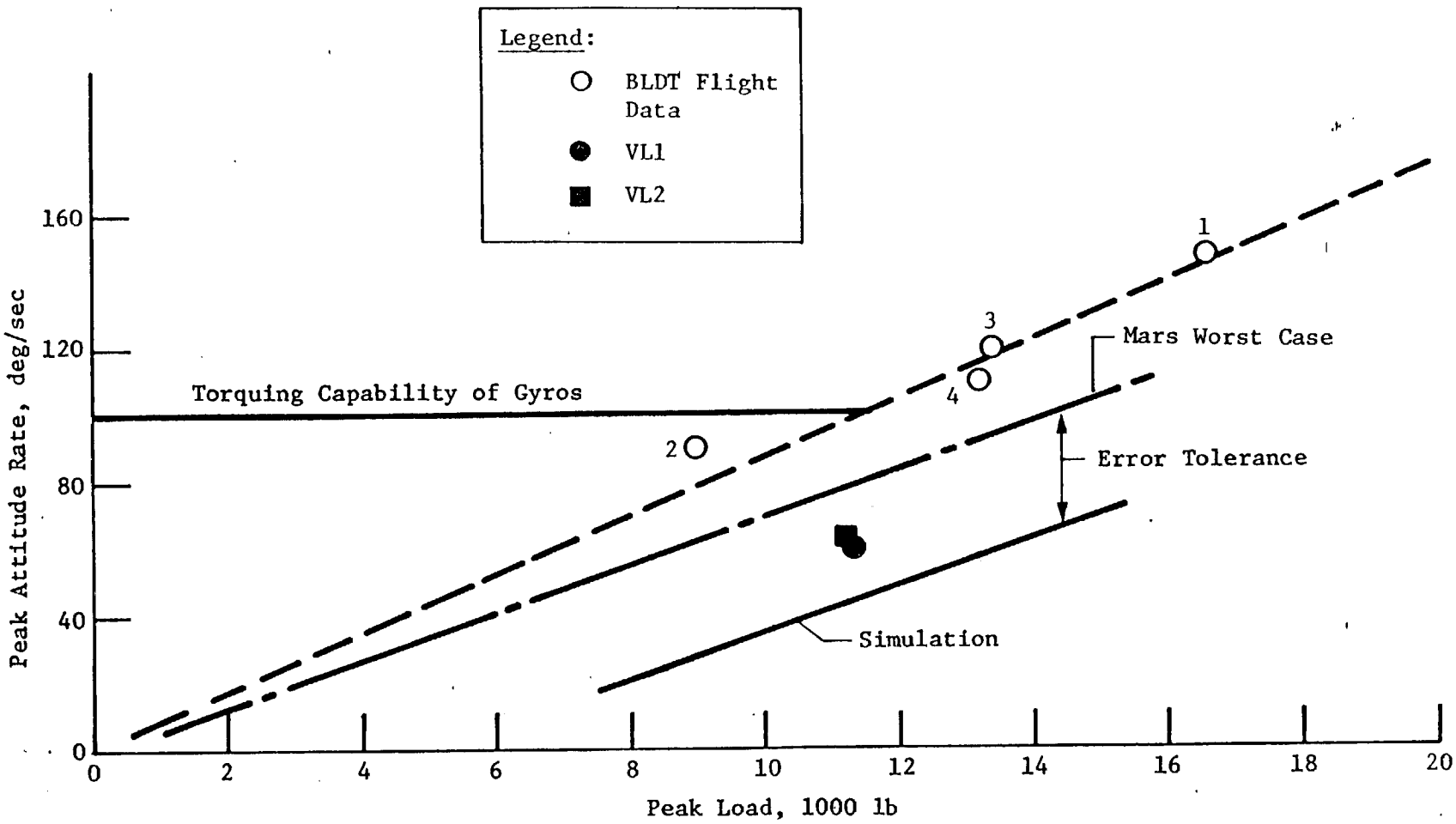

Figure V-5 Attitude Rate Sensitivity to Load

D. PARACHUTE DRAG

The drag performance of the parachute was evaluated based on the descent rate and vertical acceleration. This was done to eliminate the uncertainty involved in separating the parachute lift from winds and is similar to the method used to evaluate the drag during the high-altitude tests (BLDT). The resulting incremental parachute drag (with the forebody drag removed) is shown in Figure V-6. The somewhat higher drag obtained on Mars is reminiscent of the drag increase that occurred at low speeds in the Earth flight tests; however, these phenomena are probably not related.

E. PARACHUTE LIFT, CONING

The effects of winds and parachute lift are difficult to separate. The expected behavior of the parachute with lift is to describe a large circle when viewed from above. This motion was readily apparent during Earth tests due to the extended time for the motion to develop. This motion was not detected during the Mars descent, indicating either that negligible lift was present or the lift direction did not vary sufficiently to be separated from winds.

F. PARACHUTE SEPARATION

The lander motion at parachute release did not show any change in dynamic behavior that could be interpreted as recontact between the mortar-truss/base cover and the lander. A slight reduction in axial acceleration on VL1 just before parachute release could be interpreted as a parachute drag reduction due to engine wake; however, the separation sequence was not affected.

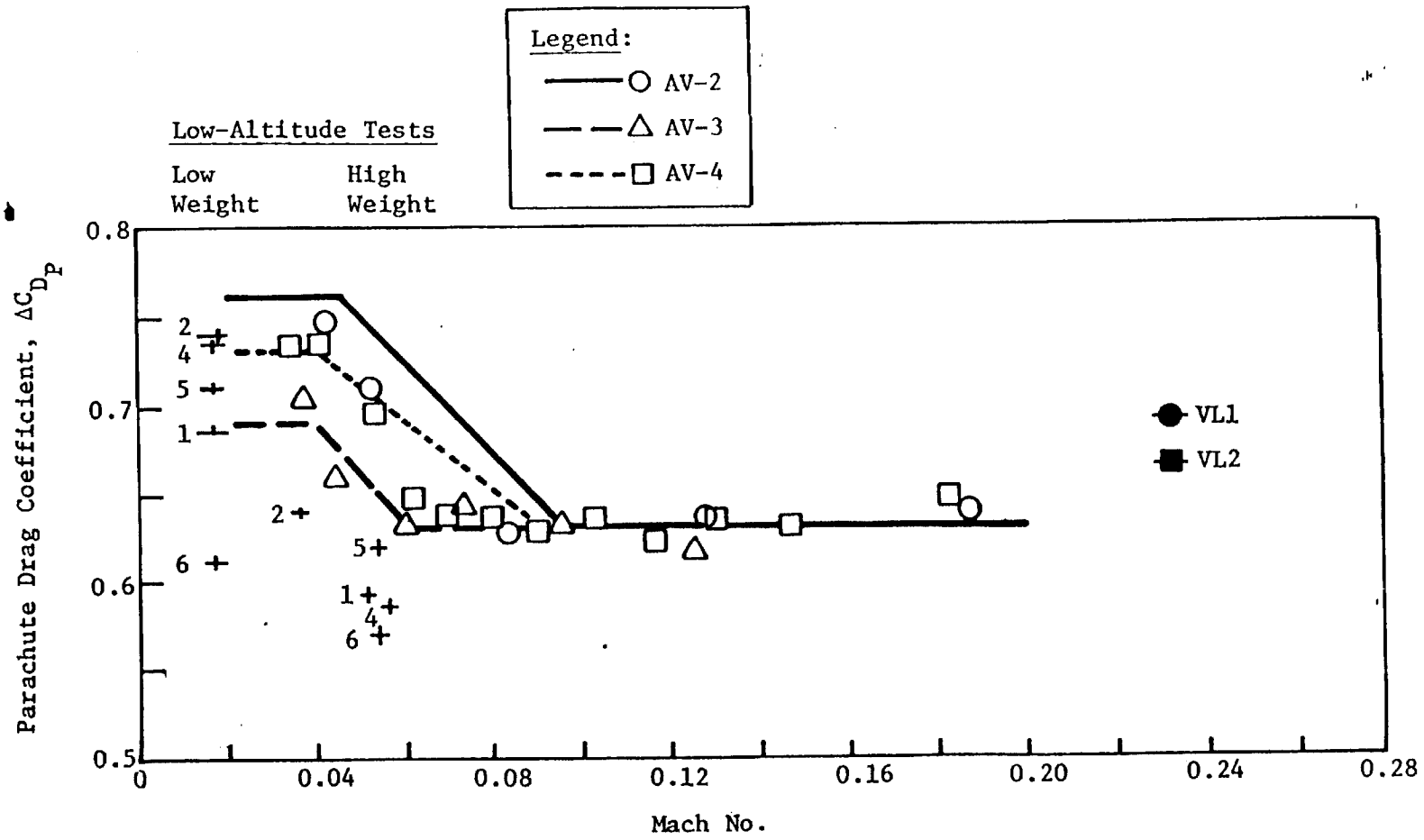

Figure V-6 Comparison of LADT and BLDT Drag

VI. TERMINAL DESCENT PERFORMANCE

Terminal descent control system performance was entirely satisfactory. System operation was smooth and stable, and fuel consumption was well within predicted limits. The following sections detail the operation of the terminal descent system.

A. TERMINAL DESCENT ENGINE THROTTLE COMMANDS

Tables IX-3 and IX-4 list the terminal descent throttle commands as functions of time for VL1 and VL2. Table VI-1 shows: (1) the time at the low throttle setting before the high-thrust phase, which should be at least 5 sec to provide sufficient time for engine warmup and tip up; (2) the time at the high-thrust setting, which should be less than 25 sec because the highest-velocity design case takes this long; (3) the average value of the high-thrust phase throttle position, which should be less than the limit of 84%; (4) the time at the constant-velocity phase position (approximately 25% average), which should be between 7.9 and 5.9 sec.

Table VI-1 Throttle Durations

	Time between Engine Start & High Thrust, sec	Time at High Thrust, sec	High Thrust Average, %	Time at CVD, sec
VL1	12.4	22.9	50.7	8.1
VL2	12.5	22.6	50.4	7.9
Criteria	>5	<25	<84	7.9 to 5.9

All criteria were met except the time at CVD setting. The longer times were caused by the higher CVD phase--approximately 63-64 ft versus 55 ft targeted. The reason for this phenomenon, as explained in Section VII.A, was primarly RA measurement error of altitude.

Figures VI-1 through VI-6 give DECSET plots of the terminal descent phase throttle positions for VL2 (VL1 plots were not available). The plots characterize smooth, stable performance and look quite similar to typical VCMU runs. The short bit of throttling at the end of CVD for the last 0.5 sec was caused by the velocity radar's sensing the dust velocity near touchdown, as explained in Section VII.B.

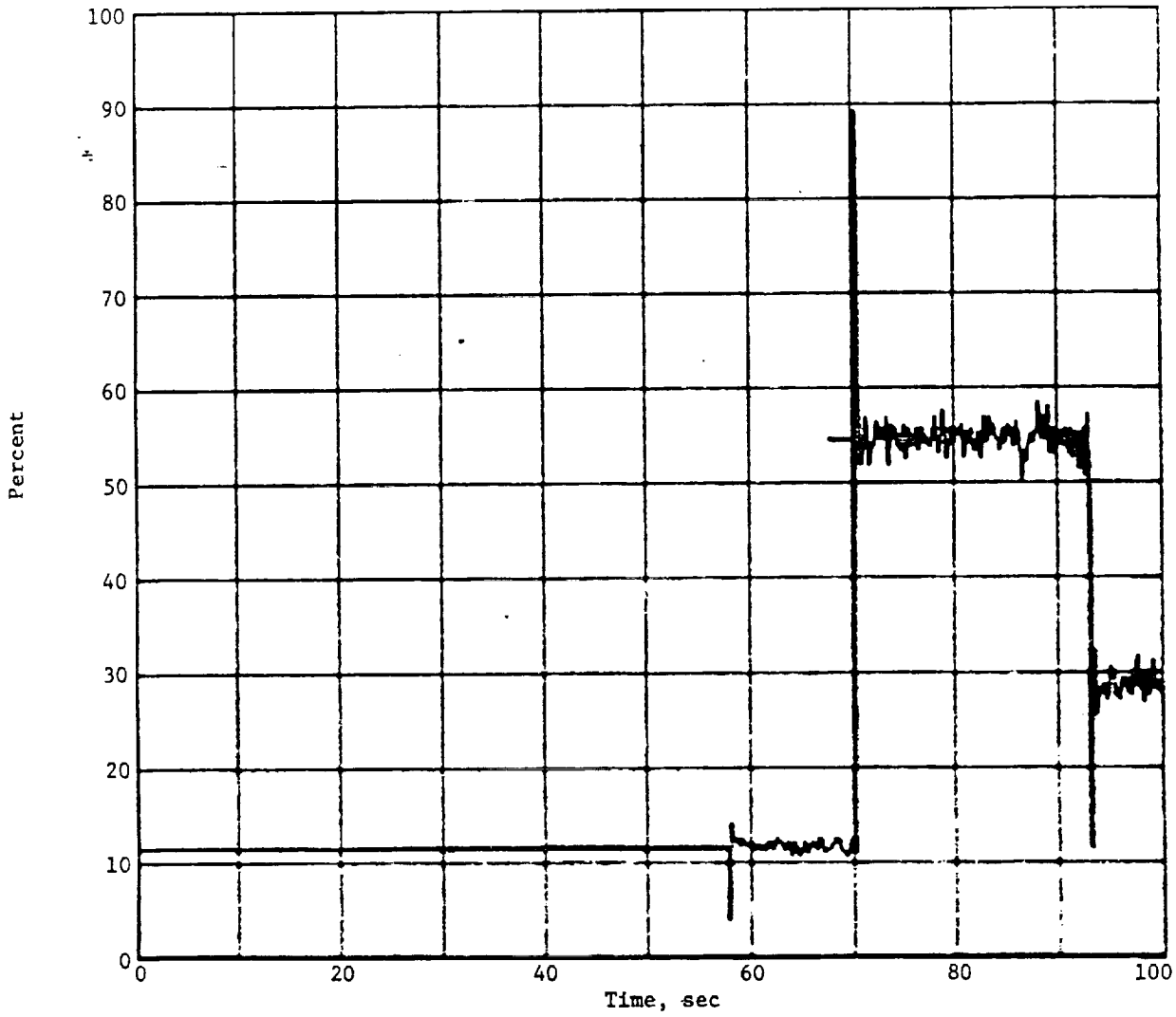

Plot Start GCSC Time 11,800
G4513 Term. Descent CMD1 FMT3

Figure VI-1 (DECSET plots of terminal descent throttle positions, VL2)

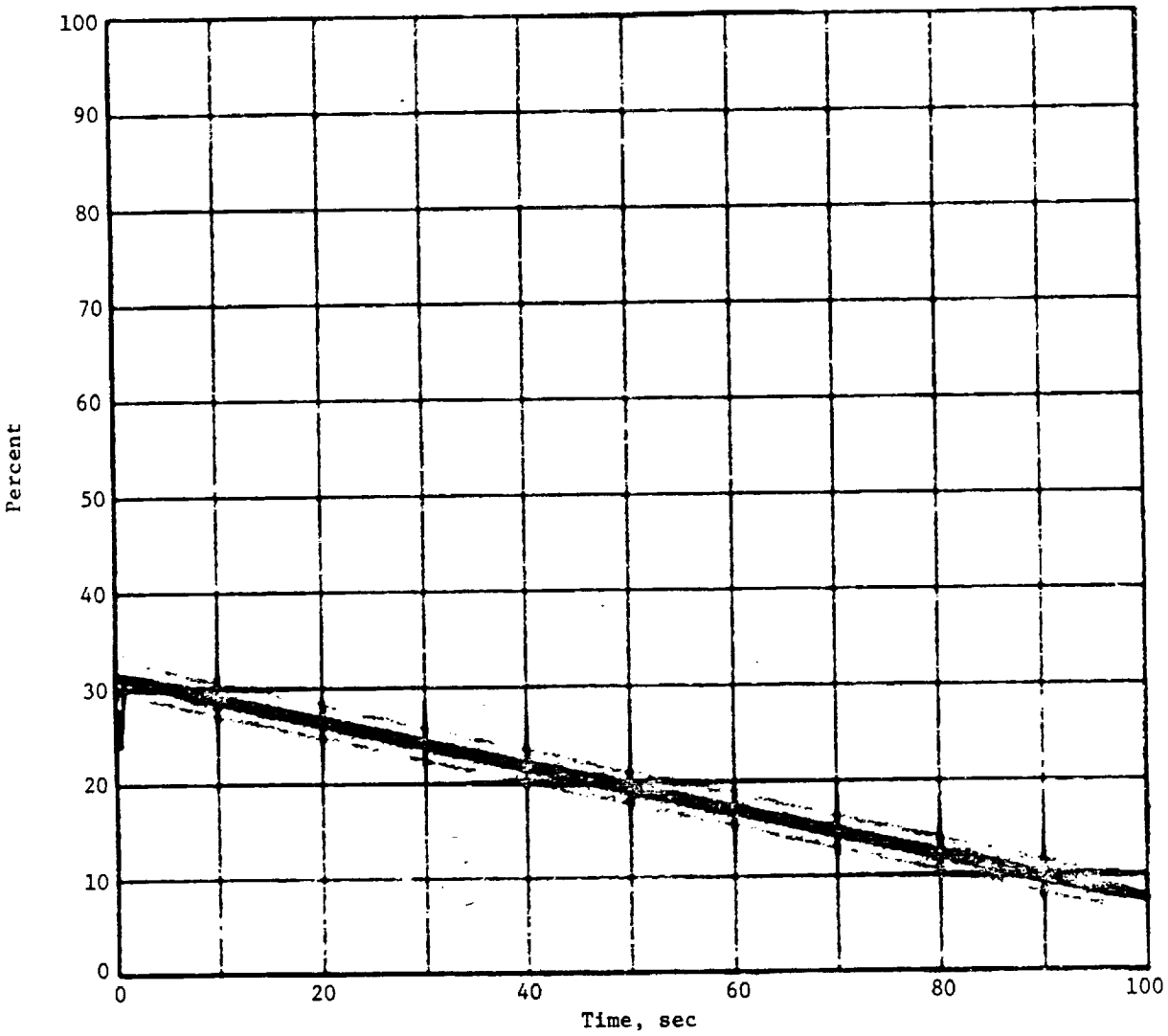

Plot Start GCSC Time 11,900
G4513 Term. Descent CMD1 FMT3

Figure VI-2 (DECSET plots of terminal descent throttle positions, VL2)

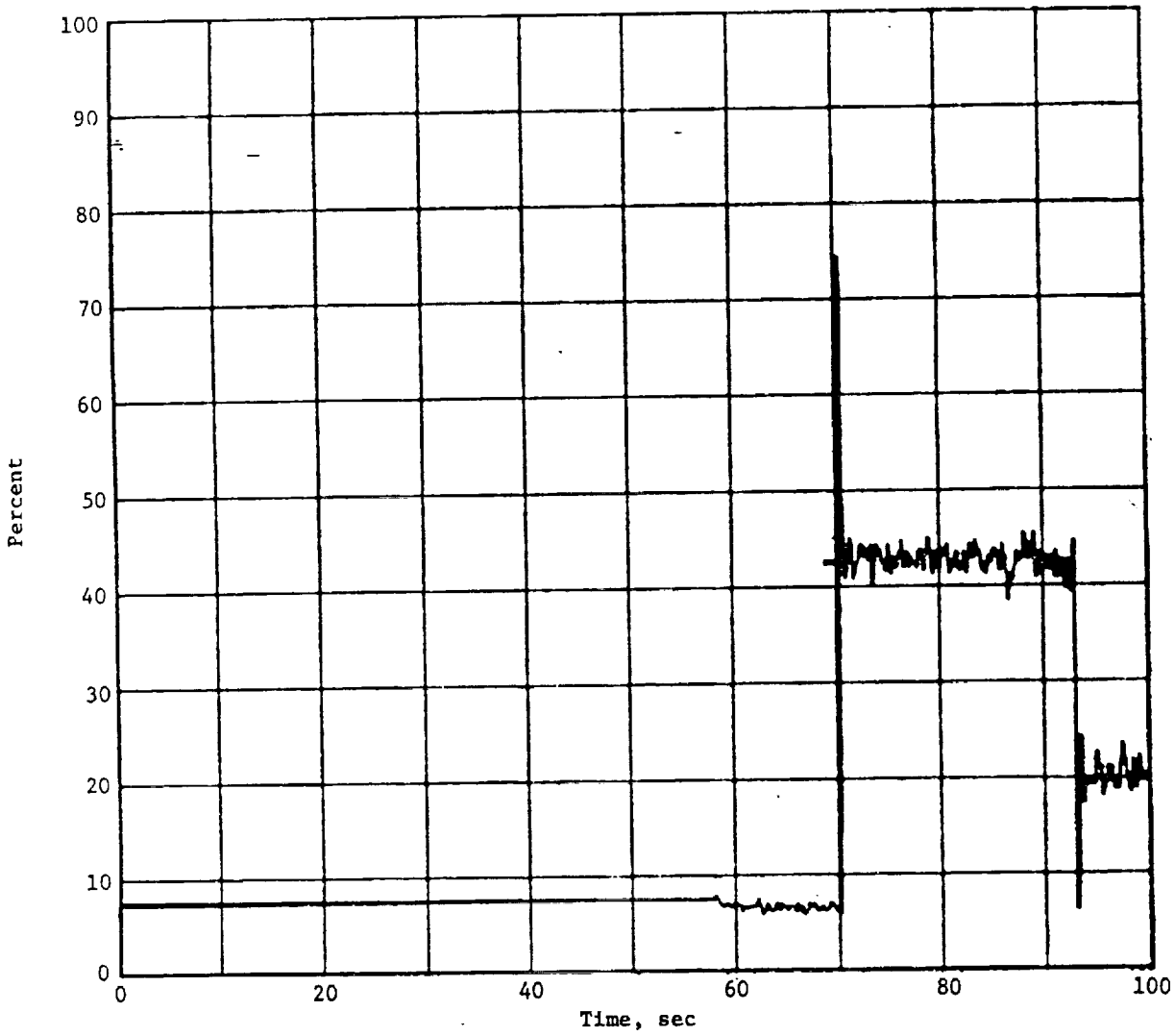

Plot Start GCSC Time 11,800
G4514 Term Descent CMD2 FMT3

Figure VI-3 (DECSET plots of terminal descent throttle positions, VL2)

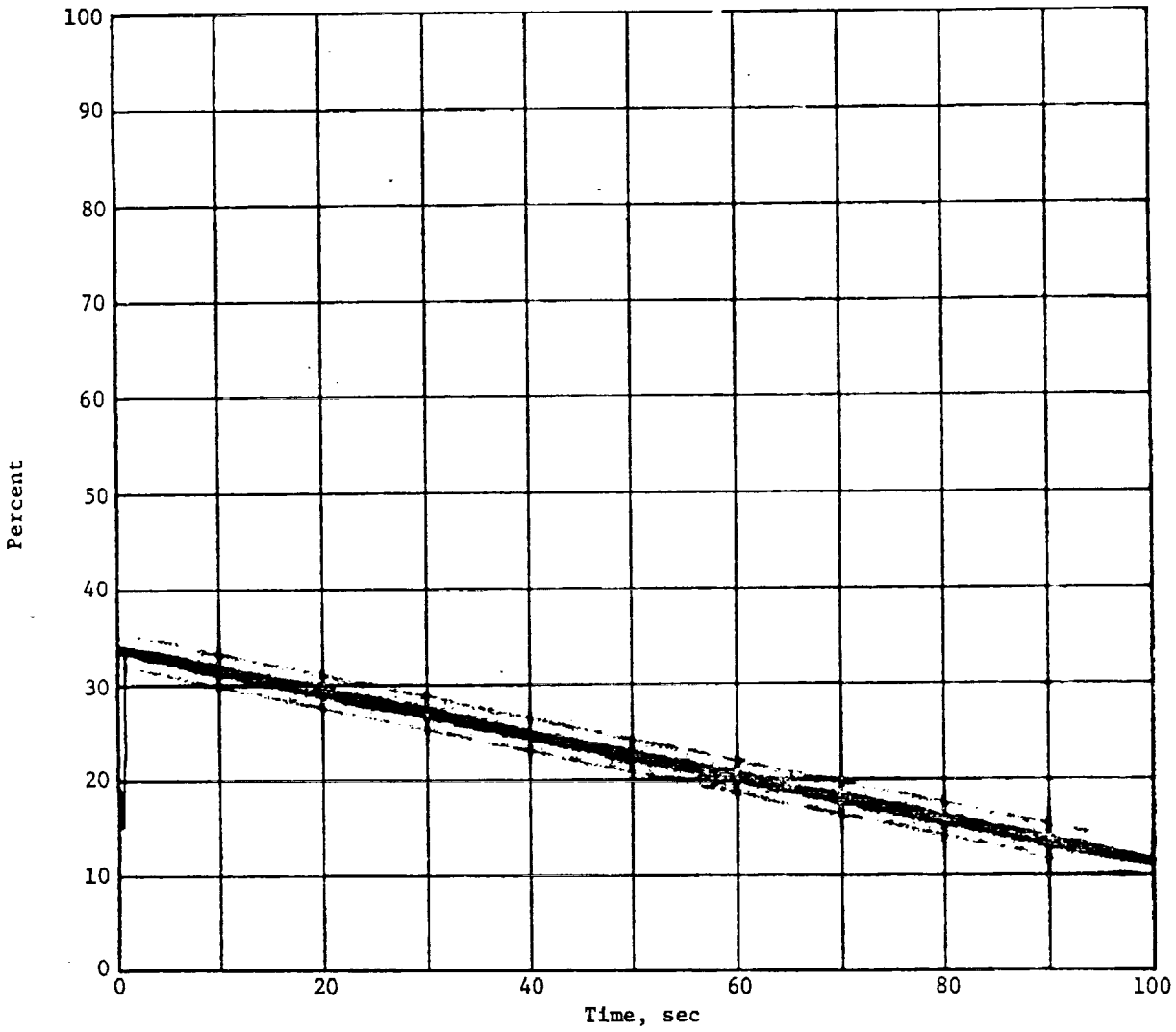

Plot Start GCSC Time 11,900
G4514 Term. Descent CMD2 . FMT3

Figure VI-4 (DECSET plots of terminal descent throttle positions, VL2)

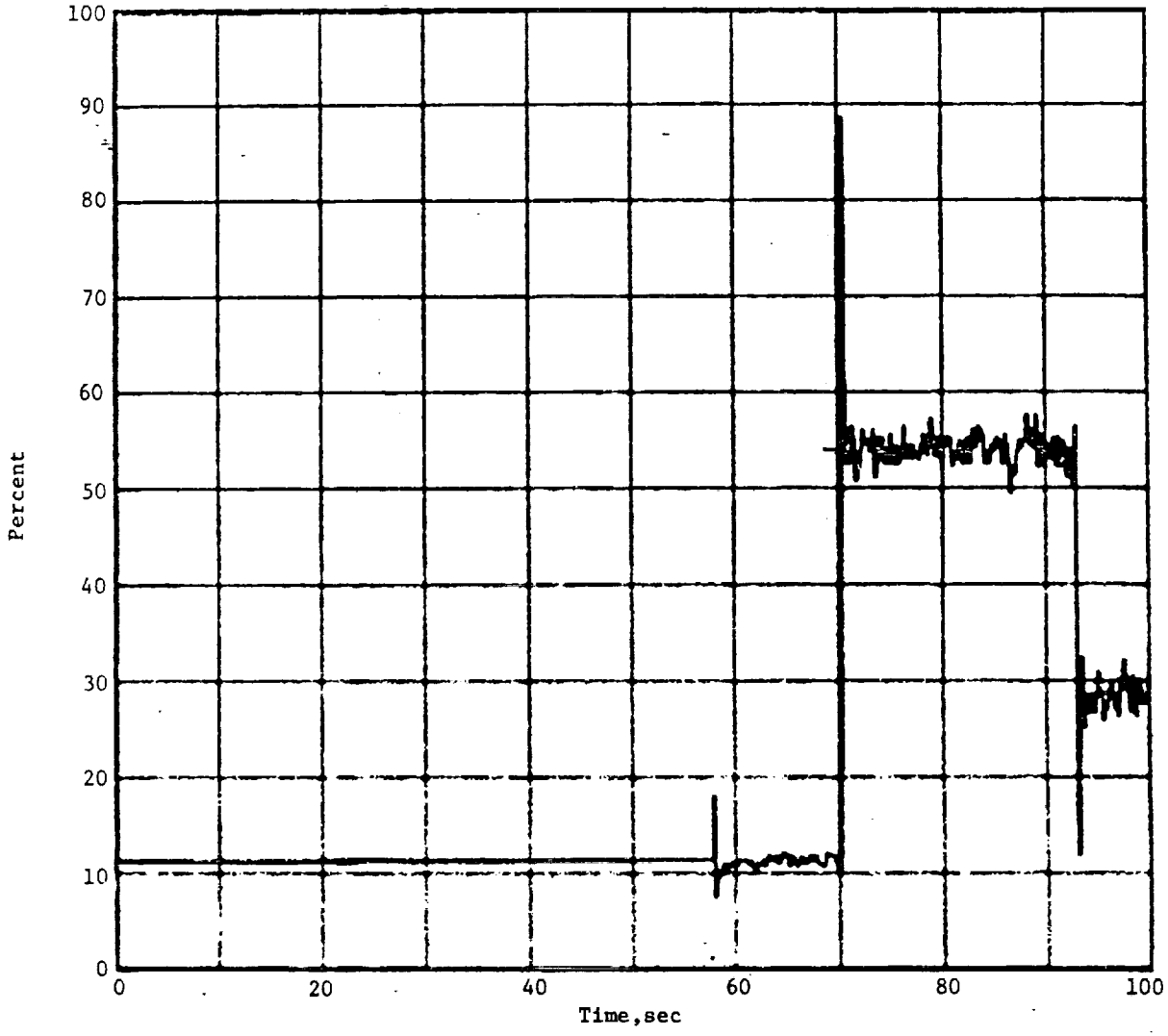

Plot Start GCSC Time 11,800
G4515 Term Descent CMD3 FMT3

Figure VI-5 (DECSET plots of terminal descent throttle positions, VL2)

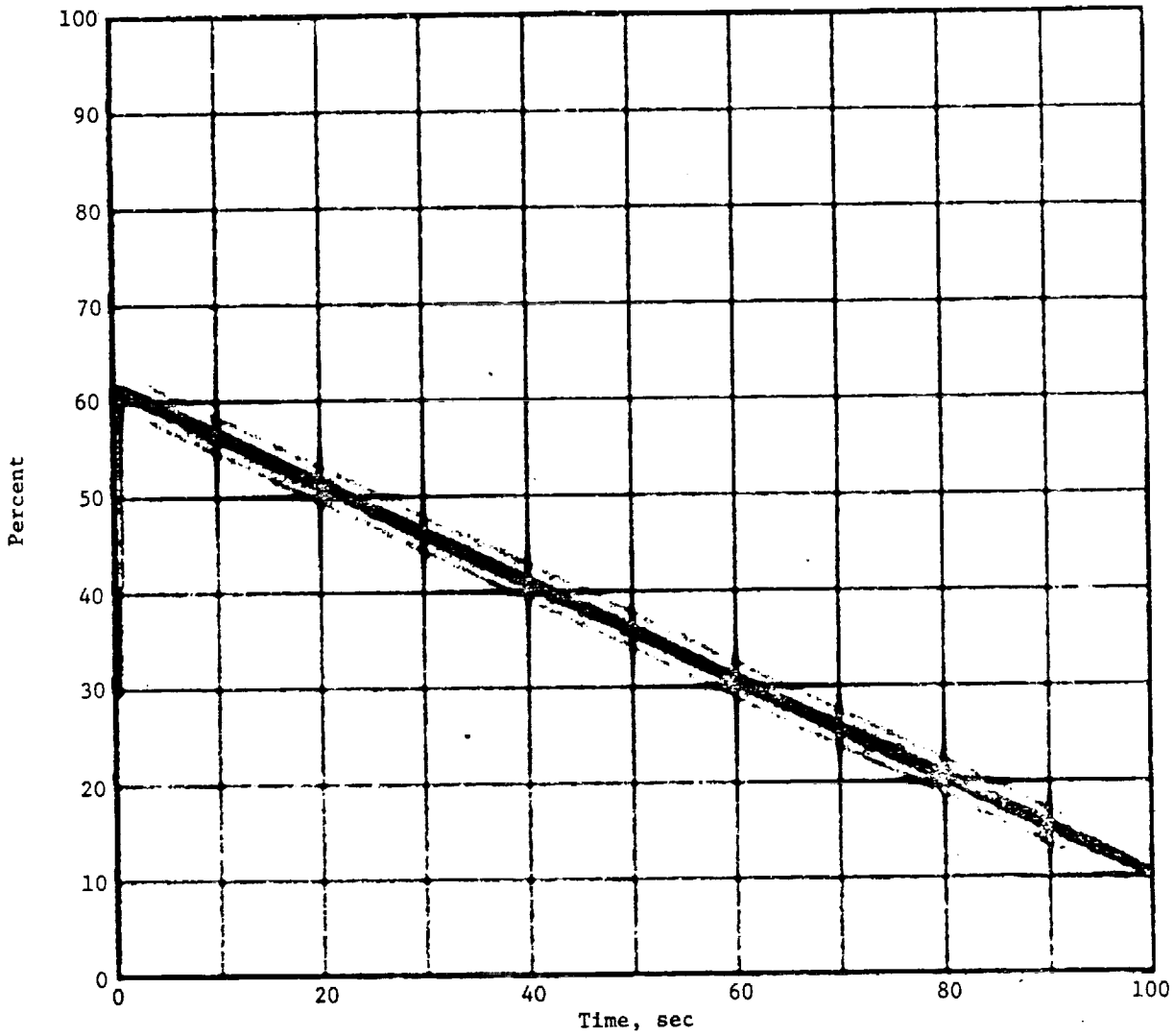

Plot Start GCSC Time 11,900
G4515 Term. Descent CMD3 FMT3

Figure VI-6 (DECSET plots of terminal descent throttle positions, VL2)

During the high-thrust phase of terminal descent, fairly high W body velocity errors are evident. Because we are velocity steering both W and V to null, these W errors must be explained. They are explained by the fact that the differential throttle command bias gains (GA1, GA2, GA3, which are designed to maintain moment balance without a W velocity error since we have an offset cg along the yaw axis) are optimized for the highest throttle setting of 84%. At any other throttle setting, they are not quite correct and require a differential throttle setting to be acquired by a velocity error, i.e., for VL2 at 11871.51 sec

$W = -13.59$ fps

$U = 183.52$ fps

which produces a pitch command of

$$\theta_c = G_q \frac{W}{U} = -1X \frac{-13.59}{183.52} = +0.074$$

The inner loop pitch gain at this time is approximately 0.35, so the delta throttle in pitch commanded by this error is

$$\Delta X_p = 0.074 \ (0.35) = 0.026$$

Working through the mixing gains, this should produce a delta of 1.3% for engines 1 and 3, and 2.6% for engine 2.

At this time, the average throttle commands were

XC1 = 54.6%

XC2 = 42.5%

XC3 = 54.0%

and we know the differential throttling produced by the bias gains was

$GA1 \times A_c = 1.055 \times 50.4 = 53.1$

$GA2 \times A_c = 0.890 \times 50.4 = 44.8$

$GA3 \times A_c = 1.055 \times 50.4 = 53.1$

Therefore, the difference between what the bias gains provided and what we really got should equal what the W Velocity error provided.

For

Engine 1: 54.6 - 53.1 = 1.5%

Engine 3: 54.0 - 53.1 = 0.9%

Average 1 & 3 = 1.2%
(Compare to 1.3%)

Engine 2: 44.8 - 42.5 = 2.3%
(Compare to 2.6%)

which explains why the W velocity errors were as they were. The difference between engine 1 and 3 commands is due either to a small yaw cg offset or, more likely, engine 3 was slightly stronger.

B. TIP-UP PERFORMANCE AND PEAK ATTITUDE RATES

After the terminal descent control system channels are closed, the vehicle begins a tip-up maneuver that aligns the vehicle thrust vector with the total relative velocity vector to begin the gravity turn descent. For the slowest vertical velocity and maximum wind condition, the predicted tip-up angle is on the order of 60°. Three seconds are provided in the contour design to allow for this maneuver. The maneuver rates are constrained to be less than 30 deg/sec by control system limits. The actual performance of the two landers for this important maneuver is:

	Max. Attitude Rates, deg/sec		Time to Complete, sec	Tip-Up Angle, deg	
	Pitch	Yaw		Pitch	Yaw
VL1	11.2	13.4	1.0	6.3	12.5
VL2	≈0	7.9	0.3	0	-5.3

There was negligible overshoot after the maneuver, and the attitude rates remained low after this maneuver was completed.

C. LANDING CONDITIONS

The landing conditions are the crucial elements of lander performance, for which all other elements of lander performance are predecessors. Table VI-2 lists these cruicial elements along with their desired values.

Table VI-2 Landed Conditions

	Velocity, fps			Attitude Rates, deg/sec			Attitude, deg	
	U	V	W	Roll	Pitch	Yaw	Pitch	Yaw
VL1	8.18	-0.04	-0.51	0.48	-0.92	-0.41	0.59	0.34
VL2	8.10	-0.09	-0.64	-0.12	-1.23	1.94	-1.16	-2.18
Desired	8 ± 3	0 ± 4	0 ± 4	0 ± 5	0 ± 7	0 ± 7	0 ± 5	0 ± 5

As can be seen, all landing conditions were easily met. Even with the engine differential throttling caused by the TDLR sensing the dust velocity just before touchdown, as explained in Sections VI.A and VII.B, all attitude rate and verticality requirements were still well within tolerance.

VII. RADAR PERFORMANCE

A. RADAR ALTIMETER PERFORMANCE

1. Overview

All evidence of RAE performance on both landers indicates nominal operation. Parameters measured during preseparation checkouts and observed during the descents were virtually unchanged from those measured during prelaunch testing. Thus, no degradation was found from launch, cruise, or entry environments.

The navigator altitude converged to the RAE data as expected. After initial navigator updates in Mode 1 (9I), the navigator remained converged with a hang-off error from inertial velocity errors. After the TDLR fixed the velocity errors, the navigator quickly converged and was within 1 ft of the RAE at the end of updates (135 ft).

One phenomenon, common to both landers, was that the constant velocity descent phase was approximately 1 sec longer than expected. This meant the vehicle was in this phase 7 to 8 ft longer than anticipated, which converts into about 2.4 lb of terminal descent fuel. Because we had about 30 lb of fuel left over in both missions, this was of no consequence. The cause of the error is discussed in Section VII A3.

Another interesting item was the absence of plasma blackout for both vehicles. This probably resulted from: (1) low sodium impurity content of the aeroshells; (2) the atmosphere resembling the nominal model rather than the extremes; (3) the conservatism (justifiable) in the blackout models.

2. Performance - Entry Phase (Mode 1)

RAE 2 is initially turned on at event 8I (approx 800,000 ft). If lock does not occur within 30 sec, the other RAE is turned on (1-sec warmup), then allowed to search for 30 sec. This sequential operation continues until one RAE maintains lock. RAE data is not used to update the navigator until approximately 258,600 ft (9I). The prime mission objective of the RAE in this mode is to converge the navigator altitude errors at parachute mortar fire to within ±550 ft.

For both landers, RAE 2 locked the first sweep after turn-on at 8I. The lock was ambiguous. An ambiguous target is one that returns to the radar after the next outgoing pulse is transmitted. Thus, the RAE believes the return is from the second transmitted pulse rather than the true one. The ambiguous range is about 700,000 ft. The indicated range is the true range minus about 700,000 ft. Knowing the specific ambiguous range (a function of pulse repetition frequency) for each serial number altimeter, the true altitude in this region may be accurately estimated. This information is a bonus for the entry scientists and trajectory reconstruction analysts. As the indicated ambiguous range approaches the minimum range gate of the RAE (10,000 ft, really 710,000 ft) the variable bandwidth and threshold control of the RAE attenuate the returned signal and unlock occurs. Relock then cannot occur until the return, now unambiguous, falls within the upper range gate of the RAE at 450,000 ft. For both missions, enough time passed between the ambiguous unlock and unambiguous relock for two RAE switches to occur (greater than 62 sec). Thus, RAE 2 was on when the target came within the gate and lock occurred on the first sweep. For both vehicles, RAE 2 was used until touchdown.

At 9I, the RAE data updated the navigator. Because the navigator altitude is output only once every 4 sec in format 2, this is the granularity that convergence could be observed. Both navigators converged within 4 sec, which is nominal with a 1-sec time constant.

Figure VII-1 shows the estimated true altitude above the terrain in Mode 1 for both VL1 and VL2. The difference between the profiles for the two missions was negligible. This figure was constructed by adjusting the raw RAE data for known scale factors and electronic biases and estimated terrain bias errors.

No RF plasma blackout occurred on either mission. No degradation, in the form of higher fluctuation or bias errors, was noted during the possible blackout region. Thus, it appears that even a partial plasma was not encountered. The lack of blackout is explained by three reasons:

1) The largest contributor to free electrons that form the plasma is the aeroshell ablator. This impurity level probably turned out to be low.

2) The atmospheres during both entries were very close to the mean model. Thus, the extreme atmospheric models, which produced the combination of high air relative velocity and high dynamic pressure, were not encountered.

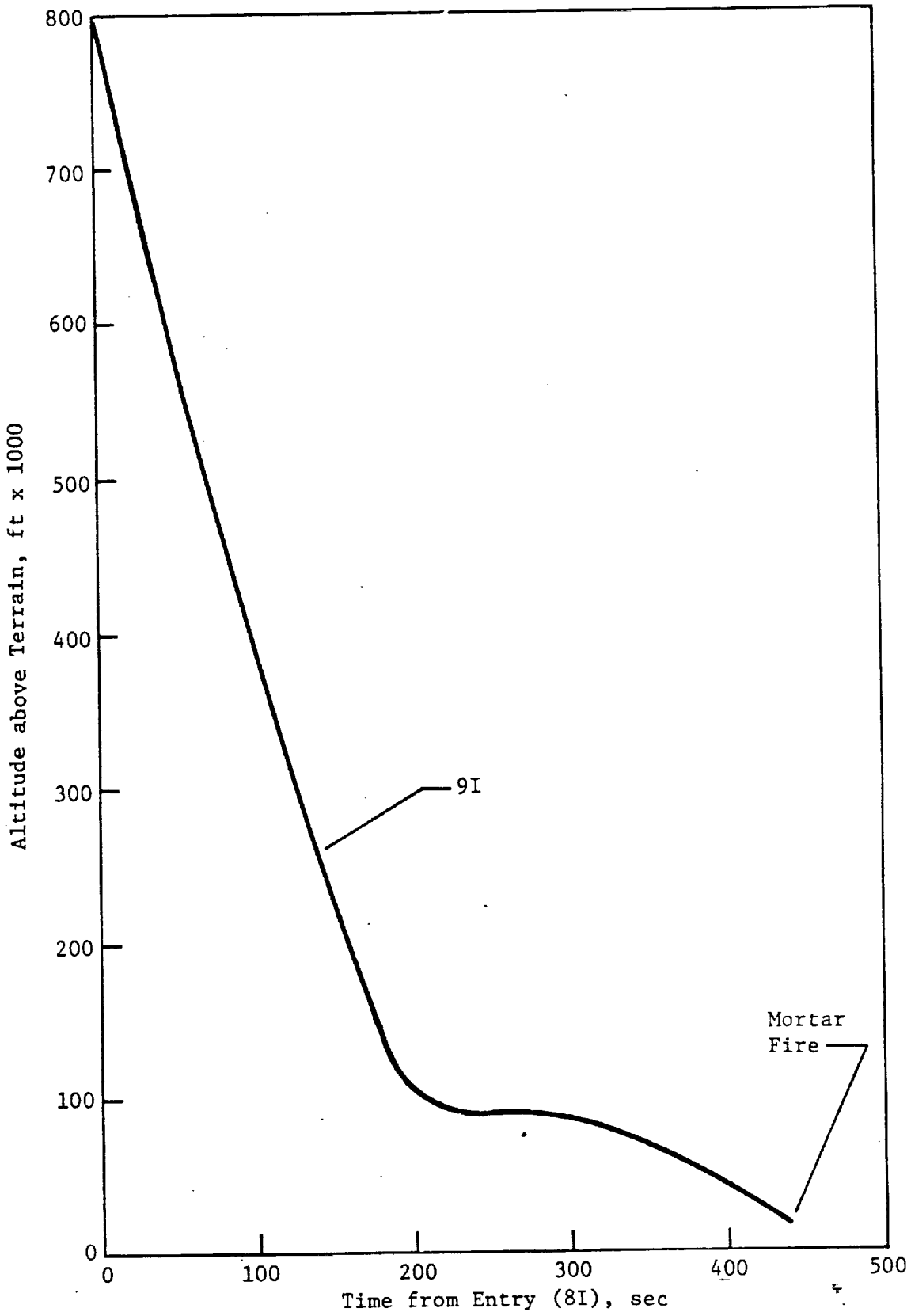

Figure VII-1

Estimated True Altitude (above Terrain) vs Time from Entry (8I) for VL 1 and VL 2, RAE Mode 1

3) The modeling of the gas physics in the blackout models was conservative. This was prudent analytically as the worst blackout duration had to be known to ensure enough RAE data before mortar fire. As it turned out, we had good RAE data from 9I to mortar fire.

Table VII-1 lists the lock regions, convergence data, and analog values for VL1 and VL2 in Mode 1.

Figure VII-2 shows the comparison between the LTARP altitude above the landing site radius and RAE data for VL1. This chart can be thought of as a terrain map, referenced to a spherical planet, as a function of downrange distance. No such comparison is possible for VL2 as the LTARP results have not yet been received.

Table VII-1 RAE Performance (Mode 1), VL1 and VL2

Parameter	VL1	VL2
Ambiguous Lock Altitude	779,439 ft	792,265 ft
Ambiguous Unlock Altitude	704,903 ft	728,025 ft
Unambiguous Lock Altitude	432,160 ft	432,704 ft
Plasma Blackout Region	None	None
Error (NAV-RAE) at 9I	+11,048 ft	-334 ft
Convergence Time	<4 sec	<4 sec
Transmitter Power (min/max)	63.5/64.1 W	58.1/59.0 W
CFAR	N/A FMT 2/2A	N/A FMT 2/2A
RAE 1 Temp	48.63°F	54.90°F
Hang-Off at Mortar Fire from Velocity Errors (NAV-RAE)	-101 ft	-56 ft

Figures VII-3 through VII-6 are DECSET plots of the format 2 navigator altitude data for VL1. Figures VII-7 through VII-10 are the same data for VL2.

Figures VII-11 and VII-12 are the DECSET plots of the RAE data for format 2A from 8I to 9I for VL1. Both the ambiguous and unambiguous lock regions are shown. Note that no navigator updating occurs in this region. Figures VII-13 and VII-14 show the same data for VL2.

Figures VII-15 through VII-18 are the DECSET RAE data for format 2 from 9I to mortar fire for VL1. Note that no unlock from blackout occurs, and that the RAE is updating the navigator in this region. Figures VII-19 through VII-22 are the same data for VL2.

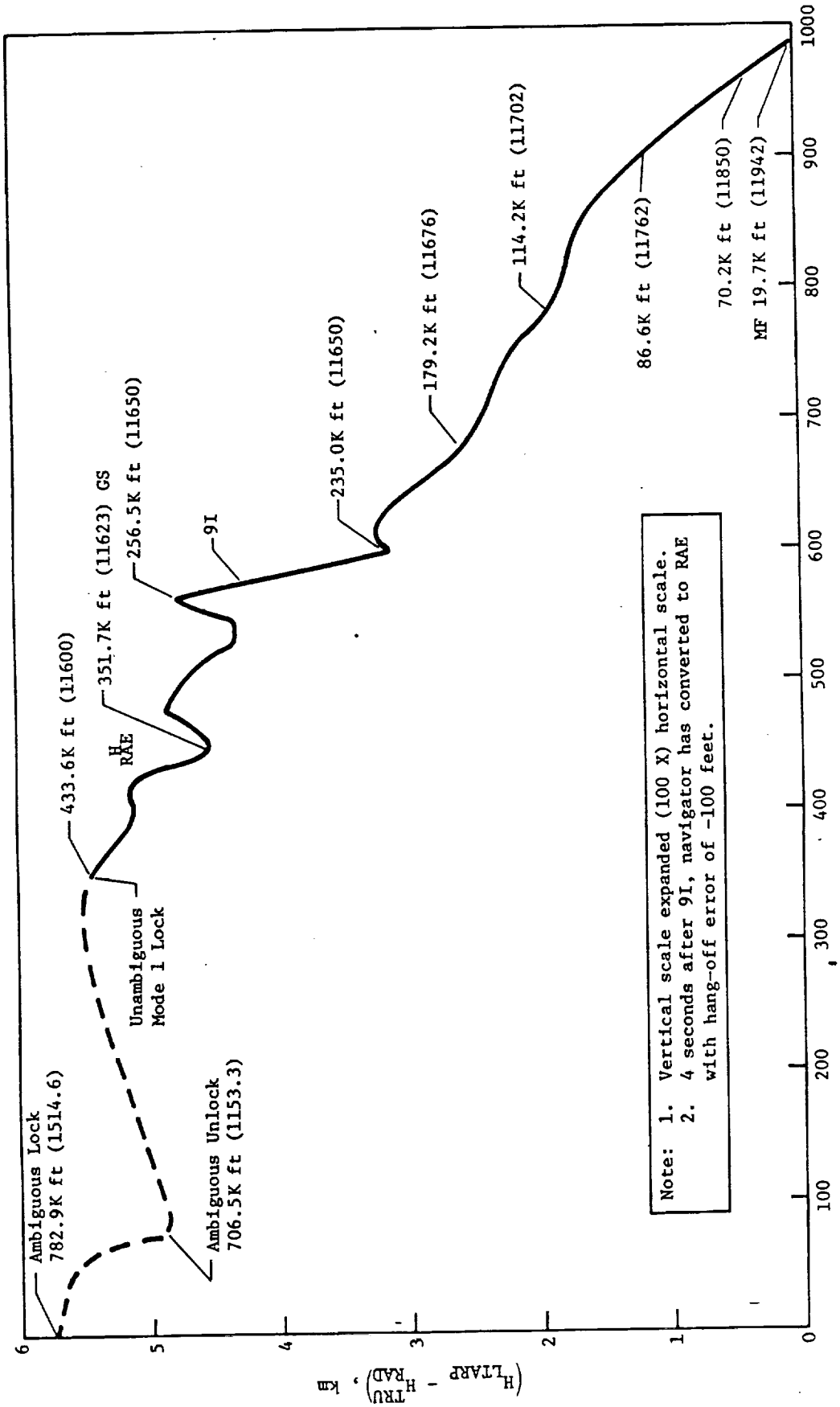

Figure VII-2

Figure VII-2 LTARP Analysis, $H_{LTARP} - H_{TRUE}$ (RAE)

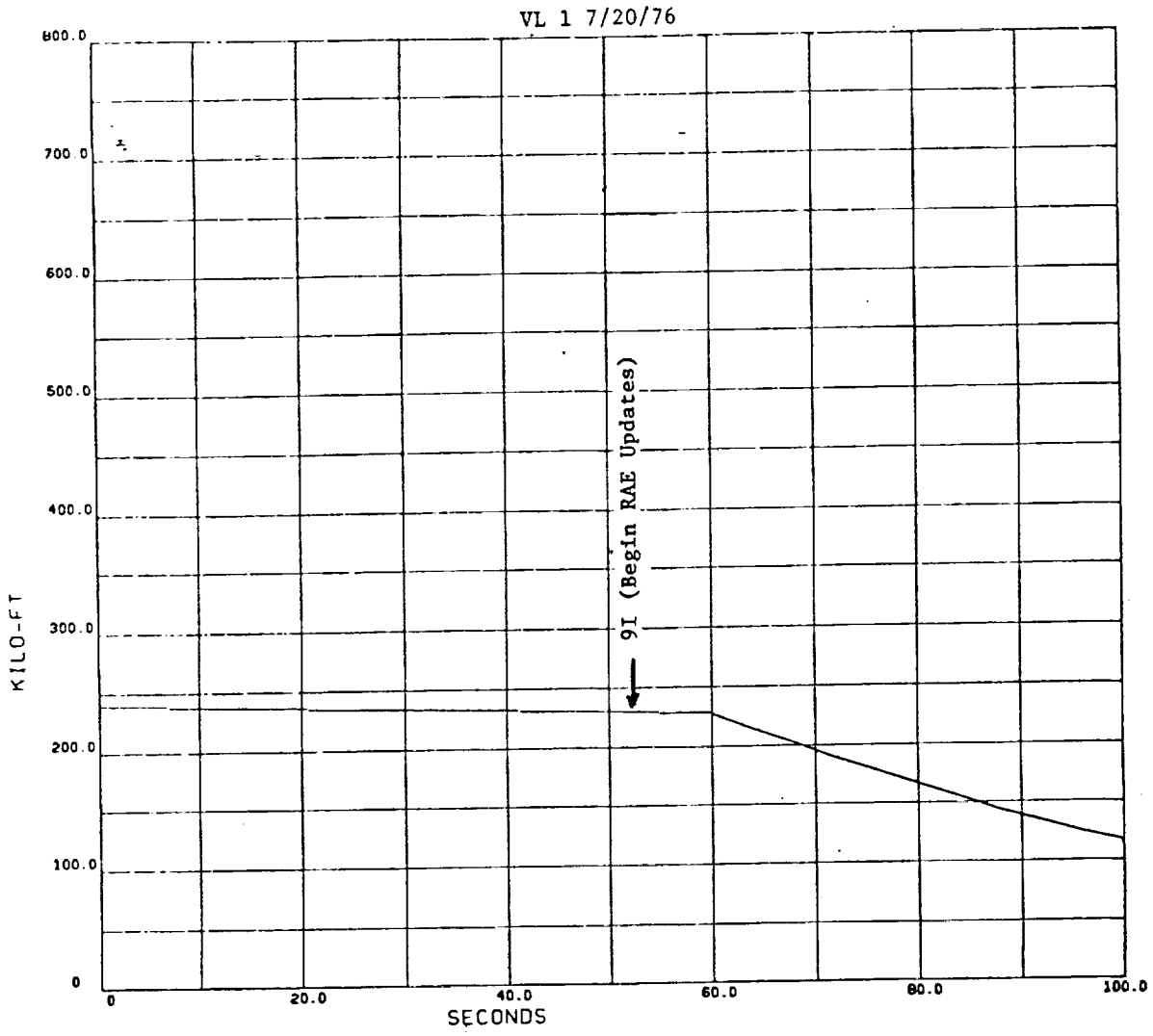
VL 1 7/20/76
800.0
700.0
600.0
500.0
400.0
300.0
200.0
100.0
0
KILO-FT
0
20.0
40.0
60.0
80.0
100.0
SECONDS
91 (Begin RAE Updates)
PLOT START GCSC TIME 11600
G 4716 NAVIGATOR ALT HI
FMT2

Figure VII-3

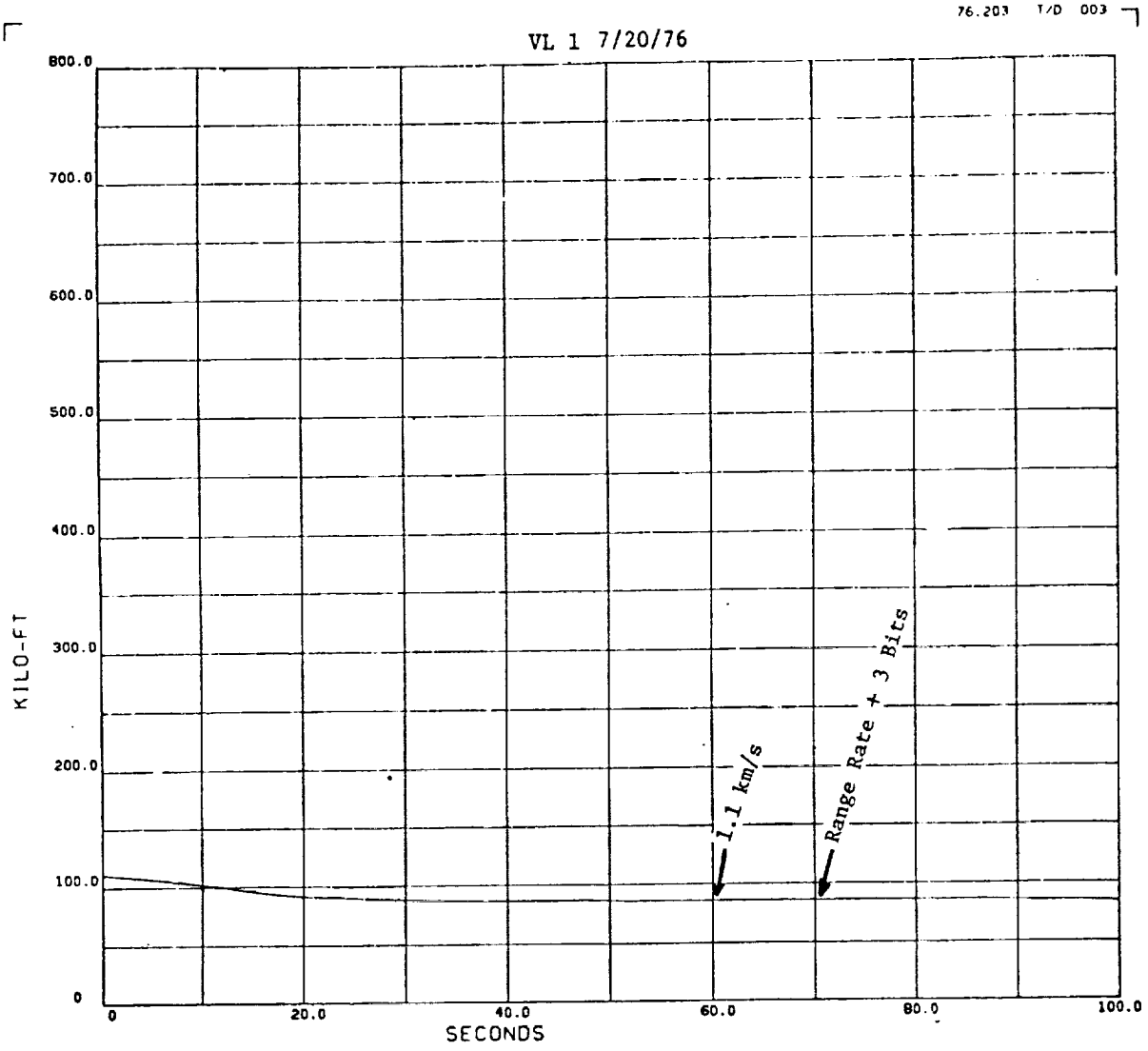

PLOT START GCSC TIME 11700
G 4716 NAVIGATOR ALT HI FMT2

Figure VII-4

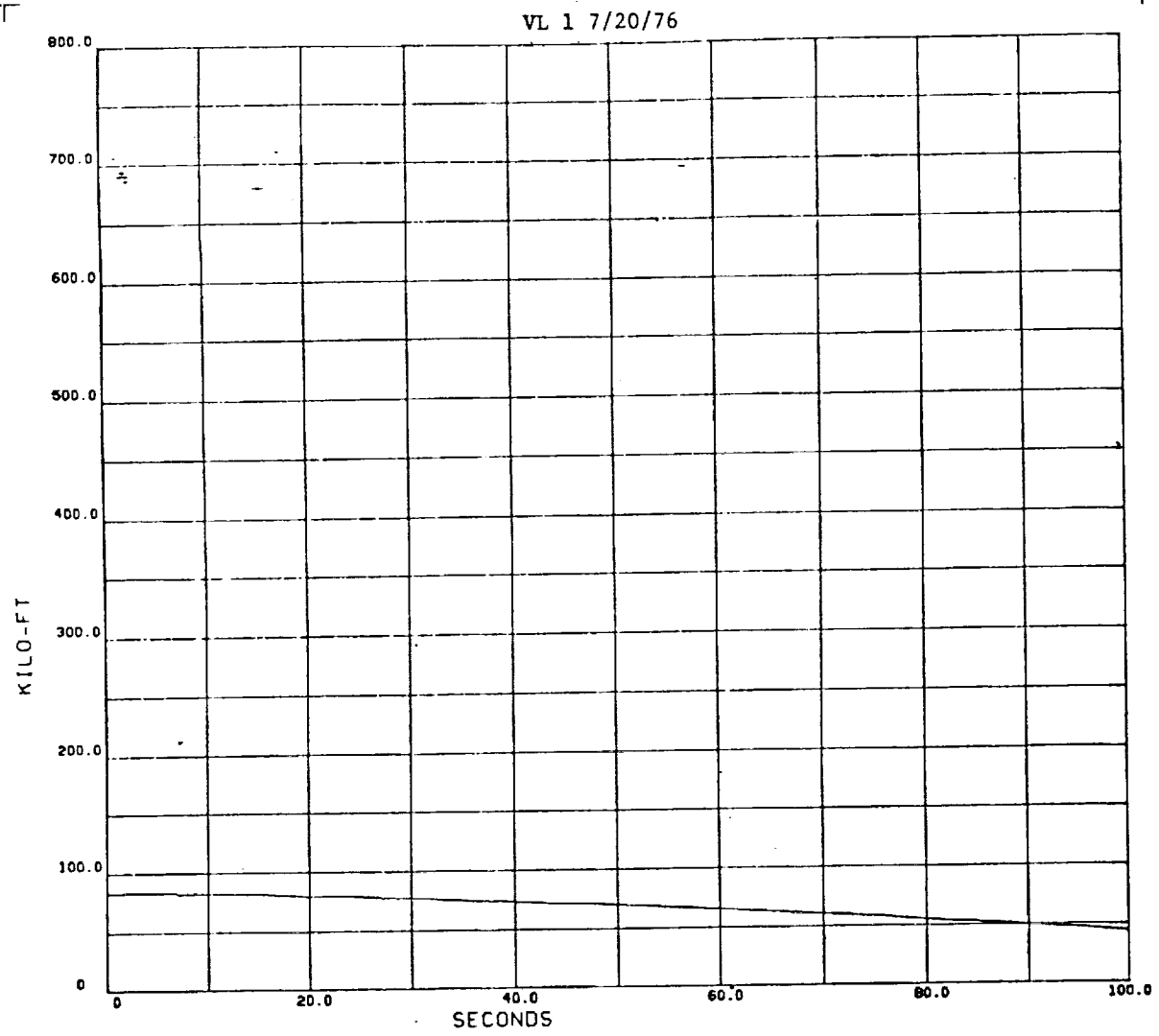

PLOT START GCSC TIME 11800
G 4716 NAVIGATOR ALT HI FMT2

Figure VII-5

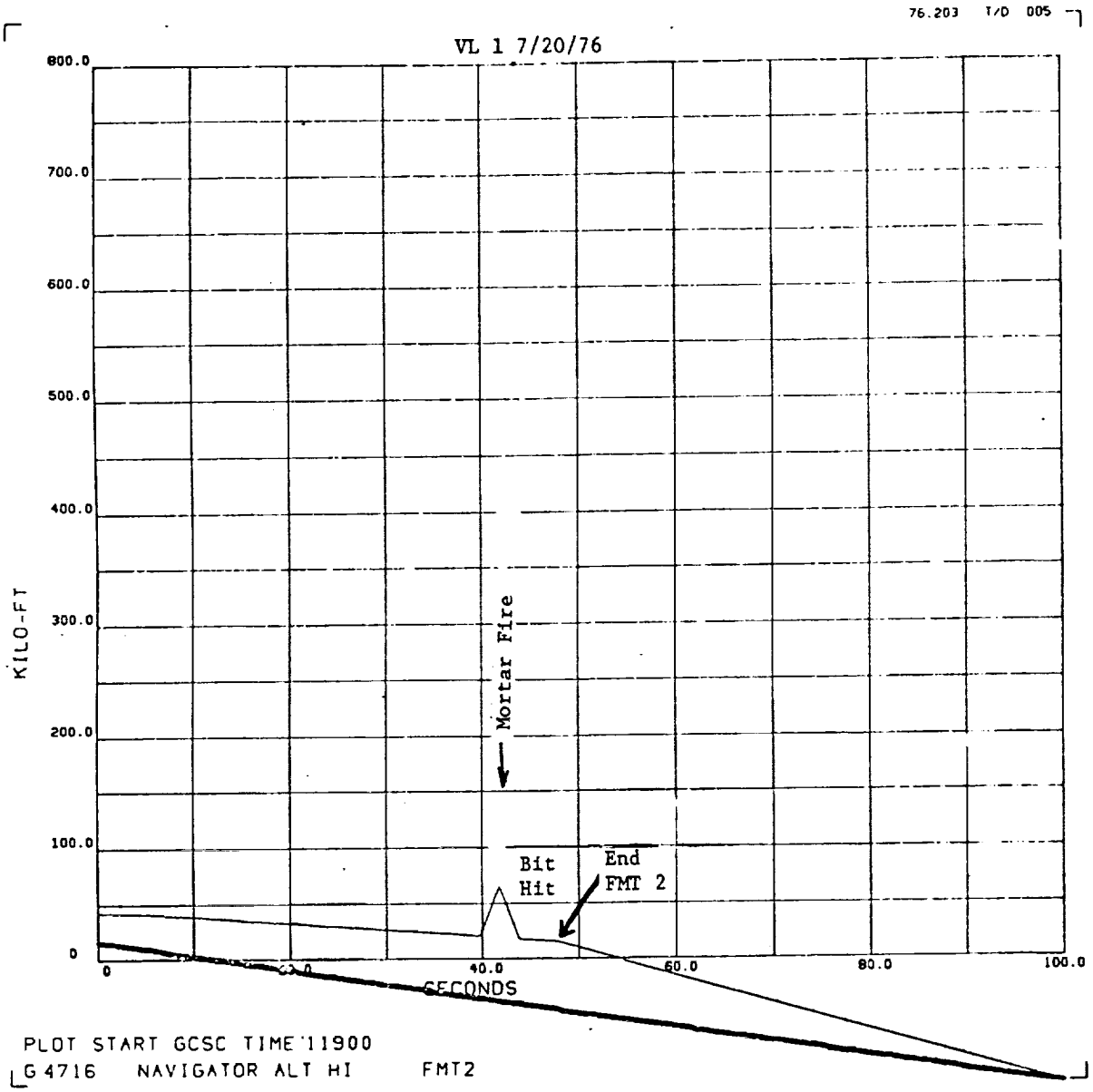
76.203 T/D 005
VL 1 7/20/76
800.0
700.0
600.0
500.0
400.0
300.0
200.0
100.0
0
KILO-FT
Mortar Fire
Bit Hit
End FMT 2
0
40.0
60.0
80.0
100.0
SECONDS
PLOT START GCSC TIME 11900
G 4716 NAVIGATOR ALT HI FMT2

Figure VII-6

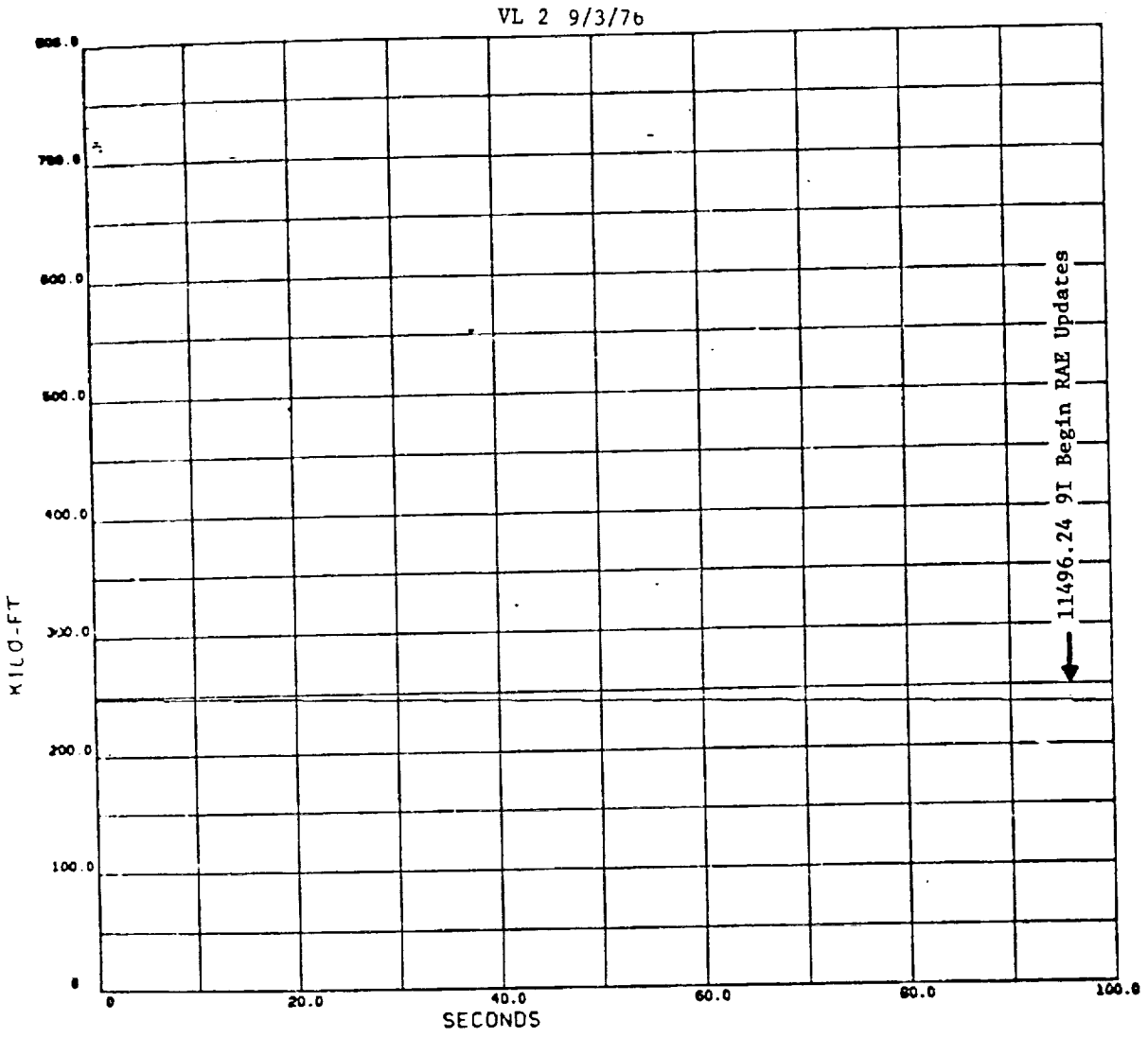
VL 2 9/3/76
KILO-FT
800.0
700.0
600.0
500.0
400.0
300.0
200.0
100.0
0
0
20.0
40.0
60.0
80.0
100.0
SECONDS
11496.24 9I Begin RAE Updates
PLOT START GCSC TIME 11400
S4716 NAVIGATOR ALT HI FMT2

Figure VII-7

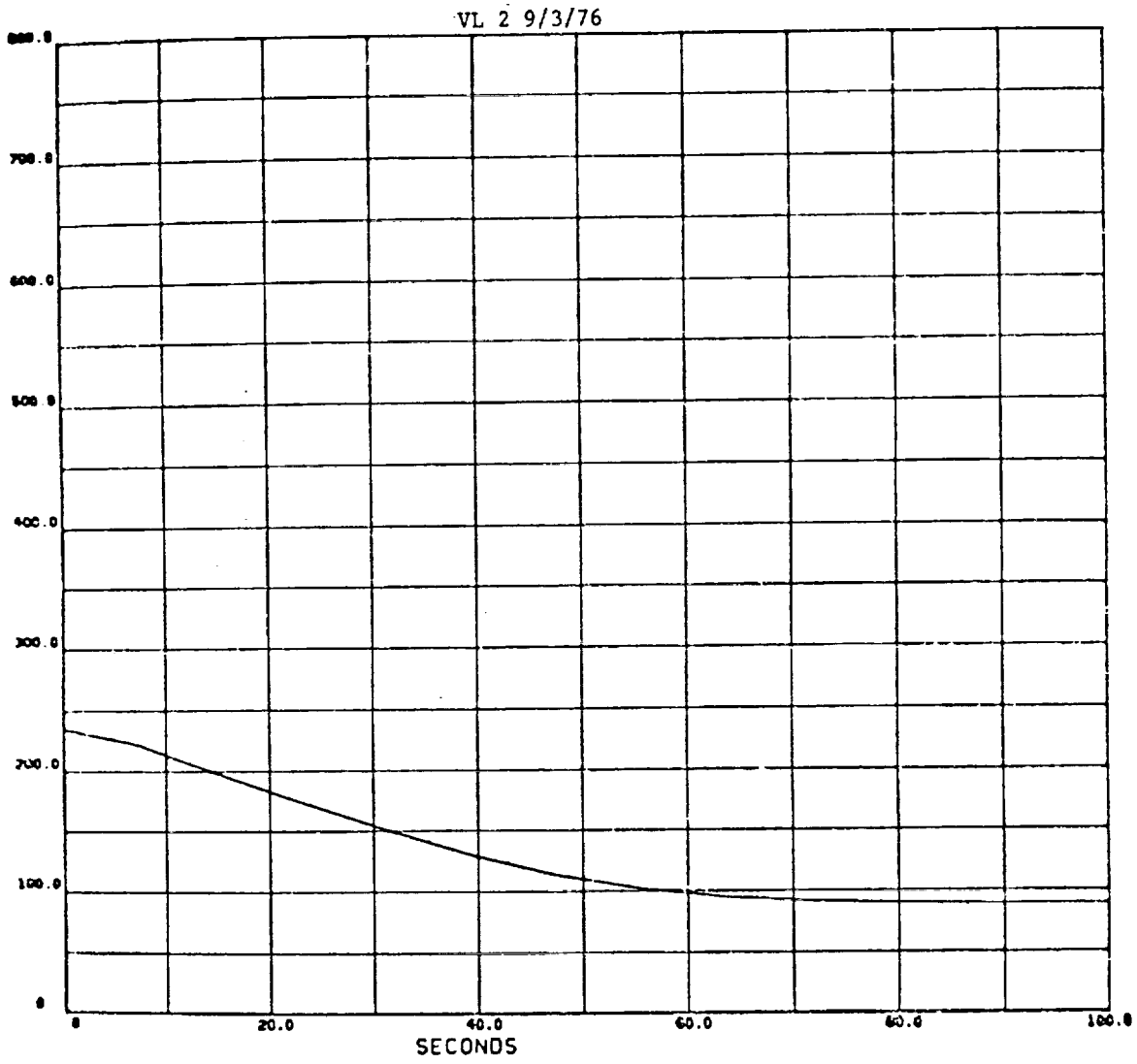

:01 START GCSC TIME 11500
4716 NAVIGATOR ALT HI FMT2

Figure VII-8

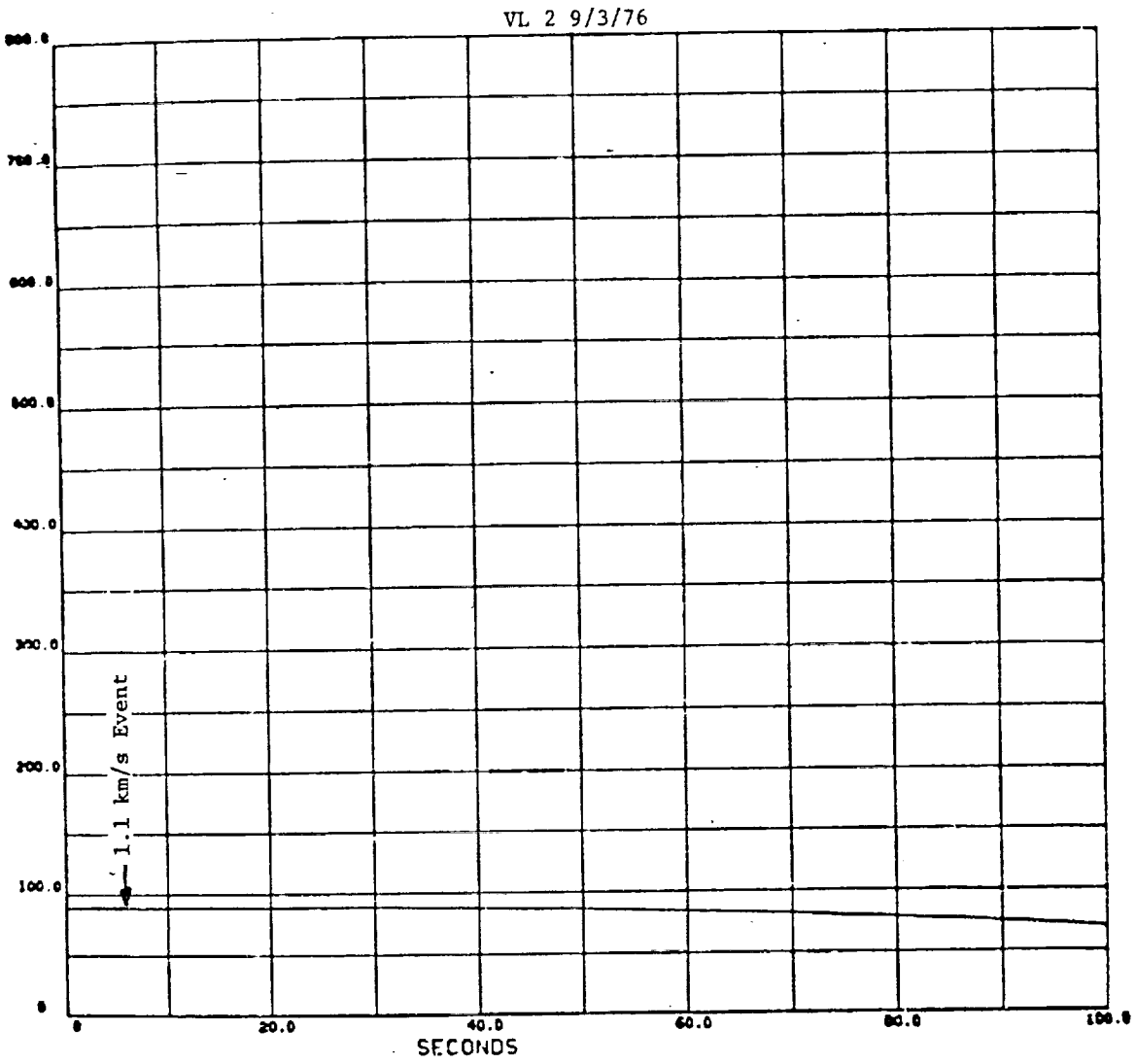
VL 2 9/3/76
800.0
700.0
600.0
500.0
400.0
300.0
200.0
100.0
0
1.1 km/s Event
0
20.0
40.0
60.0
80.0
100.0
SECONDS
PLOT START GCSC TIME 11600
54716 NAVIGATOR ALT HI FMT2

Figure VII-9

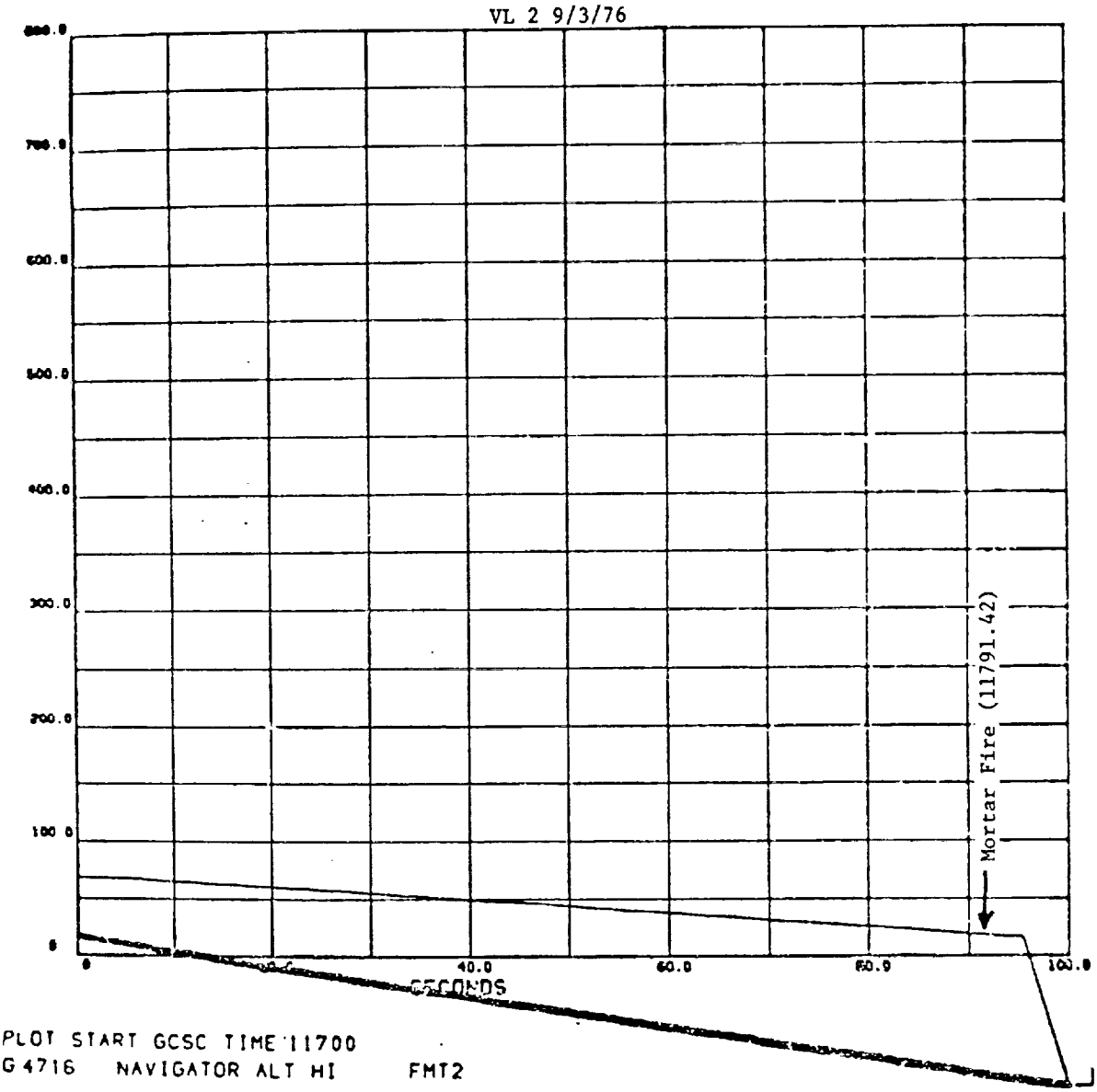

PLOT START GCSC TIME 11700
G4716 NAVIGATOR ALT HI FMT2

Figure VII-10

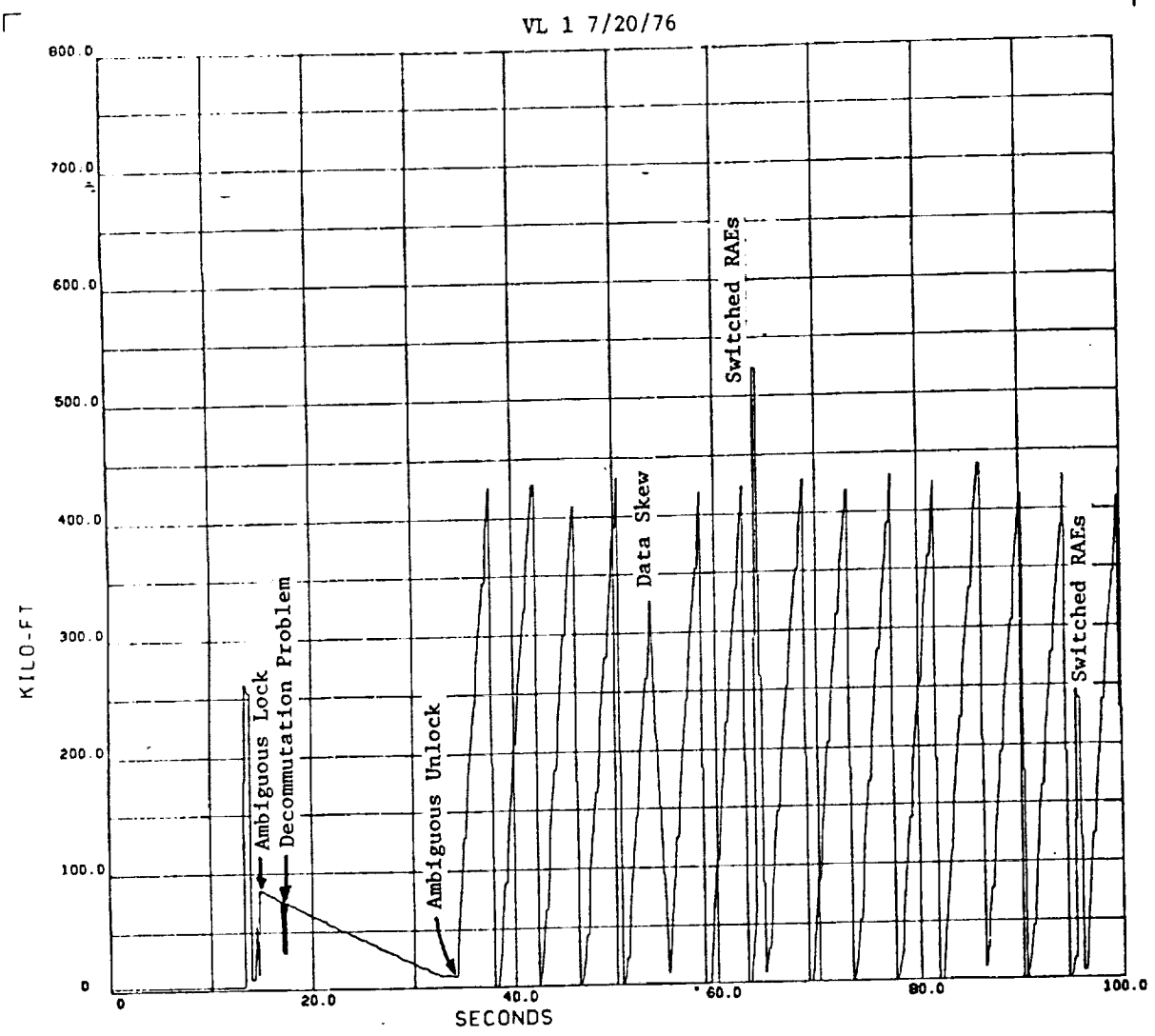

Figure VII-11

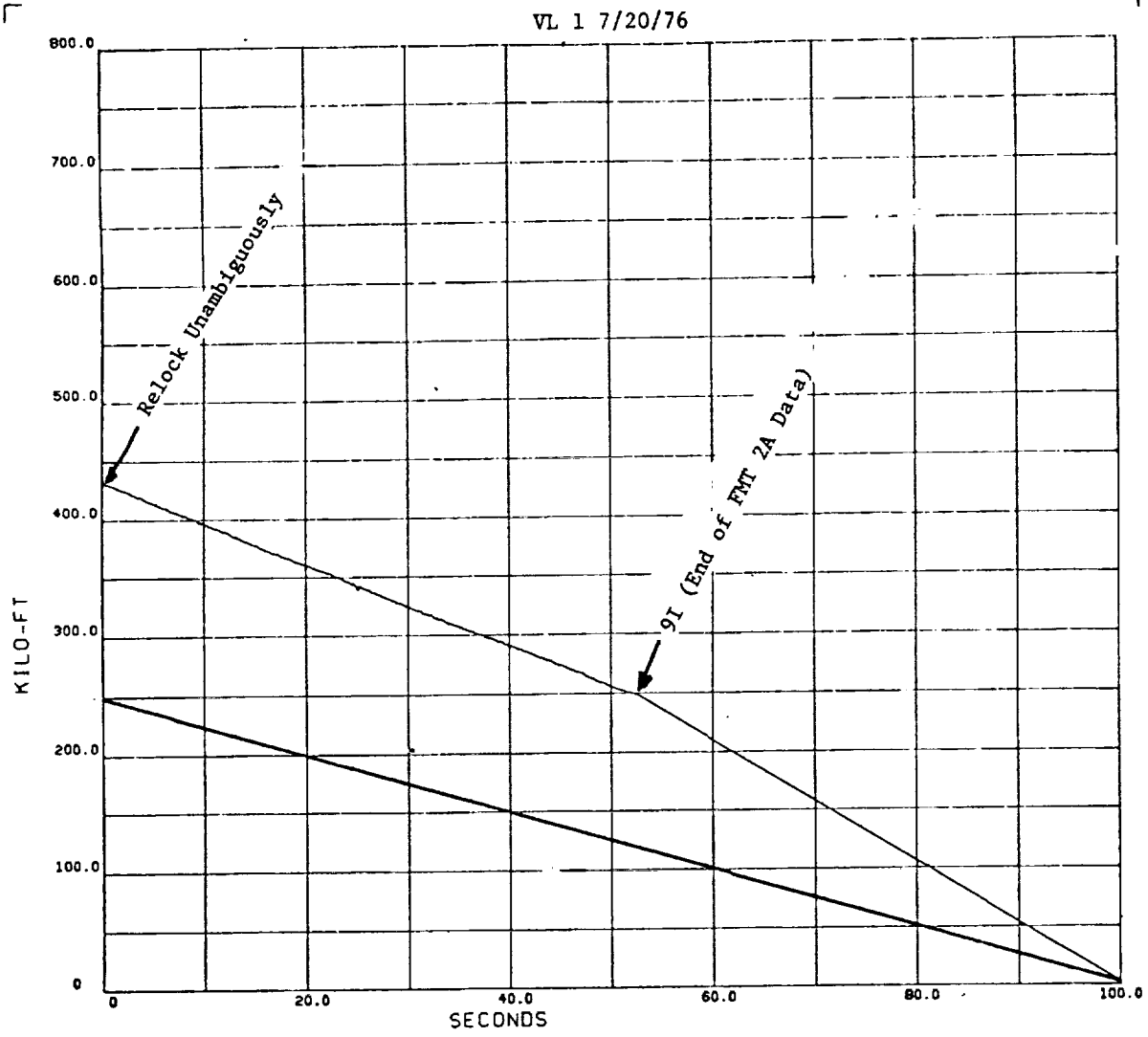

Figure VII-12

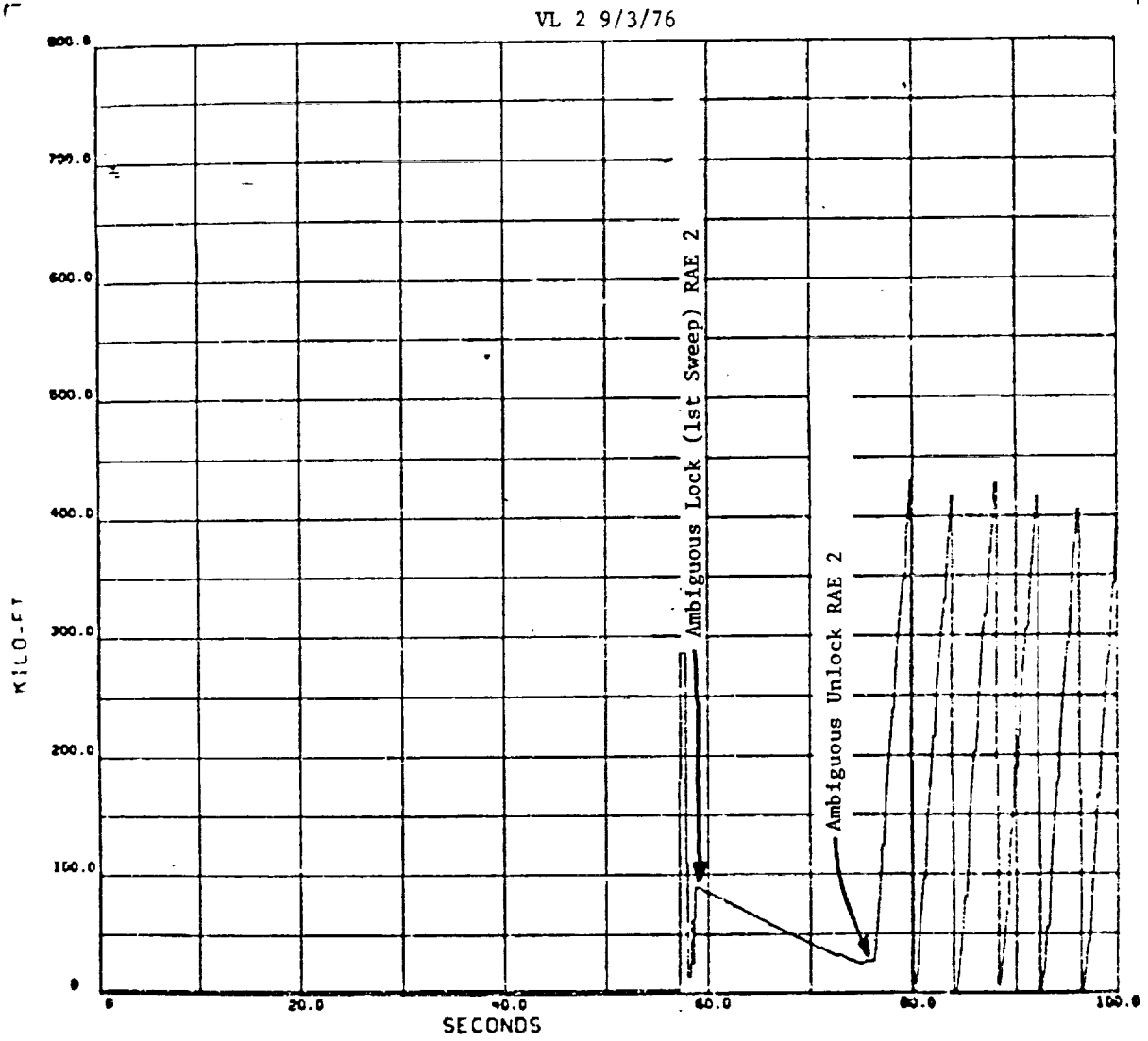

PLOT START GCSC TIME 11300
G4501 RADAR ALTITUDE HI FMT2A

Figure VII-13

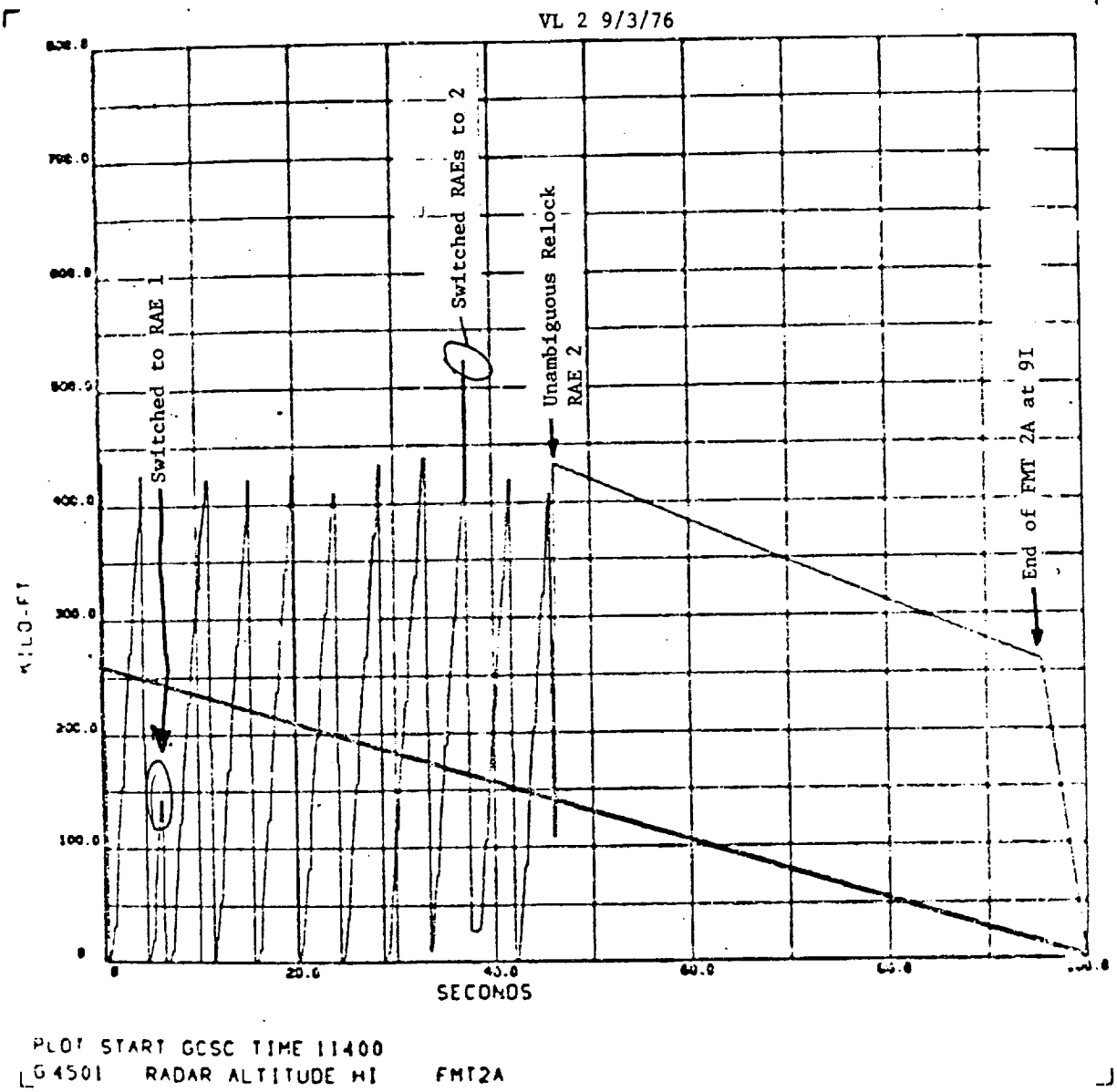

Figure VII-14

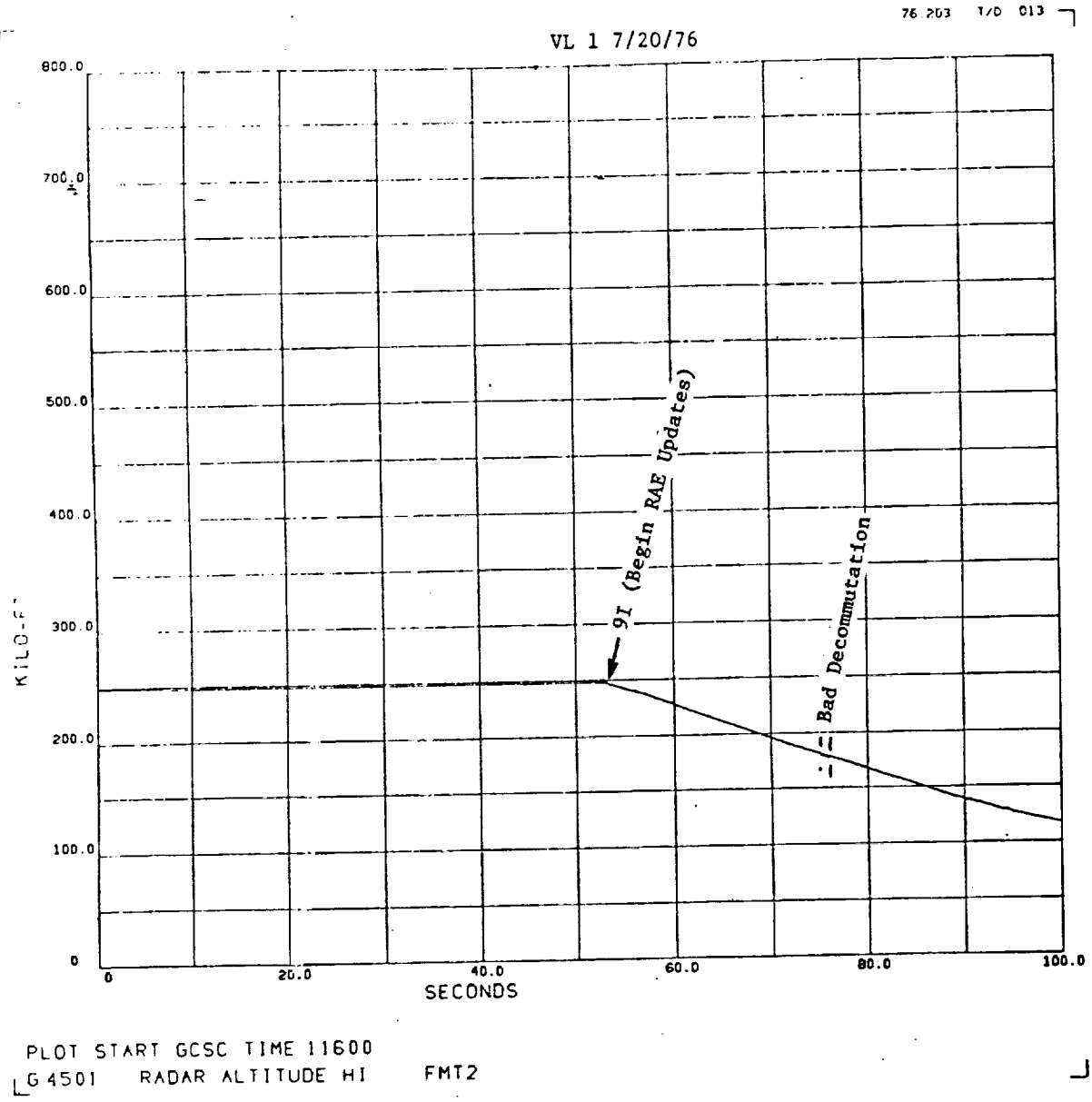

Figure VII-15

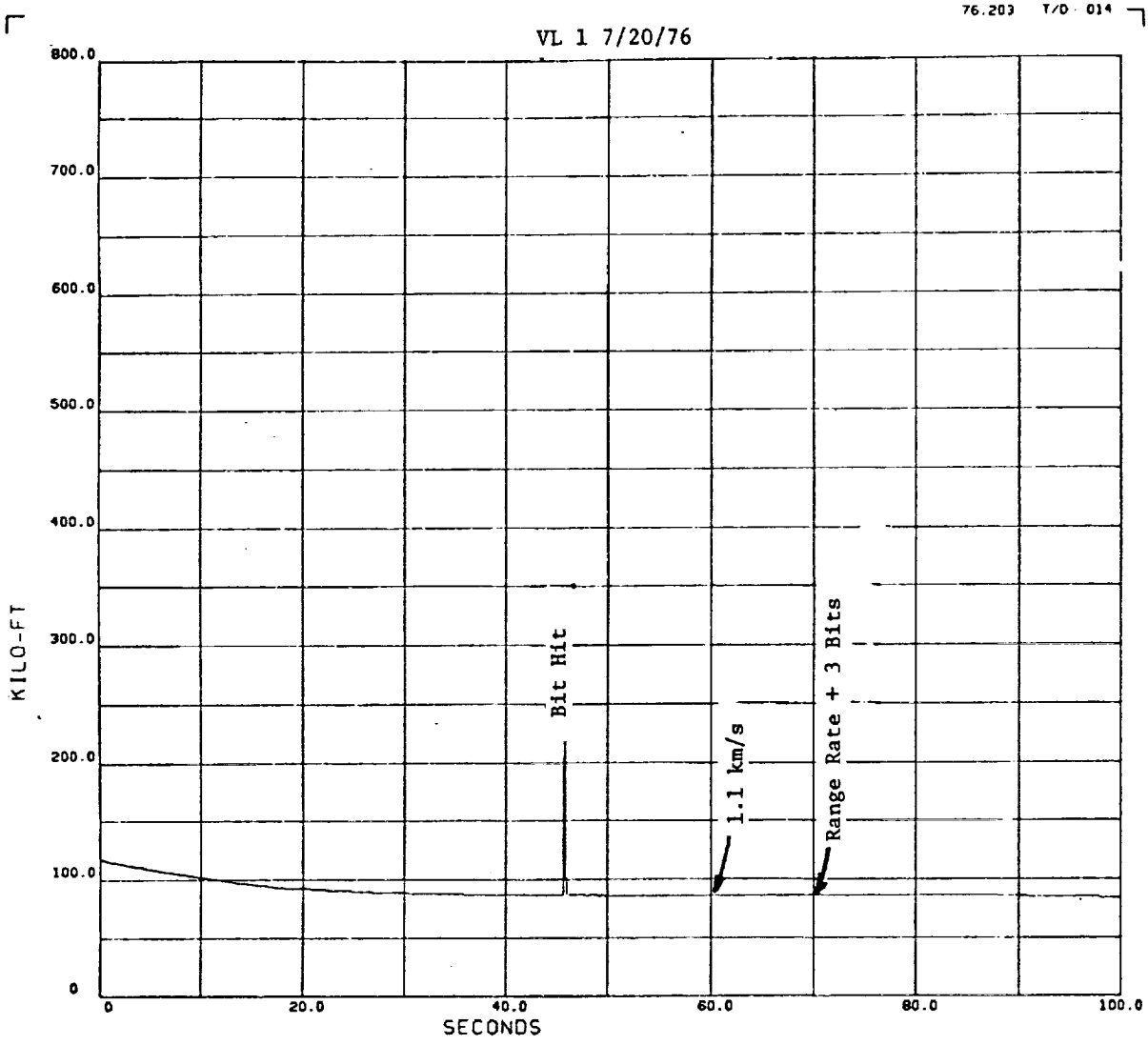

Figure VII-16

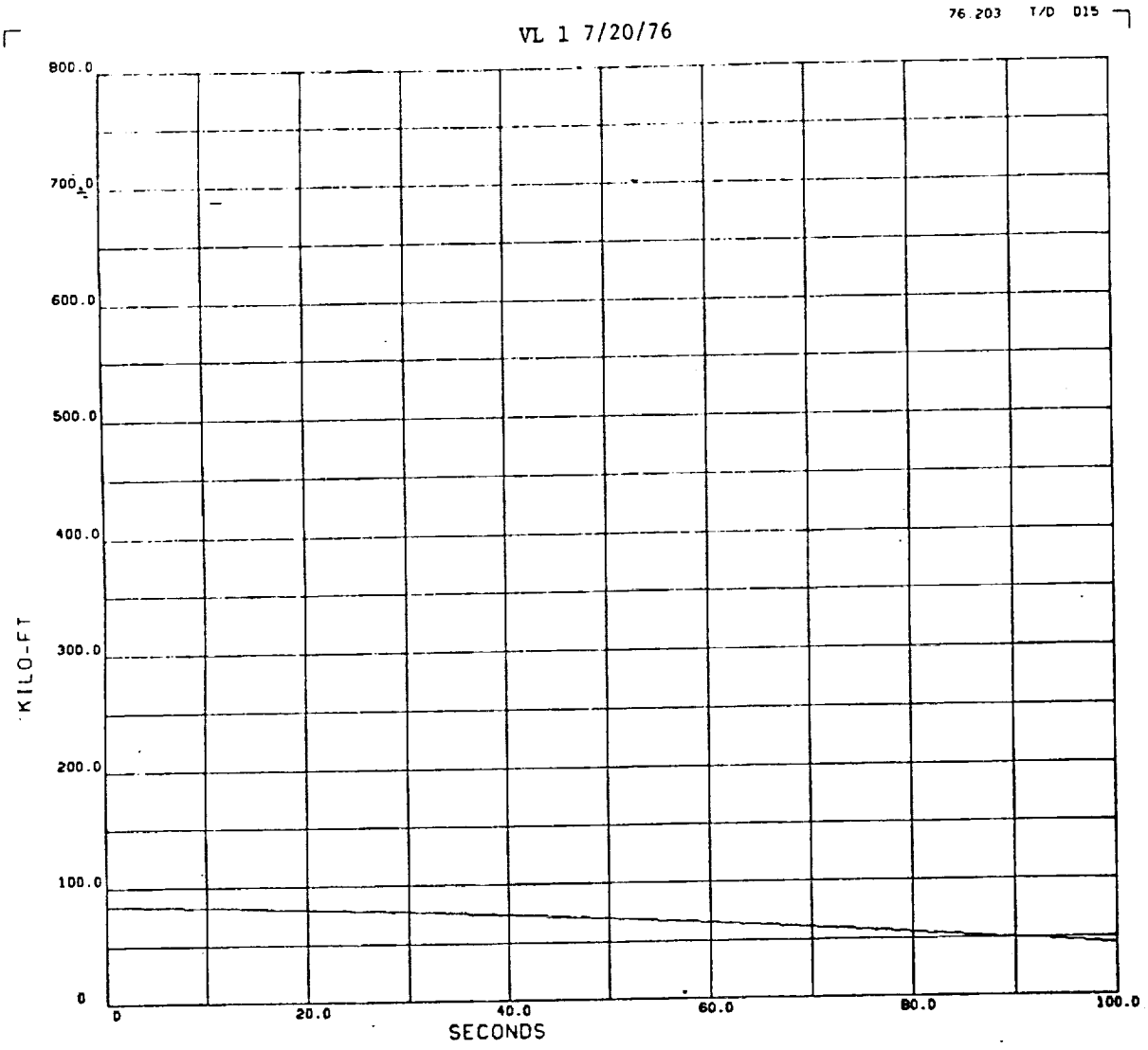

Figure VII-17

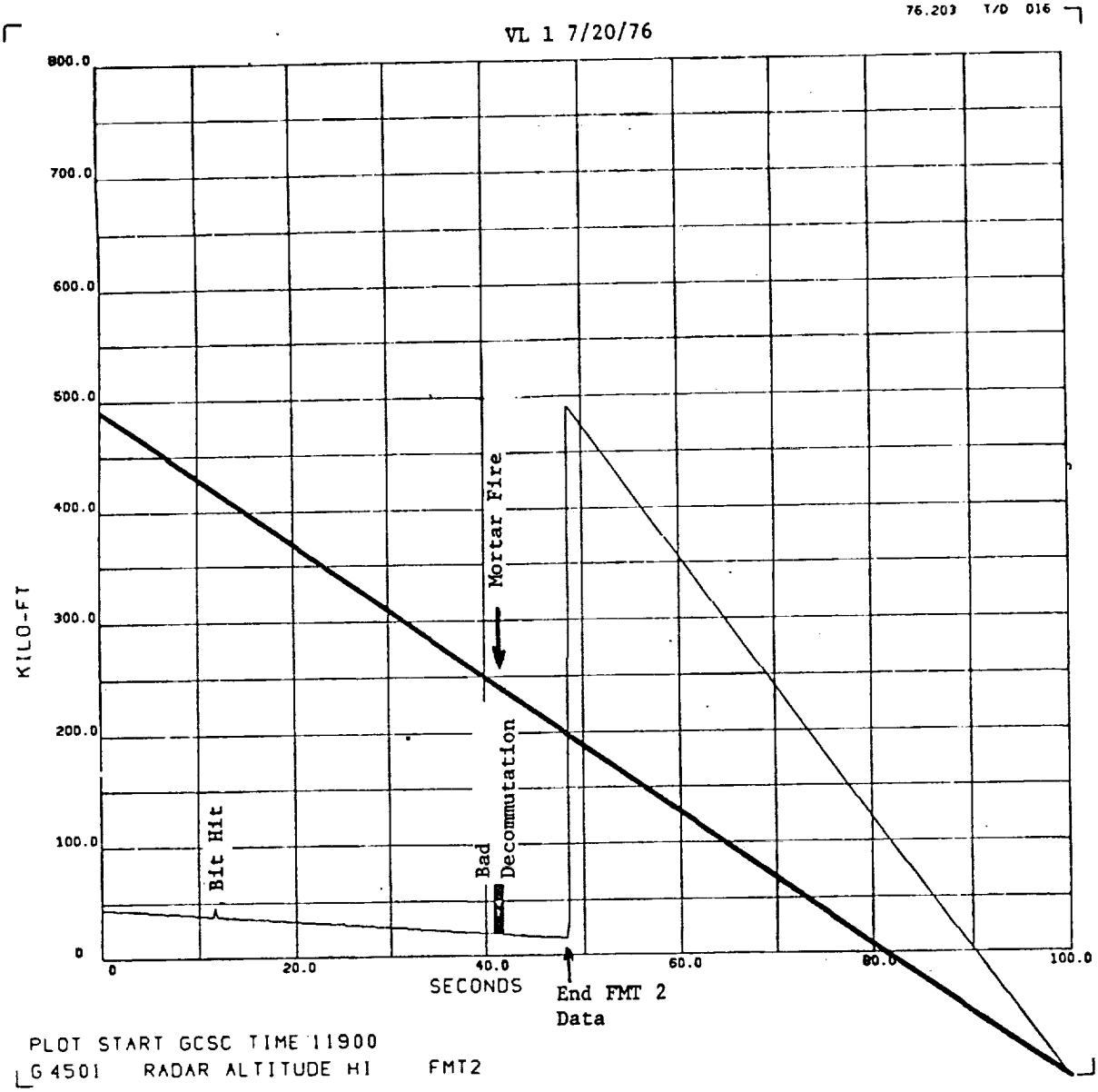

Figure VII-18

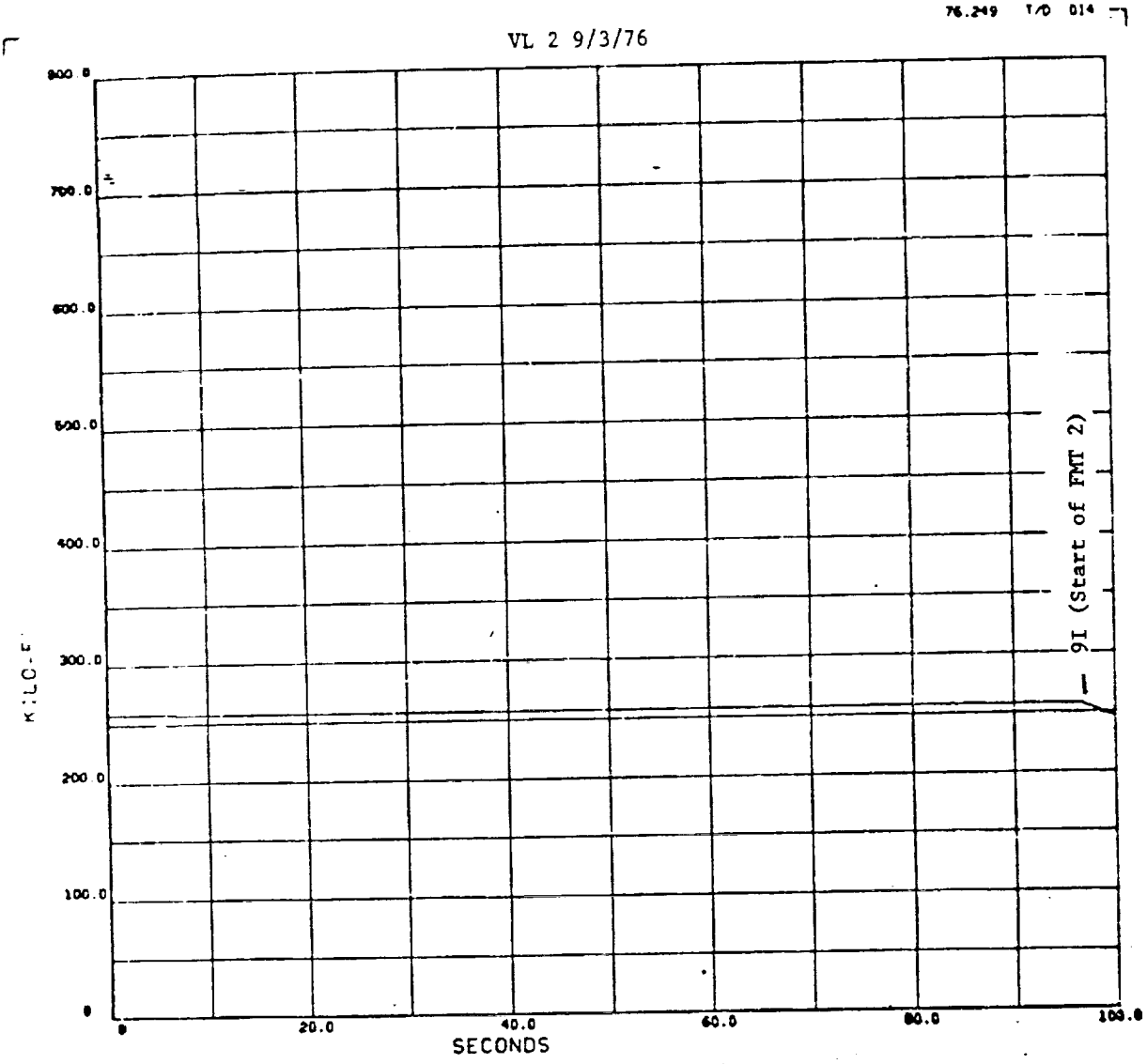

Figure VII-19

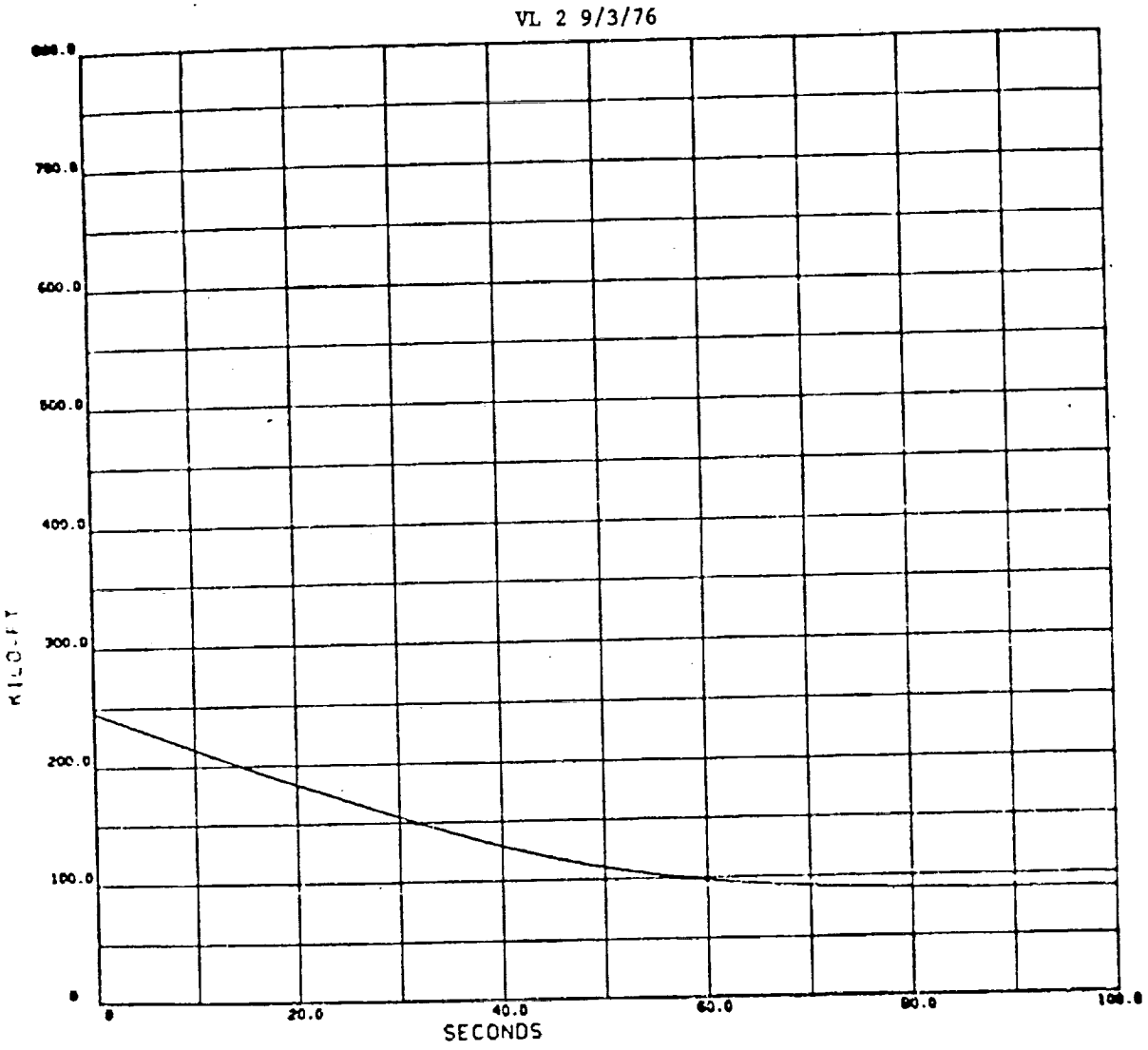

Figure VII-20

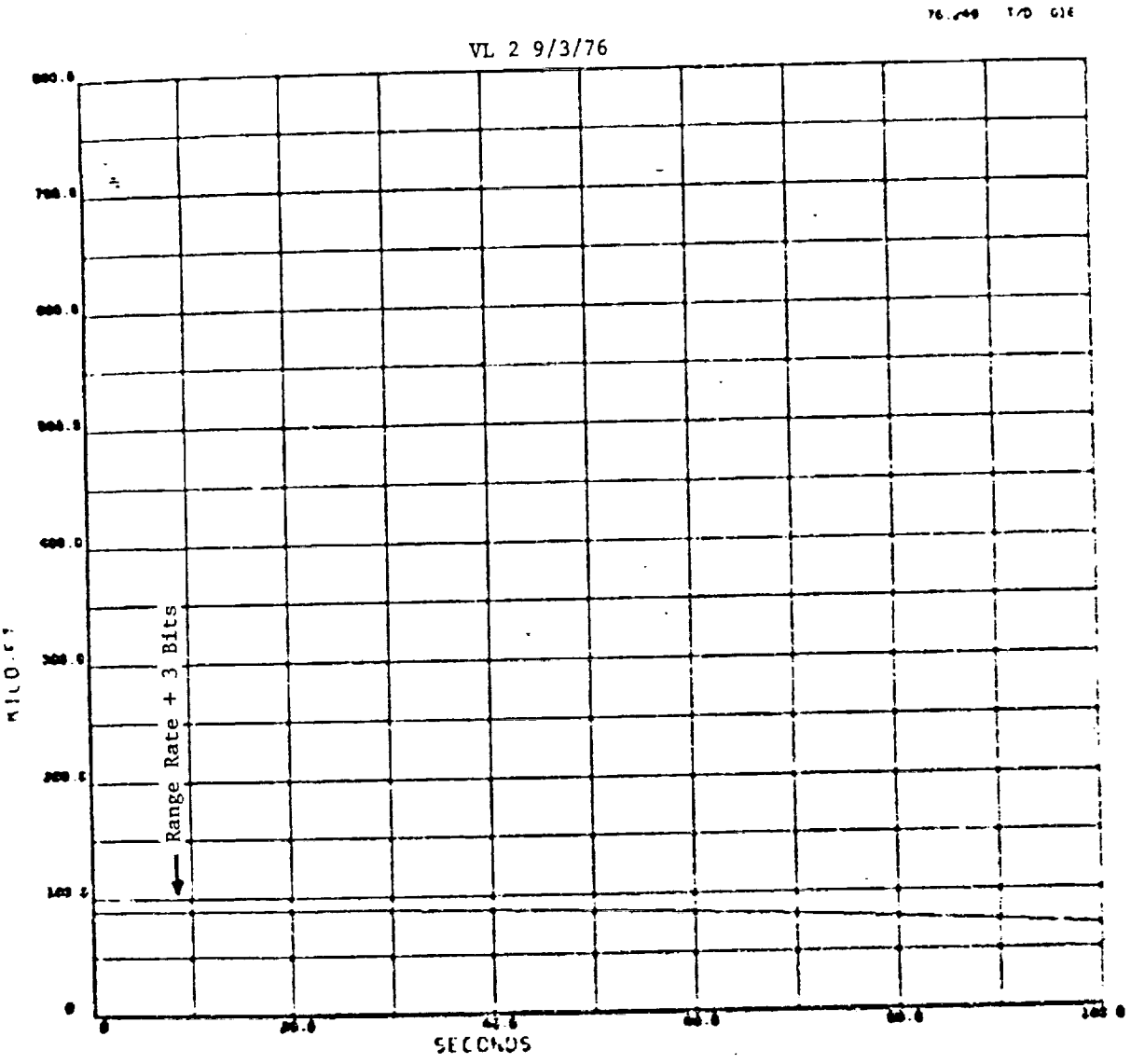

Figure VII-21

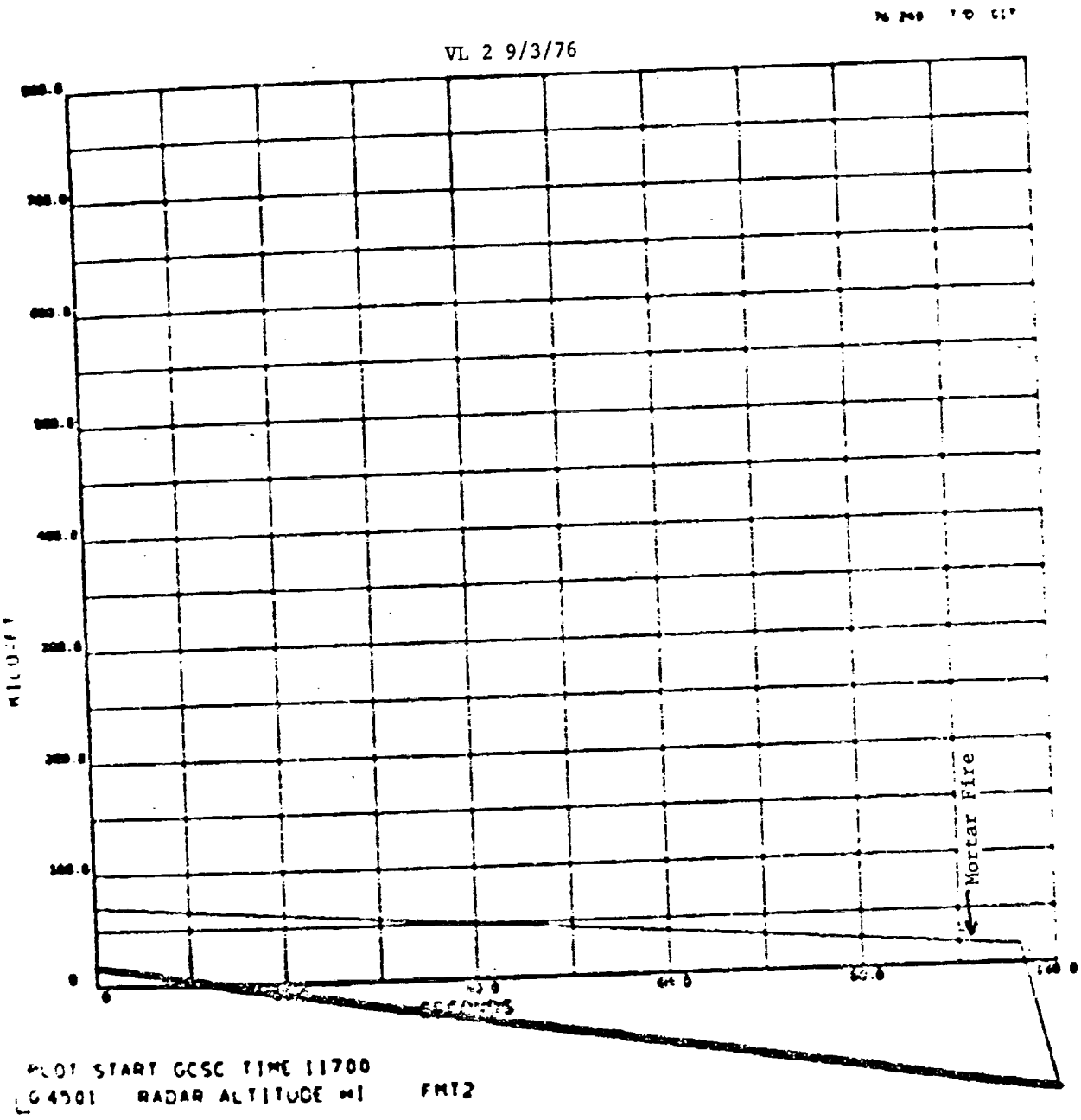

Figure VII-22

3. Performance - Terminal Descent Phase (Modes 2, 3, and 4)

RAE performance during the parachute and terminal descent phases was nominal for both missions with the exception of 7 to 8 ft of error in the constant velocity descent (CVD) start altitude.

Before aeroshell separation minus 1 sec, when transmitter inhibit was initiated, RAE 2 was locked for both missions. As transmitter inhibit was on for 4 sec, RAE 2 unlocked after the 1.1-sec drop track proof time, then reacquired first sweep after the inhibit was turned off at aeroshell separation plus 3 sec.

After the TDLR converged the velocity errors at handover, the navigator converged to the RAE within 3 sec. RAE lock was maintained continuously through the end of updates at 135 ft. The navigator was converged to within 1 ft of the RAE at 135 ft.

No false target locks were encountered.

On both missions, approximately 8 ft extra were spent on the constant velocity descent phase over nominal. This means that either there was a bias in the RAE at the end of updates or there was a navigation error accrued between 135 ft and 63 ft. Examination of the TDLR, velocity navigator, RAE, and altitude navigator rates at 135 ft show no reason to believe there was a navigation error in the altitude rate estimate. Thus, the cause must be in the RAE bias error.

As both landers were about 8 ft high in the CVD start altitude, the error seems systematic. Three possible causes exist. The bias error compensation in the software is computed as follows:

1)	RAE electronic and cable bias to LRAA port (J06) on the RAE antenna switch	B
2)	LRAA cable and connectors (electrical)	3.8 ft
3)	LRAA itself (electrical)	0.8 ft
4)	Distance from LRAA to bottom of footpad (leg extended)	1.1 ft
	Total bias error	B + 5.7 ft

The quantity B was measured at KSC before launch using a 160-ft calibrated delay line. One possible error cause is that this line, which was fabricated after the extension of RAE FSTC blanking, was in error. Mr. G. A. Murdock of Teledyne Ryan Aeronautical checked the values taken at KSC against those measured during testing at Ryan and found them to be systematically about 4 to 5 ft high for all four flight altimeters. As delay line cables are quite sensitive devices, an error of 5 radar feet or 10 nsec in delay is possible. It is strongly recommended that, if there are future Viking missions, the delay lines be recalibrated before use on the spacecraft by time domain reflectometer or otherwise.

Second, a 50-dB pad is used in line with the delay line to prevent reflections along every little imperfection in the cable. With the approximately 6 dB of two-way loss in the cable, this yields a path loss of about 106 dB from J06. In the missions, because of the high-reflectivity surface and hardware margins, the path loss was likely closer to 85 dB at 135 ft. This results in slightly less bias error as the received pulse takes slightly less time to cross the threshold. This error is estimated to be 1 to 2 ft.

The third error source is the nature of the terrain. As the RAE is a leading-edge tracking device, the first target appearing in time will be acquired. Because both landing sites were full of rocks and, in the case of VL1, knolls, it is likely that 1 to 2 ft of error was caused by the terrain.

If one adds up these three error sources, the result is about an 8-ft negative error in RAE measurement, which causes an 8-ft positive error in CVD start.

With today's knowledge of Mars, errors 2 and 3 (about 3 ft total) should be compensated for in any future missions.

Table VII-2 summarizes the performance of the RAE for VL1 and VL2.

Figures VII-23 and VII-24 are the DECSET plots of navigator altitude in format 3 for VL1. Figure VII-25 contains the same data for VL2.

Figures VII-26 and VII-27 are the DECSET plots of the raw RAE data for VL1 in format 3. Figure VII-28 contains the same data for VL2. To estimate true altitude above the surface for this phase, the following expression is used:

$$H_T = \left(H_A/0.9965\right) - B_T$$

where H_T = True altitude in feet

H_A = Raw RAE altitude in feet

B_T = Total S/W bias compensation in feet
= 55.7 ft (VL1)
= 58.7 ft (VL2)

For the aforementioned reasons, approximately 8 ft may be subtracted from B_T.

Table VII-2 RAE Performance (Modes 2, 3, and 4), VL1 and VL2

Parameter	VL 1	VL 2
Mode 2 Lock Altitude	14,924 ft	14,968 ft
Unlocks before Blanking	None	None
False Target Locks	None	None
Error at Handover (NAV-RAE)	-101 ft	-56 ft
Convergence Time after Handover	3 sec	3 sec
Error at End of Updates (NAV-RAE)	+1.0 ft	-1.6 ft
FSTC Blanking Altitude	132 ft	134 ft
Transmitter Power		
Mode 2/3	63.5 W	57.6 W
Mode 4	58.4 W	57.1 W
CFAR Analog (Min/Max)		
Mode 2	8.5/14.3 dB	10.0/14.6 dB
Mode 3	10.6/12.6 dB	11.2/13.1 dB
Mode 4	12.1/12.8 dB	13.1/13.4 dB
RAE 1 Temperature	48.6°F	54.9°F

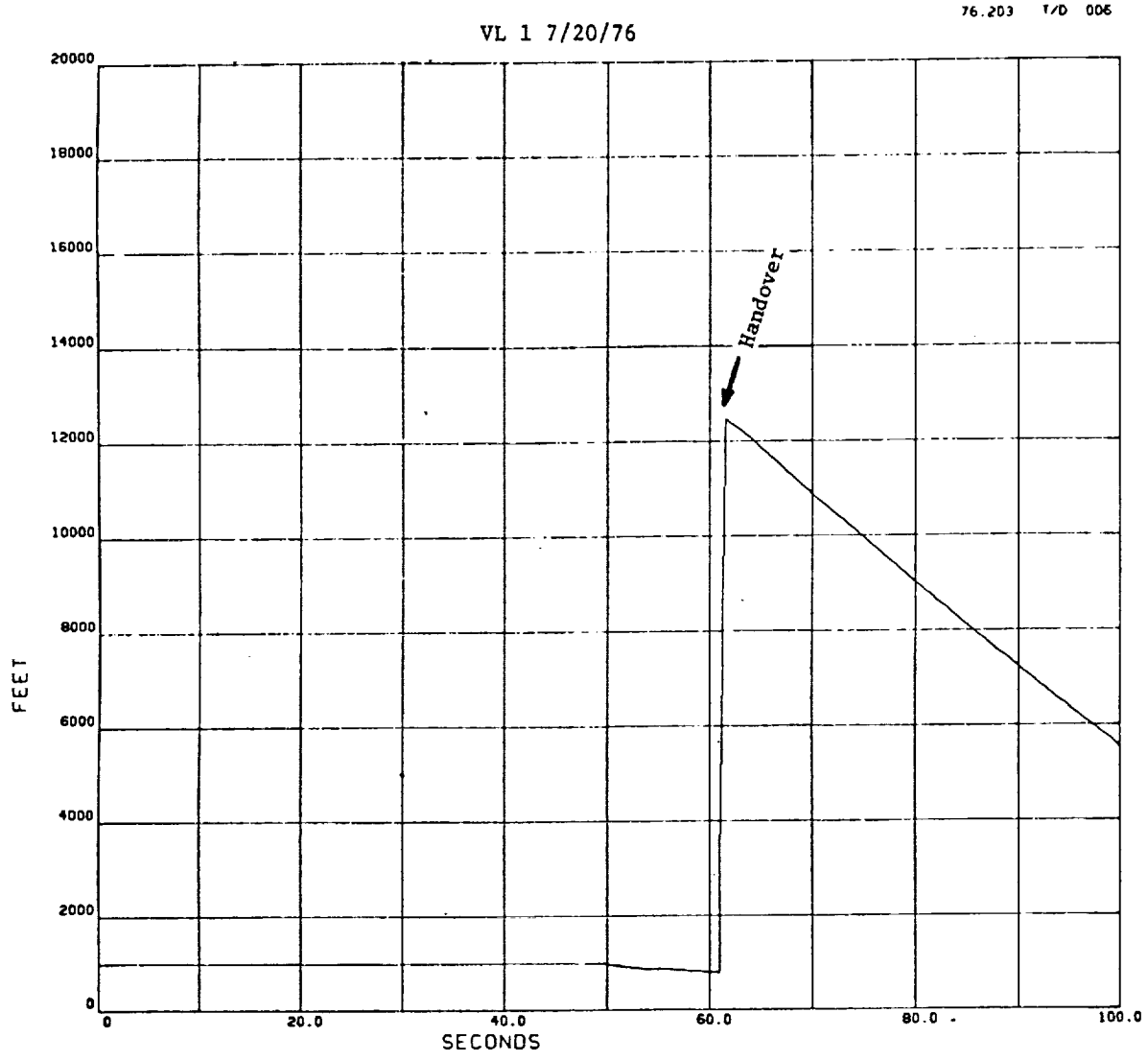

PLOT START GCSC TIME 11900
G 4726 NAVIGATOR ALTITUDE FMT3

Figure VII-23

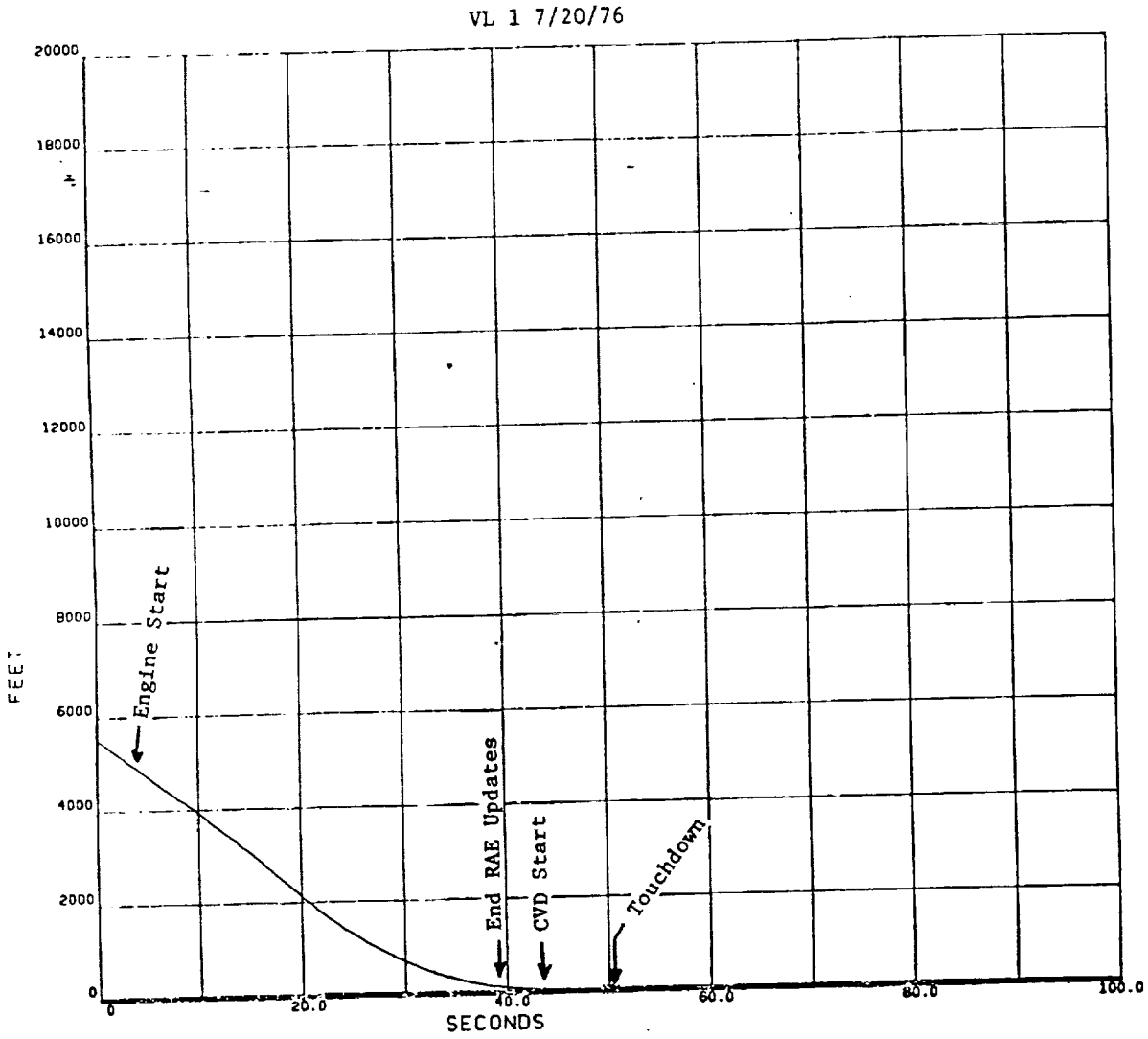

PLOT START GCSC TIME 12000
LG 4726 NAVIGATOR ALTITUDE FMT3

Figure VII-24

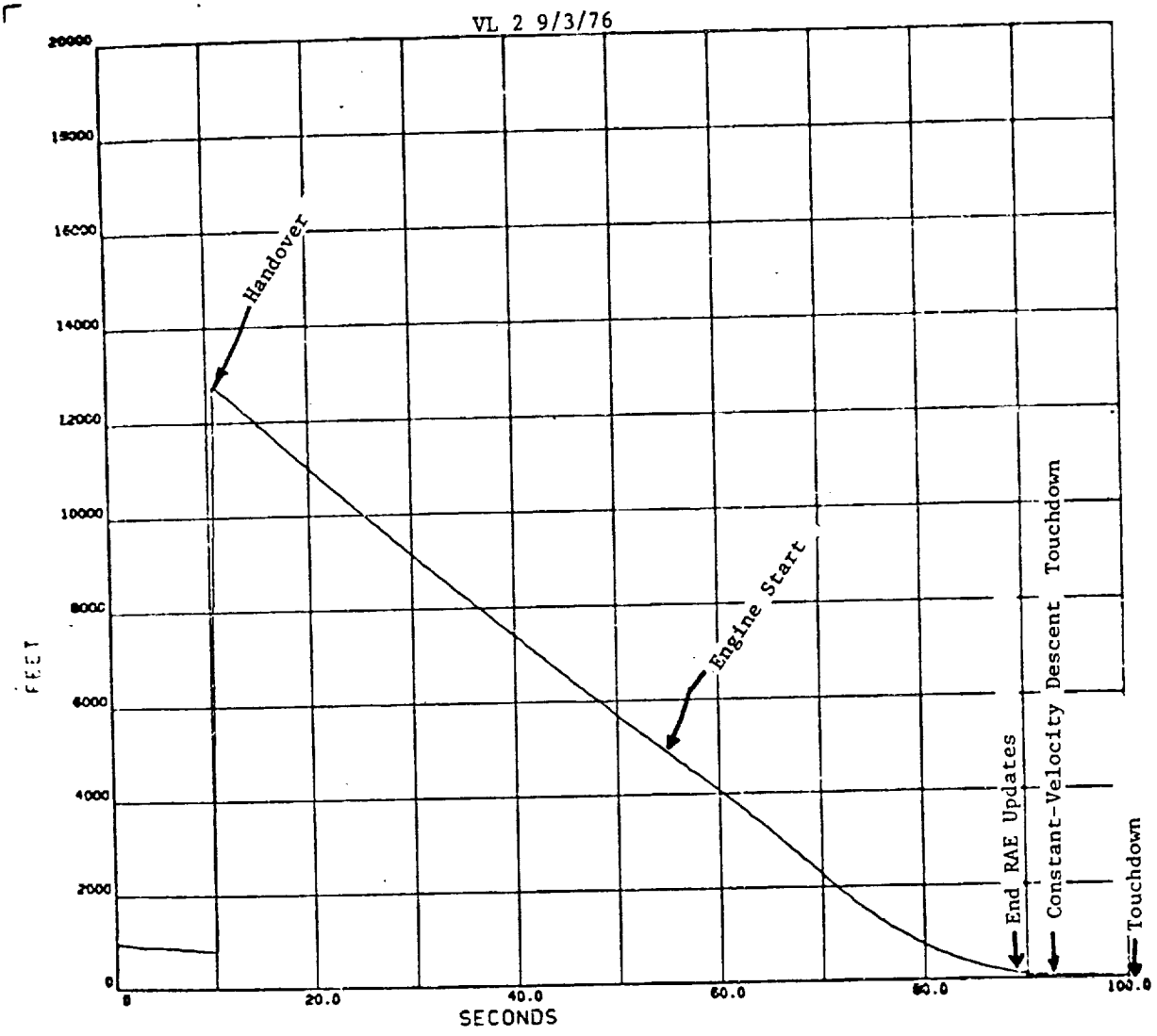

PLOT START GCSC TIME 11800
LG 4726 NAVIGATOR ALTITUDE FMT3

Figure VII-25

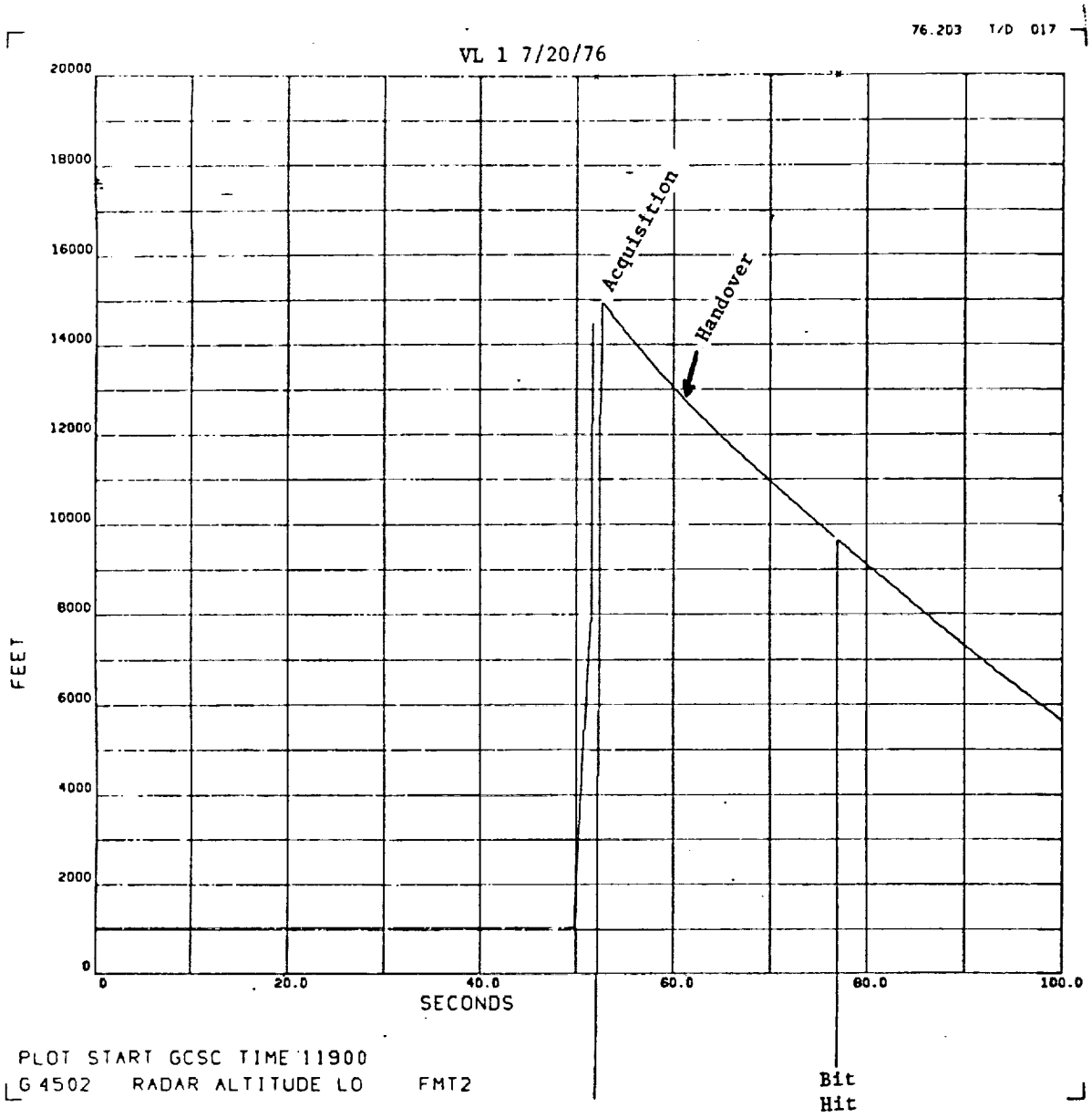

Figure VII-26

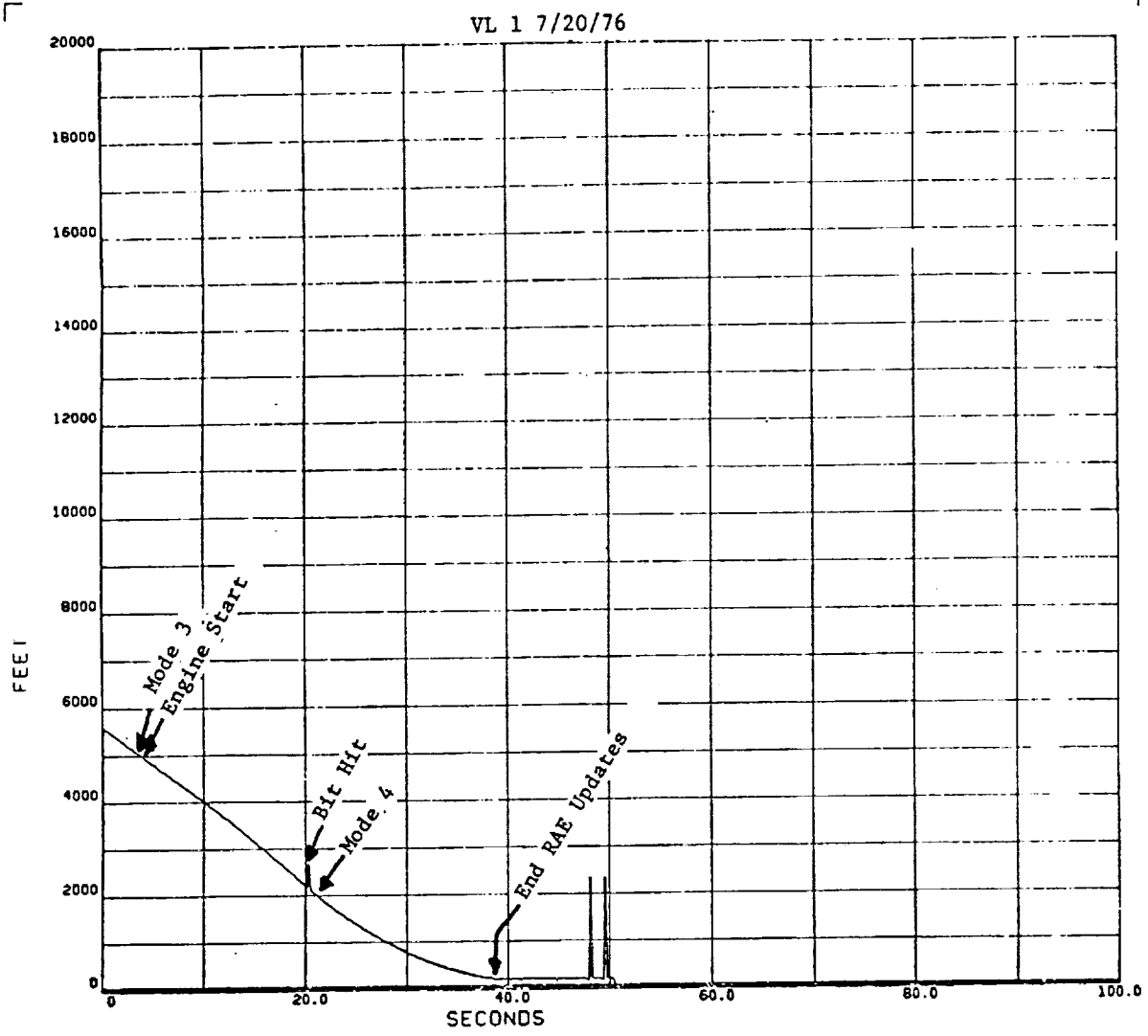

Figure VII-27

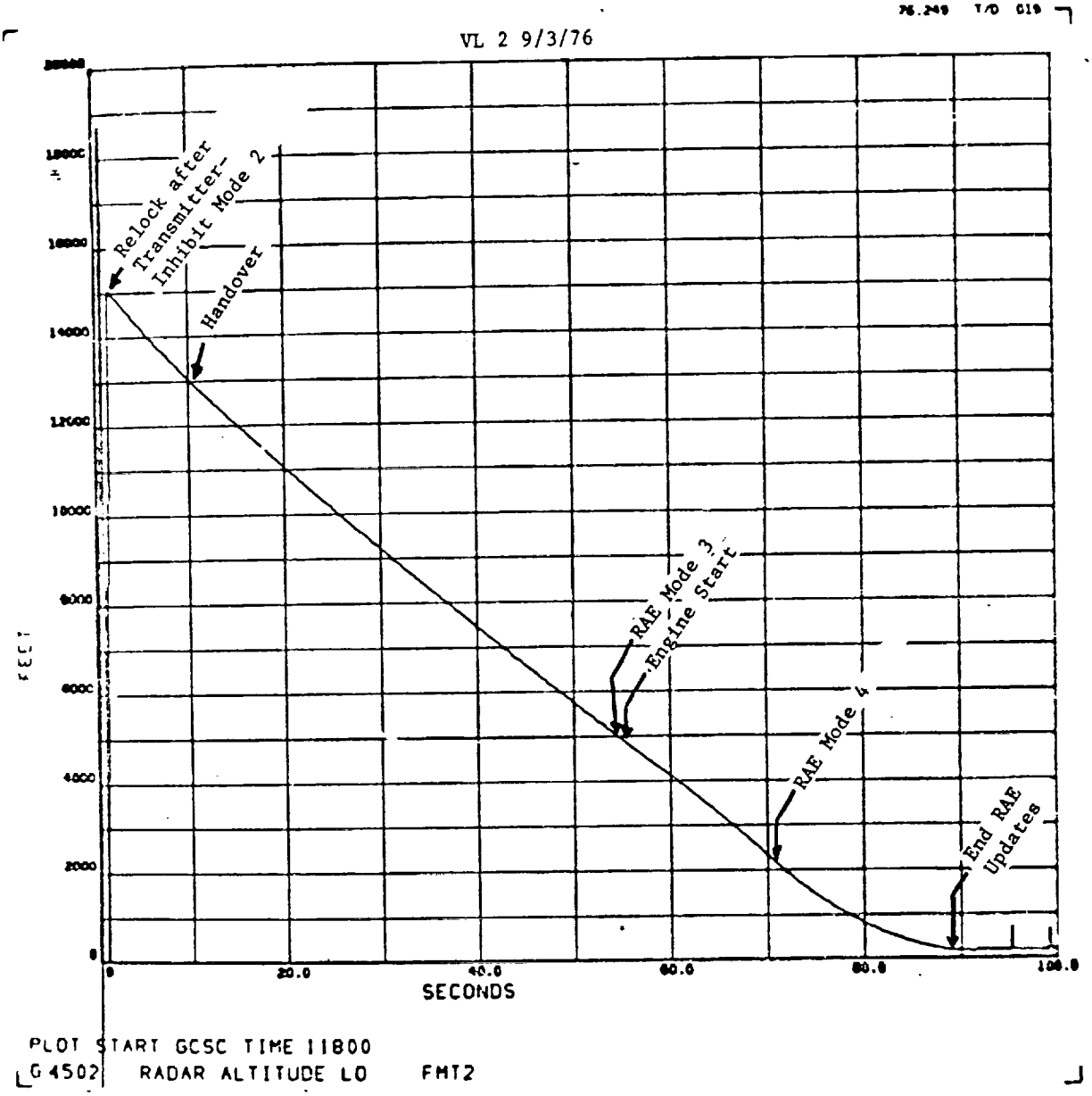

Figure VII-28

B. TERMINAL DESCENT AND LANDING RADAR (TDLR)

The TDLR is a four-channel Doppler velocity-measuring radar used to provide four velocity vectors to the Viking Guidance Control and Sequencing Computer (GCSC). The navigation software in the GCSC resolves TDLR velocities into vehicle body axis coordinates for use in navigation to a soft landing. Any three of the four TDLR channels provide sufficient data for a successful landing.

Performance of the TDLRs on both Viking landers was near nominal during preseparation checkout and terminal descent. Two anomalies occurred in TDLR operation and are discussed here.

Preseparation checkout of TDLR S/N 0000006 on VL1 was nominal in all respects, with all parameters well within tolerance of expected conditions. TDLR S/N 0000004 on VL2 was also nominal except for a series of four anomalous tracker acquisitions that occurred during the 5-min "false lock" test. The specified limit is for no locks during the test. Four definite locks occurred, which indicated that there was a signal present in Channel 2 of the TDLR.

Because there is no T/M data available to determine the actual source of the problem and analyze the probability of a solid false lock during descent, which could cause a mission failure, the radar analysis team decided to command the GCSC to ignore the Channel 2 data and use the other three channels. All concerned felt that there was little chance of such a false lock occurring but that any chance at all was unacceptable. In fact, the performance of Channel 2 during descent was nominal in all respects.

Some possible sources of the anomaly include:

1) Vibration of structure in proximity to the TDLR antenna. A check of conditions showed that there was no activity on the spacecraft to excite vibrations.

2) Electrical noise coupling into the TDLR. There were no indications of any such activity and only one channel showed a problem.

3) Internal TDLR circuit failures that generated low-frequency noise in the affected channel. Several possibilities exist, including the receiver mixer diodes and the solid tantalum filter capacitors as likely candidates.

Descent performance was normal for both landers until just before touchdown, when some channels showed an increase in indicated velocity. Performance is summarized in the following paragraphs.

1) All channels acquired valid signals on first sweep after power on. On both landers, TDLR Channel 2 detected the presence of the aeroshell in the antenna beam and unlocked for one sweep interval and then all channels remained locked until touchdown.

2) The velocity performance is shown in Figures VII-29, VII-30, and VII-31. Navigator estimates and resolved radar values are plotted. Within the limitations imposed by the limited samples (1 out of 25) of the navigator, the overall performance is nominal. The Lander Trajectory Reconstruction Program (LTRP) data tracks the direct data and is not separately plotted.

3) The indicated transmitter power for all channels was well within normal tolerance of expected values. Measurements were:

	VL1, mW		VL2, mW	
	Turn On	Touchdown	Turn On	Touchdown
Ch 1	204.9	206.9	167.2	167.2
Ch 2	172.0	173.4	149.3	150.7
Ch 3	152.9	154.3	159.1	160.9
Ch 4	172.6	172.6	177.6	179.3

4) Temperatures of the TDLRs were within expected limits and posed no constraints

VL1, °F		VL2, °F	
Turn On	Touchdown	Turn On	Touchdown
29.02	30.59	31.37	32.94

5) Navigator velocity errors at Mission Event 38 (handover) were as shown. Convergence of the navigator to the radar data was complete in 3 sec for VL1 and 2 sec for VL2. Errors were:

VL1, fps			VL2, fps		
U (X axis)	V(Y axis	W(Z axis)	U(X axis)	V(Y axis)	W(Z axis)
78.0	-51.5	-42.8	47.9	88.1	102.4

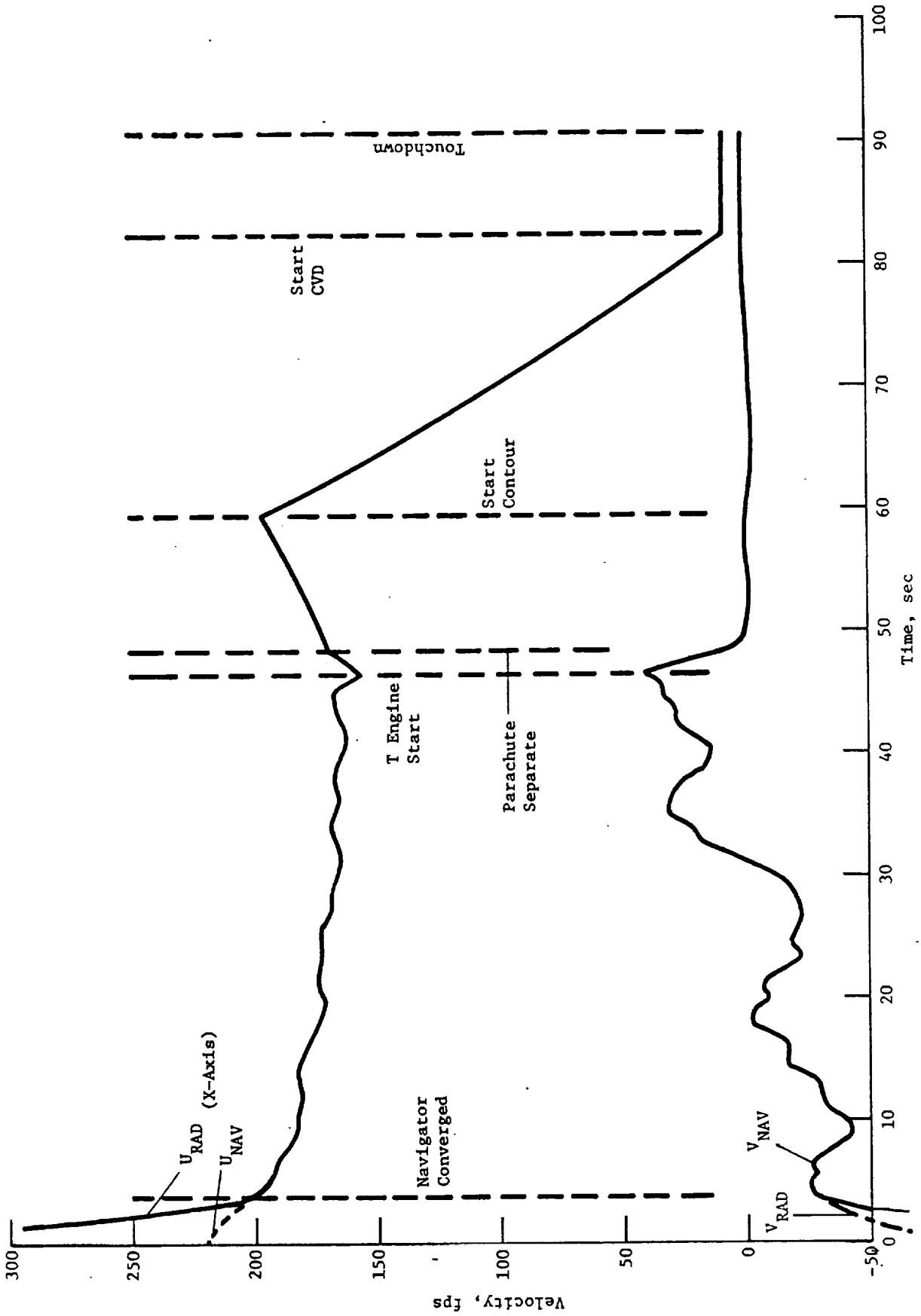

Figure VII-29 VL 1 Terminal Descent Velocity, Channels U and V

Figure VII-29

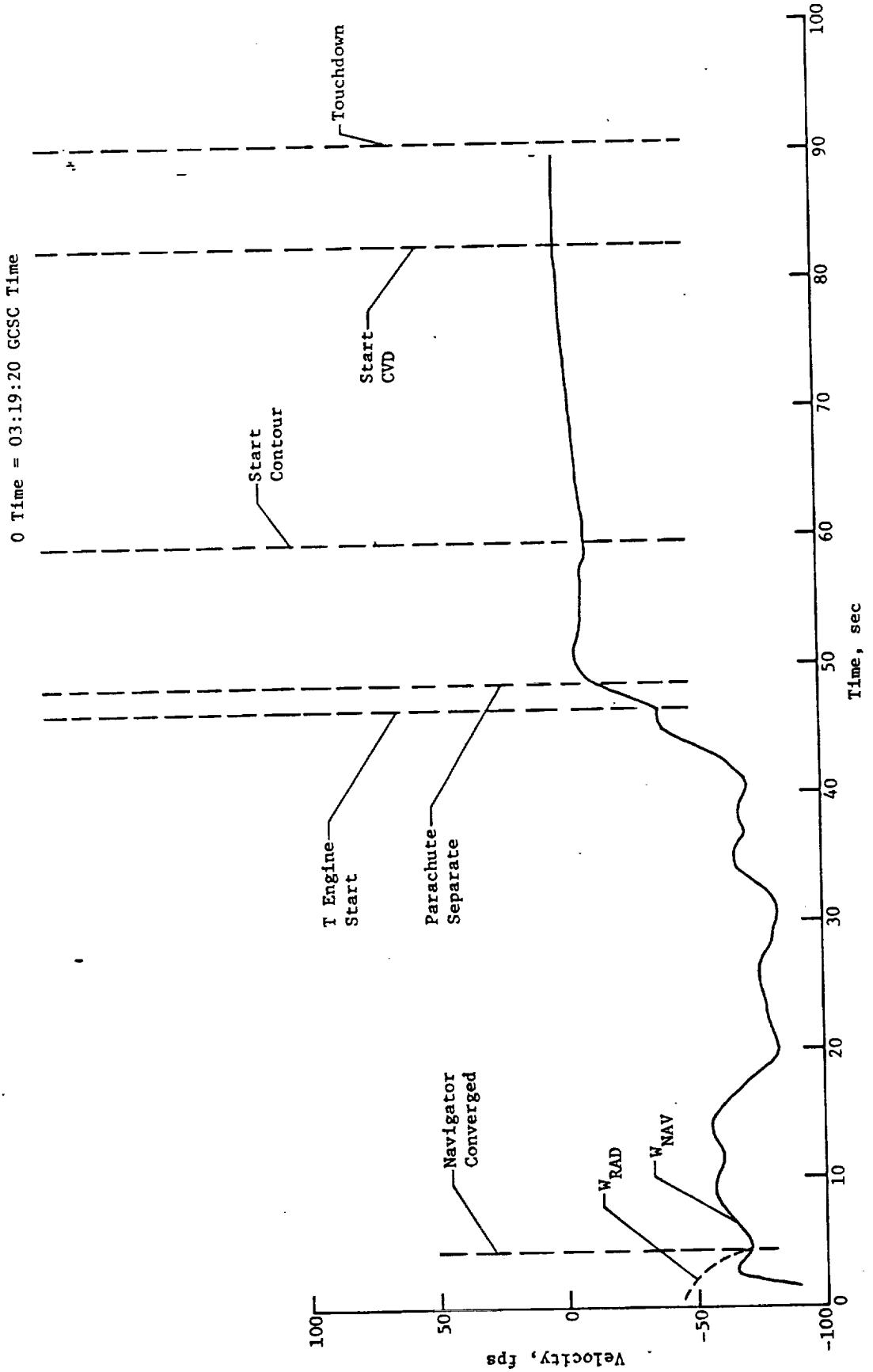

Figure VII-30 Terminal Descent Velocity, Channel W

Figure VII-30

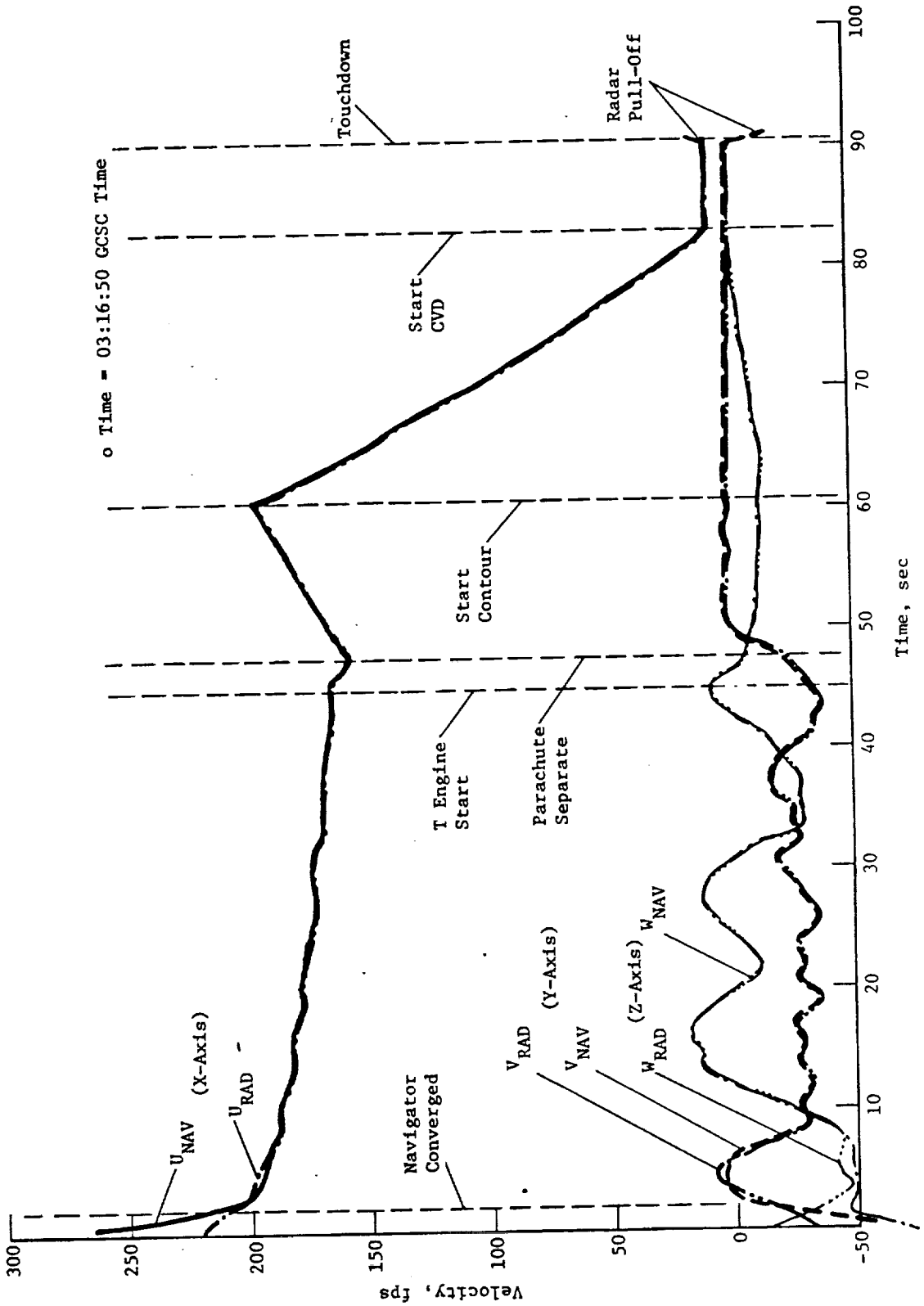

Figure VII-31 Terminal Descent Velocity, Channels U, V, and W

Figure VII-31

An anomalous increase in velocity indications occurred just before touchdown on both landers. Channel 3 of VL1 increased from 7.75 fps to 8.12, 9.22, and 13.10 fps; Channel 4 increased from 7.90 fps to 8.11, 9.77 and 15.12 fps for the last three 200-ms samples; Channel 1 increased from 7.40 to 8.87 fps at the same time. Channel 3 of VL2 increased from 7.75 fps to 9.96 and 16.23 fps for last two 200-ms samples and Channel 1 increased from 7.77 to 9.06 fps on the last sample. In both vehicles, the indicated increase occurred within 3 ft of the Martian surface.

Probable cause of the indication is displacement of surface material and deflection upward by the rocks under the lander. Such material can cause the noted indications. Analysis and previous tests showed that material displaced over a smooth surface would not cause measurement errors. The displaced material, as seen on the landing pads and high-gain antenna, appears quite cohesive and seems to contain a relatively high content of magnetic material. Both conditions can contribute to a relatively high radar cross section.

The net effect (on VL2) of the indicated increase of velocity was to cause the thrust of engine 3 to increase (about 3 times), thus slowing the descent and causing about 2° of attitude error at touchdown.

VL1 was affected less than VL2 due to the averaging effect of using all four channels instead of only three.

Channels 3 and 4 are more sensitive to this effect than 1 and 2 because of proximity of those antenna beams to engines 1 and 3.

Additional logic could be provided to protect against any deleterious effects from the previously noted anomaly.

1) During the constant velocity phase of the descent, the indicated velocities in each channel change by less than 5% between samples except when the "kickback" of surface material occurs. This factor could be used to suppress the TDLR data at any time a change exceeding 10% occurred. This approach is valid only for the final part of CVD after the initial transients have damped out (i.e., use only at a navigator altitude below 10 ft).

2) When all four channels are used, the sum of Channels 1 and 3 is equal to the sum of Channels 2 and 4 within narrow limits. Actual data from VL1 and VL2 shows nearly all data within 2.5%, with only very few points outside the limit except for the "kickback" anomaly, which unbalanced by as much as 33.9% (Fig. VII-32).

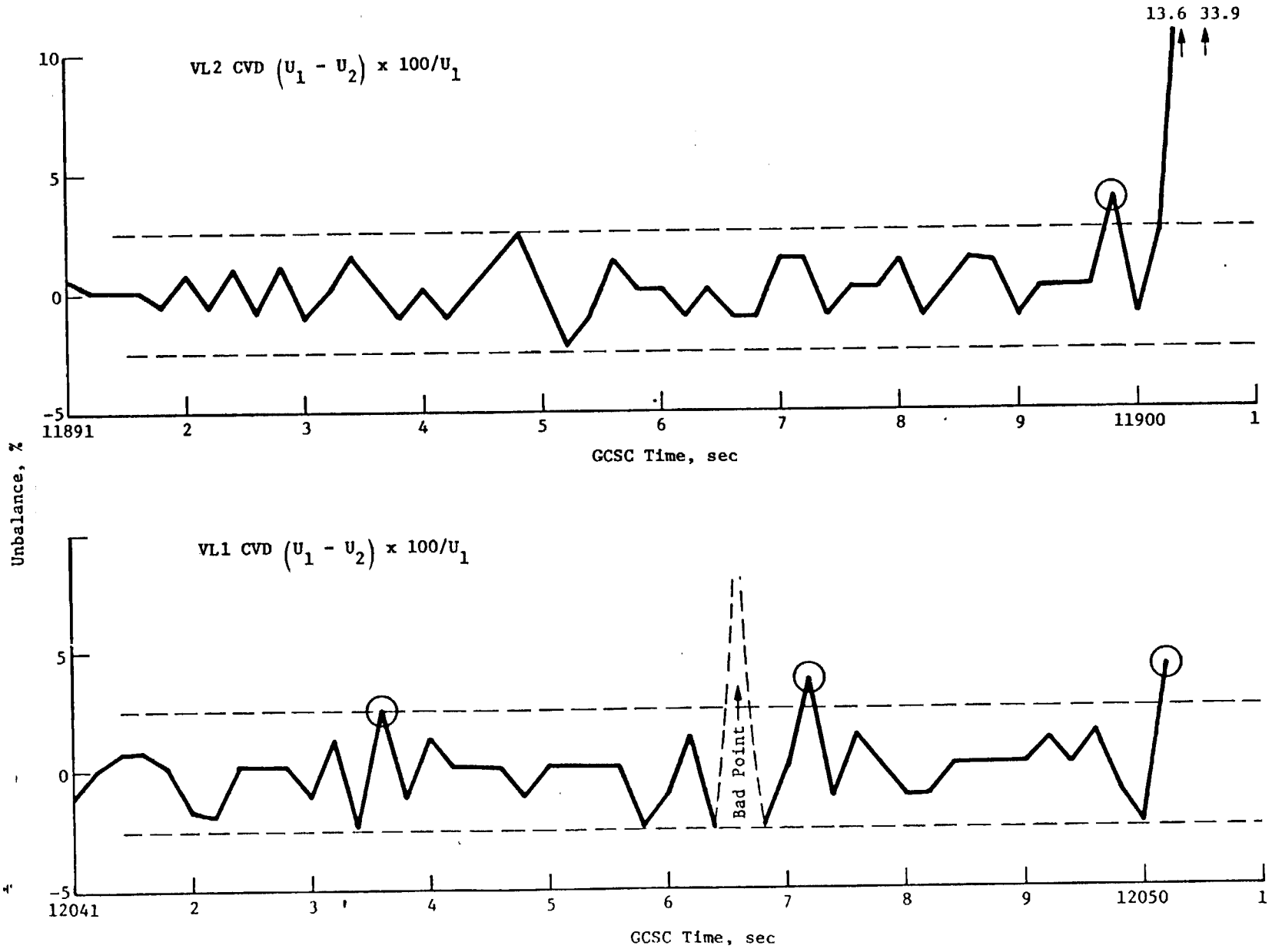

Figure VII-32

Figur: VII-32 TDLR Channel Balance, Constant-Velocity Descent

3) If altitude can be determined to sufficient accuracy, the navigator can ignore TDLR data at 5 to 10 ft above the surface.

If the TDLR or similar radar is used for planetary landings, some technique (as above) should be provided to prevent anomalous effects near touchdown.

VIII. INERTIAL REFERENCE UNIT (IRU) PERFORMANCE

Both Viking landings were flown using the primary triad of sensors in the IRU. The gyro and accelerometer biases determined in preseparation checkout repeated the values determined in cruise checkout so closely that no up-link was required at S-9.5 hr.

The apparent bias instability of the Y gyro on VL2 during the preseparation checkout was attributed to an orbiter sensor scale factor error. To show that this was actually true, the raw gyro pulse counts and computed biases were used to perform a gyro consistancy computation on the IRU. The sensed rate of the redundant gyro is equal to the sum of the sensed rate of the three primary gyros divided by $\sqrt{3}$. The gyro consistancy of the IRU gyros is computed as follows:

$$GC = \frac{\omega x + \omega y + \omega z}{\sqrt{3}} - \omega_R$$

In performing this calculation over all 302.4-sec computation periods during preseparation checkout, the maximum difference between the primary gyros sensed rate when projected onto the redundant gyro sensed rate was ±0.032 deg/hr. This indicates that all gyros were performing properly with all parameters well within expected limits.

A. TEMPERATURE VERSUS TIME

The IRU cover temperature rise during deorbit burn was 1.9°F on VL1 and 1.6°F on VL2. This type of cover temperature change is normal and occurs during normal operation of the IRU. Based on the observed temperature change during deorbit and the calculation of accelerometer bias (Table VIII-1) after deorbit, it is concluded that there was no accelerometer deterministic bias shift occuring during deorbit on either lander due to thermal heating of the cover by the deorbit engines.

The IRU cover temperature increased a maximum of 14.59°F on VL1 and 12.97°F on VL2. The maximum cover temperature occurred during high mode operation on the parachute.

The IRU electronics temperature decreased by 1.48°F on VLC1 and 0.74°F on VL2. These changes are nominal and well within the operating temperature range of the IRU (155 to 165°F).

Table VIII-1 IRU Data

IRU Gyro Bias Stability

VL1	Baseline Bias Hamilton Standard 4-14-75, deg/hr	Cruise Checkout 11-10-76, deg/hr	Preseparation Checkout 7-19-76, deg/hr
X Gyro	6.504	6.488	6.452
Y Gyro	5.688	5.786	5.763
Z Gyro	0.688	0.694	0.655
R Gyro	2.600	2.733	2.710

VL2	Baseline Bias Hamilton Standard 3-19-75, deg/hr	Cruise Checkout 11-19-75, deg/hr	Preseparation Checkout 9-2-76, deg/hr
X Gyro	1.869	1.954	1.929
Y Gyro	3.760	4.081	4.070
Z Gyro	5.335	5.261	5.232
R Gyro	1.282	1.328	1.331

Postseparation Accelerometer Bias

	VL1, μg	VL2, μg
X Accel	1165	2053
Y Accel	-1108	686
Z Accel	- 732	-1035
Uncertainty: X axis = ±6.1 μg; Y and Z axis = ±1.5 μg		

Accelerometer Bias Stability

	VL1		VL2	
	Cruise to Postsep, μg	Presep to Postsep, μg	Cruise to Postsep, μg	Presep to Postsep, μg
X Accel	+16	+54	-41	+ 4
Y Accel	-66	+21	-22	-13
Z Accel	- 9	+31	-14	0
Uncertainty: X axis = ±6.1 μg; Y and Z axis = ±1.5 μg				

Table VIII-1 (concl)

Accelerometer Bias Shift across Deorbit Burn

	VL1	VL2	
	S+0:30:00, μg	S+0:30:00, μg	S+2:57:00, μg
X Accel	-10	-20	+19
Y Accel	+26	- 3	+22
Z Accel	+16	- 3	0

Uncertainty

X Axis	±21.1	±25	±18.5
Y Axis	± 5.27	± 6.25	± 4.6
Z Axis	± 5.27	± 6.25	± 4.6

Attitude Rates during Accelerometer Calibration

	VL1, deg/sec	VL2, deg/sec
Roll	+0.001	-0.038
Pitch	-0.380	-0.133
Yaw	-0.358	-0.042

Maximum Attitude Rate after Maneuvers before Phase 9

	VL1, deg/sec	VL2, deg/sec
Roll	-0.41	+0.39
Pitch	-1.81	-2.08
Yaw	+1.09	-2.07

Maximum Attitude Rates at Parachute Opening

	VL1, deg/sec	VL2, deg/sec
Roll	1.40	1.19
Pitch	60.13*	48.52*
Yaw	6.59	-16.17

*0.1 sec averages, see Section V-B.

Maximum Attitude Rates at Aeroshell Separation

	VL1, deg/sec	VL2, deg/sec
Roll	1.06	1.24
Pitch	-9.23	-19.52
Yaw	8.54	-20.36

Maximum Attitude Rates at Terminal Descent Initiate

	VL1, deg/sec	VL2, deg/sec
Roll	- 0.66	0.25
Pitch	11.19	0.53
Yaw	13.44	-8.06

B. SPIN MOTOR ROTATION DETECTIONS (SMRDs) VERSUS TIME

The IRU SMRDs indicated proper operation of the gyro spin motors from separation through landing.

C. HIGH-MODE TORQUE DISCRETES

The high-mode torque discretes indicated that the gyros operated in the high mode during the parachute deployment phase of the mission. The total time of high-mode operation for each lander is shown below:

	VL1, sec	VL2, sec
X gyro	7.70	10.9
Y gyro	20.95	20.94
Z gyro	11.70	16.14
R gyro	23.0	18.0

D. VELOCITY INCREMENTS

The IRU velocity increments were normal throughout the mission. This was observed during periods of quiescent operation (coast and constant velocity periods). The maximum pulse variations during these periods were observed to be about ±1 pulse on both vehicles.

The IRU data table gives the accelerometer bias variation during various mission phases. The accuracy of the bias calculation depends on the time over which the accelerometer pulse counts were averaged. Cruise and preseparation checkout bias calculations are based on the average of the last 1 hr of data and therefore have the least uncertainty (X axis uncertainty ≈ 0.3 µg y and z axis uncertainty ≈ 0.08 µg). The uncertainty for each of the other bias determinations is listed in the IRU data table.

The bias shifts across deorbit burn were determined during the period after completion of the coast maneuver before the start of the RPA sequences. On VL2, a bias was determined at $\approx$ S+2: 57:00 before 0.05 g as noted in the data table. Determination of the accelerometer bias for VL1 was very difficult because of data losses. The bias was an average of 83 sec worth of data over a total time of 135 sec. In other words, this was not a continuous 83 sec worth of data and therefore may be biased in one direction since the maximum period of continuous data

was ≈ 3 sec. However, based on data from both landers, it is felt that the 3σ bias stability of 50 μg is a good number. To reduce this number significantly would require additional testing and evaluation of the IRU accelerometers.

The pitch and yaw rates during accelerometer calibration were negligible, i.e., the $\omega^2 r$ terms were

VL1: $\omega_Y^2 R_Z = \left(\frac{0.380}{57.3}\right)^2 \frac{36.79}{12} = 1.348 \times 10^{-4}$ ft/sec^2 = 4.2 μg

VL2: $\omega_Y^2 R_Z = \left(\frac{0.133}{57.3}\right)^2 \frac{36.79}{12} = 1.652 \times 10^{-5}$ ft/sec^2 = 0.5 μg

The velocity increments indicated peak loads during entry of -7.28 g on VL1 and -7.14 g on VL2.

Vertical constant velocity descent was indicated for the last 7.9 sec on VL1 and the last 7.5 sec on VL2.

E. ATTITUDE INCREMENTS

The IRU attitude increments were normal throughout the mission, measuring vehicle attitude as a function of time. See Table VIII-1 for a summary of vehicle rates during the mission. High-mode operation of the IRU gyros occurred only during the parachute phase of the mission. The high-rate mode operation time for each gyro is listed in the high-mode torque discrete section of this report.

IX. PROPULSION SYSTEM PERFORMANCE

A. SUMMARY

The Viking RCS/deorbit and terminal descent propulsion systems performed without anomalies on both vehicles. Thrust levels and specific impulse were within expected tolerances. Tank pressures on both systems during blowdown were higher than predicted. The polytropic expansion coefficient was very close to isothermal during the deorbit burn and 1.295 during terminal descent. The higher pressures provided additional thrust margin.

B. RCS/DEORBIT PERFORMANCE

The telemetry data available for RCS/deorbit propulsion system performance evaluation were tank pressures and temperatures, engine commands, and velocity change increments as well as vehicle attitude and attitude rate.

The approach used to verify performance was:

1) Determine propellant consumed from tank pressures and temperatures and compare to the prediction;

2) Determine thrust from vehicle acceleration and compare to the predictions.

The initial conditions were:

	VL1	VL2
1) Vehicle Weight	2330 lb	2326 lb
2) Tank Pressure	352.0 psia	348.3 psia
3) Tank Temperature		
T1	71.9°F	72.9°F
T2	75.5°F	70.0°F
4) Propellant Load	187 lb	187 lb

Propellant Used

Propellant consumption was determined for deorbit burn, coast, 800,000 ft to sense 0.05 g, sense 0.05 g to mortar fire, and mortar fire to aeroshell separation.

Deorbit Burn - The predicted propellant required to completion of deorbit burn was 162.0 lbm or 164.2 lbm including trapped propellant. The actual used was determined from tank pressures and temperatures. A plot of pressure and temperatures versus time is shown in Figures IX-1, IX-2, and IX-3. Because the tank temperature (wall measurement on the gas side) started recovering immediately after completion of the burn, it was assumed that the wall temperature was an accurate measurement of gas temperature. Before flight, it was anticipated that the gas temperature would be lower than the tank wall measurements and a continuing decay of wall temperature would occur until the gas and wall reached equilibrium.

The perfect gas law was used to determine volume change and thus propellant used:

$$\frac{V_1}{V_2} = \frac{P_2}{P_1}\frac{T_1}{T_2}$$

where

$$V_1 = V_{tank_1} - V_{prop_1},$$

and

$$V_2 = V_{tank_2} - V_{prop_2},$$

$$\text{Also for VL1, } V_{tank_1} = V_0 \left| \frac{11.075 + \frac{352.0(11.075)^2 0.75}{32(10)^6 0.028}}{11.075} \right|^3$$

to account for tank stretch from pressure loading.

$$\text{For VL2, } V_{tank_1} = V_0 \left| \frac{11.075 + \frac{348.3(11.075)^2 0.75}{32(10)^6 0.028}}{11.075} \right|^3$$

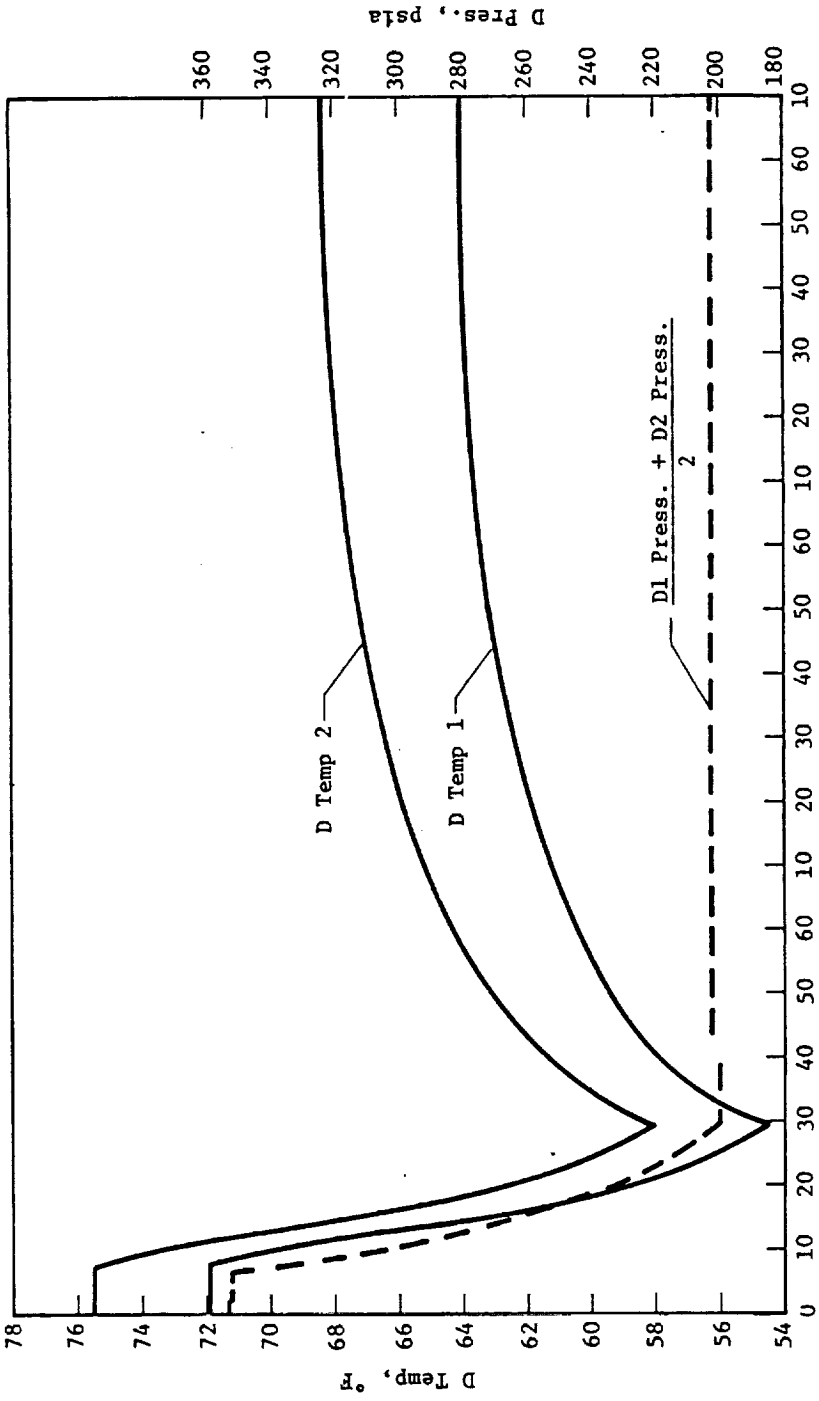

Figure IX-1 VL1 Deorbit Pressure and Temperature

Figure IX-1

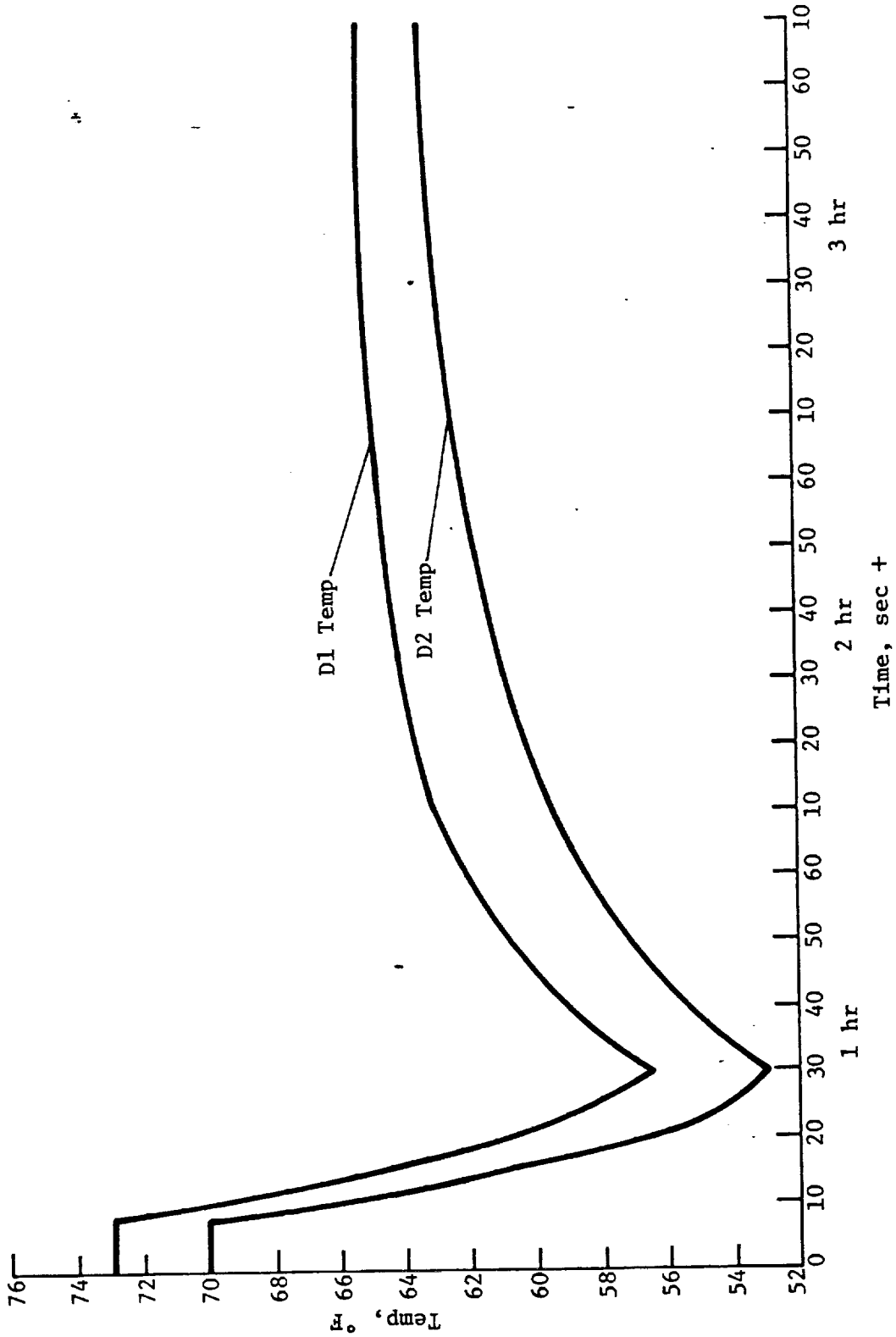

Figure IX-2 VL2 Temperatures

Figure IX-2

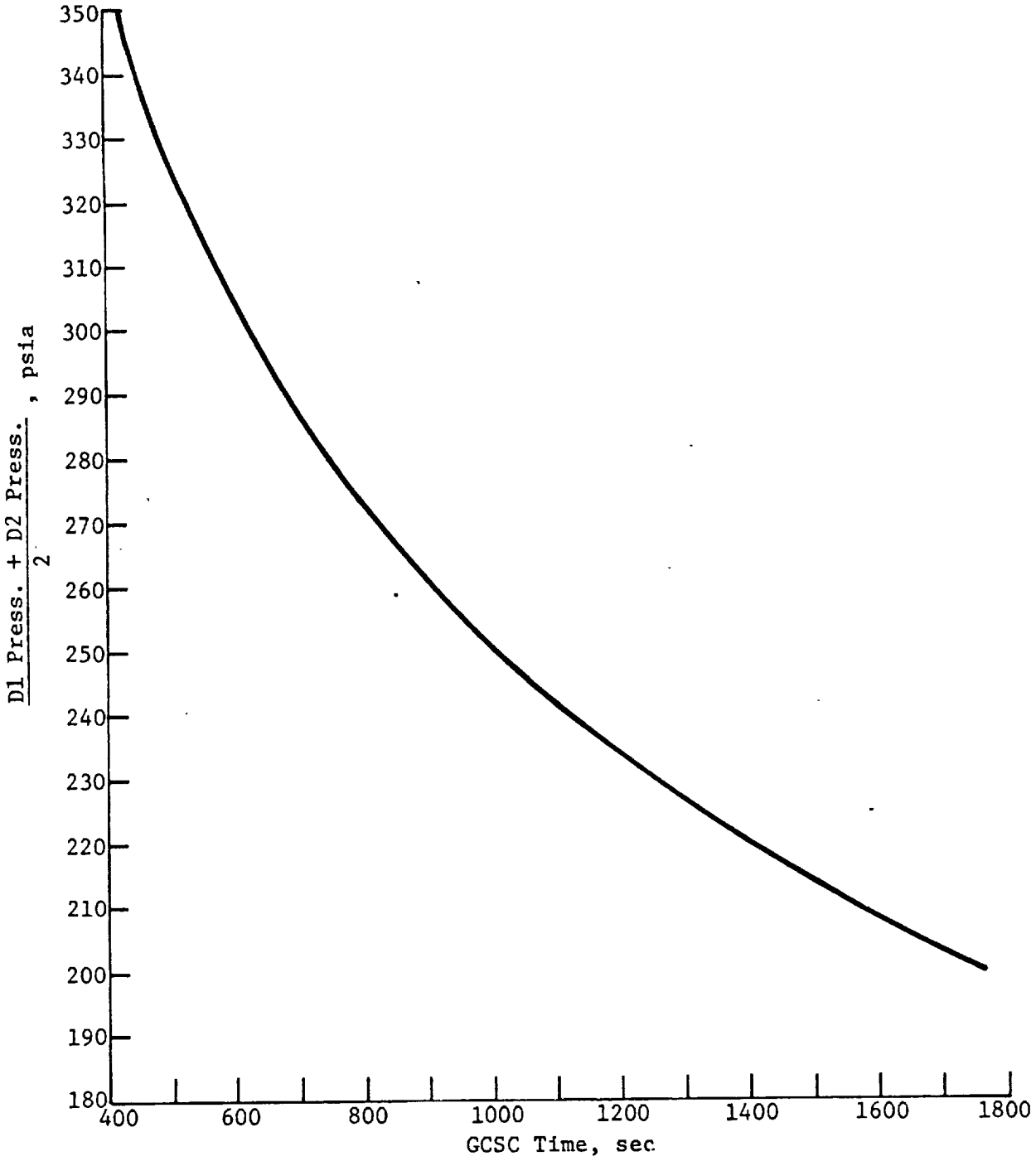

Figure IX-3 VL2 Tank Pressure

Likewise for VL1, $V_{tank_2} = V_0 \left| \frac{11.075 + \frac{200.2(11.075)^2 0.75}{32.(10)^6 0.028}}{11.075} \right|^3$

and VL2, $V_{tank_2} = V_0 \left| \frac{11.075 + \frac{199.3(11.075)^2 0.75}{32(10)^6 0.028}}{11.075} \right|^3$

where

VL1	VL2
V_0 = 11180 in.^{3}	11180 in.^{3}
P_2 = 200.2 psia	199.3 psia
P_1 = 352.0 psia (after bleed in)	348.3 psia
T_1 = 533.7°R	531.5
T_2 = 516.2°R	515.5

Solving for $V_{prop_1} - V_{prop_2}$ gives: For VL1, 4349 in.^{3} or at a density of 0.0363 lb/in.^{3} a propellant consumption of 157.9 lb and for VL2 4311 in.^{3} or 156.5 lb.

Coast - The predicted fuel consumed during coast was 2.6 lbm. Again:

$\frac{V_2}{V_1} = \frac{P_1}{P_2}\frac{T_2}{T_1} = \frac{200.2}{202.5}\frac{526.2}{516.2} = 1.00779$ for VL1;

and

$\frac{199.2}{202.5}\frac{524.6}{515.5} = 1.00158$ for VL2;

and

$V_2 - V_1 = 0.00779\ (10{,}530) = 82.07$ in.^{3} for VL1;

and

$0.00158\ (10{,}402.4) = 16.34$ in.^{3} for VL2;

and

$W_{P_{coast}} = 2.98$ lb for VL1 and 0.6 lb for VL2.

Because calculation of propellant used is very sensitive to the accuracy of telemetry data on tank pressure (a one DN error represents 3 lb of propellant), another approach was used to evaluate propellant remaining after the tanks had thermally stabilized. The final stabilized tank temperature is a function of propellant remaining. Before flight, predictions were made for the temperature drop of the tank and propellant from the stable condition before deorbit burn to a 3-hr stable condition after separation. Figure IX-4 shows this prediction. The flight temperature data shows for VL1 a tank 1 ΔT of: 71.86 - 64.04 = 7.82°F, and tank 2 ΔT of: 75.51 - 68.26 = 7.25°F. The respective values for VL2 were 7.5 and 6.5°F.

From Figure IX-4 the total usable propellant remaining at separation +3 hours is determined to be 19.4 lb for VL1 and 21.5 for VL2. This compares to a predicted margin of 20.1 lb.

Entry - The prediction was 1.4 lbm required. The actual was determined by summing engine on time, multiplying by engine thrust, and dividing by pulse specific impulse. The results are summarized in Table IX-1.

Table IX-1 Entry Propellant Consumption

Event	VL1 (I_{sp} = 170)			VL2 (I_{sp} = 170)		
	No.* Pulses	Thrust	W_p	No.* Pulses	Thrust	W_p
1. 800,000 ft to Sense 0.05 g	320	3.42	0.13	98	3.59	0.04
2. Sense 0.05 g to Mortar Fire	2848	3.42	1.15	1332	3.59	0.56
3. Mortar Fire to Parachute Separation	1680	3.42	0.68	1070	3.59	0.45
TOTAL			1.96			1.05

*Pulses are the total summation of all engine 20-msec pulses.

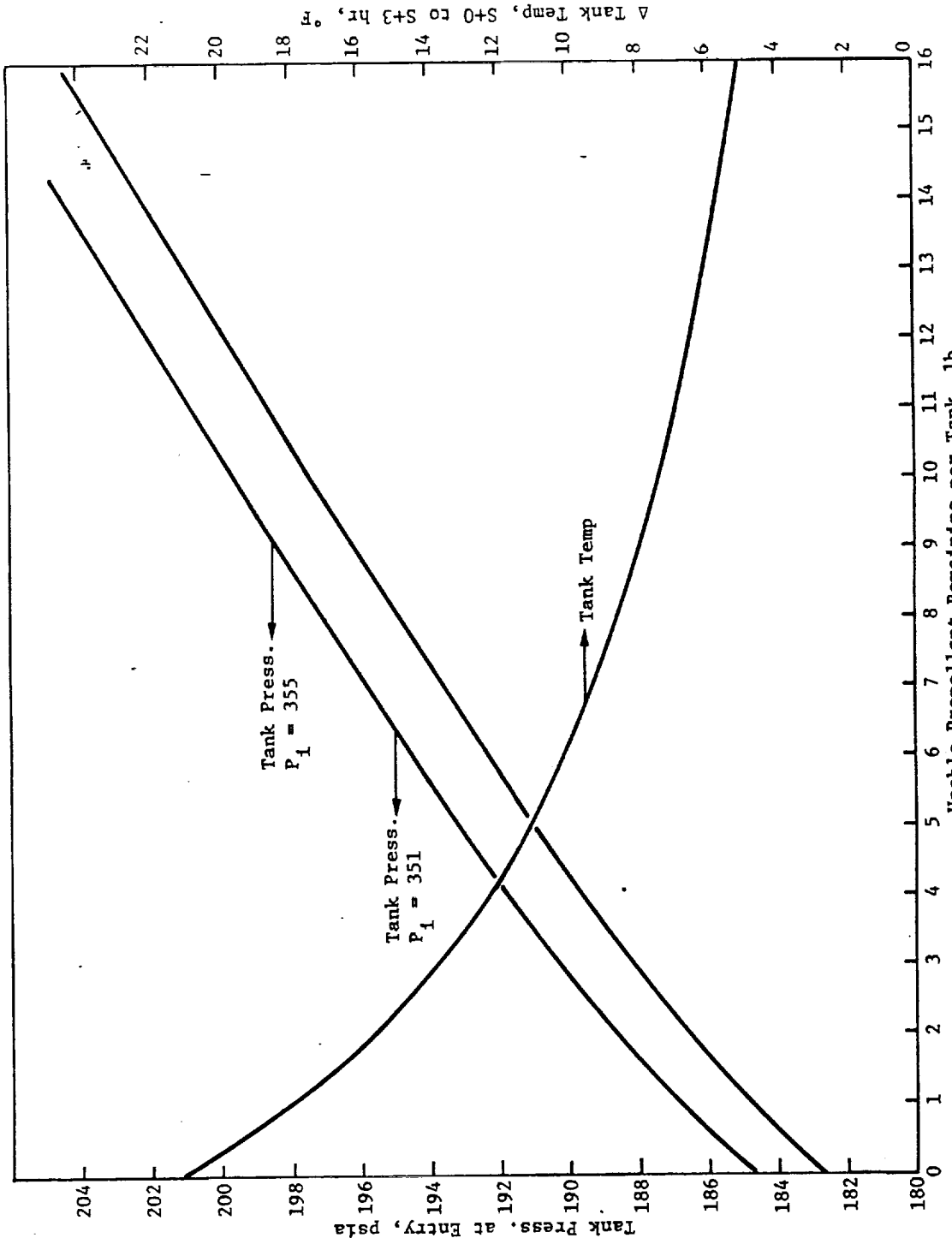

Figure IX-4 RCS/Deorbit Entry Parameters

Figure IX-4

A summary of the propellant analysis is shown in Table IX-2.

Table IX-2 RCS/Deorbit Propellant Used Summary

Item	Prediction	Pressure Derived		Temp Derived	
		VL1	VL2	VL1	VL2
Trapped	2.2	2.2	2.2	2.2	2.2
Deorbit	162.0	157.9	I56.5	162.8	160.7
Coast	2.6	3.0	0.6	2.6*	2.6*
Entry	1.4†	2.0	1.0	2.0	1.0
Total	168.2	165.1	160.3	169.6	166.5
Loaded	187.0	187.0	187.0	187.0	187.0
Margin	18.8	21.9	26.7	17.4	20.5

*Based on predicted coast usage.

†Does not include an estimate for the period from parachute deployment to aeroshell separation.

The temperature-derived propellant used is considered the most accurate and provides the most consistent data. For example, for VL2 with a higher thrust than assumed (discussion in next paragraph), a higher average I_{sp} should have occurred as shown in Figure IX-5. This translates into 1.1 lb less fuel used for deorbit. Table IX-2 shows that the difference was 1.3 lb.

2. Thrust

Tank pressure and engine acceptance test data were used to predict thrust as a function of deorbit burn time. Figure IX-6 presents the mission design thrust levels as a function of tank pressure. Acceptance test levels were degraded by 5.5%.

Axial thrust was computed by the equation:

$$F = \frac{W \cdot a_x}{g_c \times \text{duty cycle}}$$

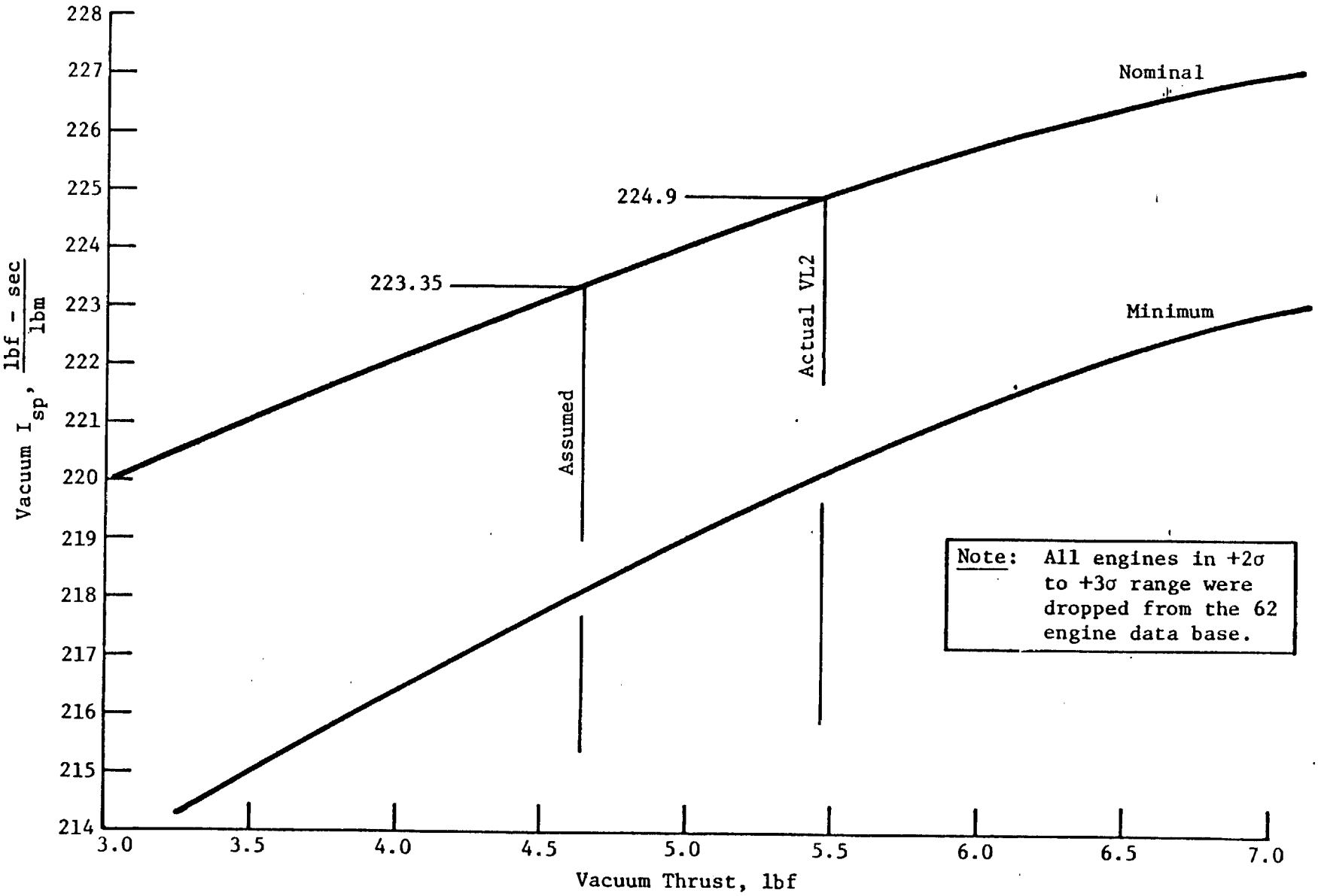

Figure IX-5 Specific Impulse versus Vacuum Thrust

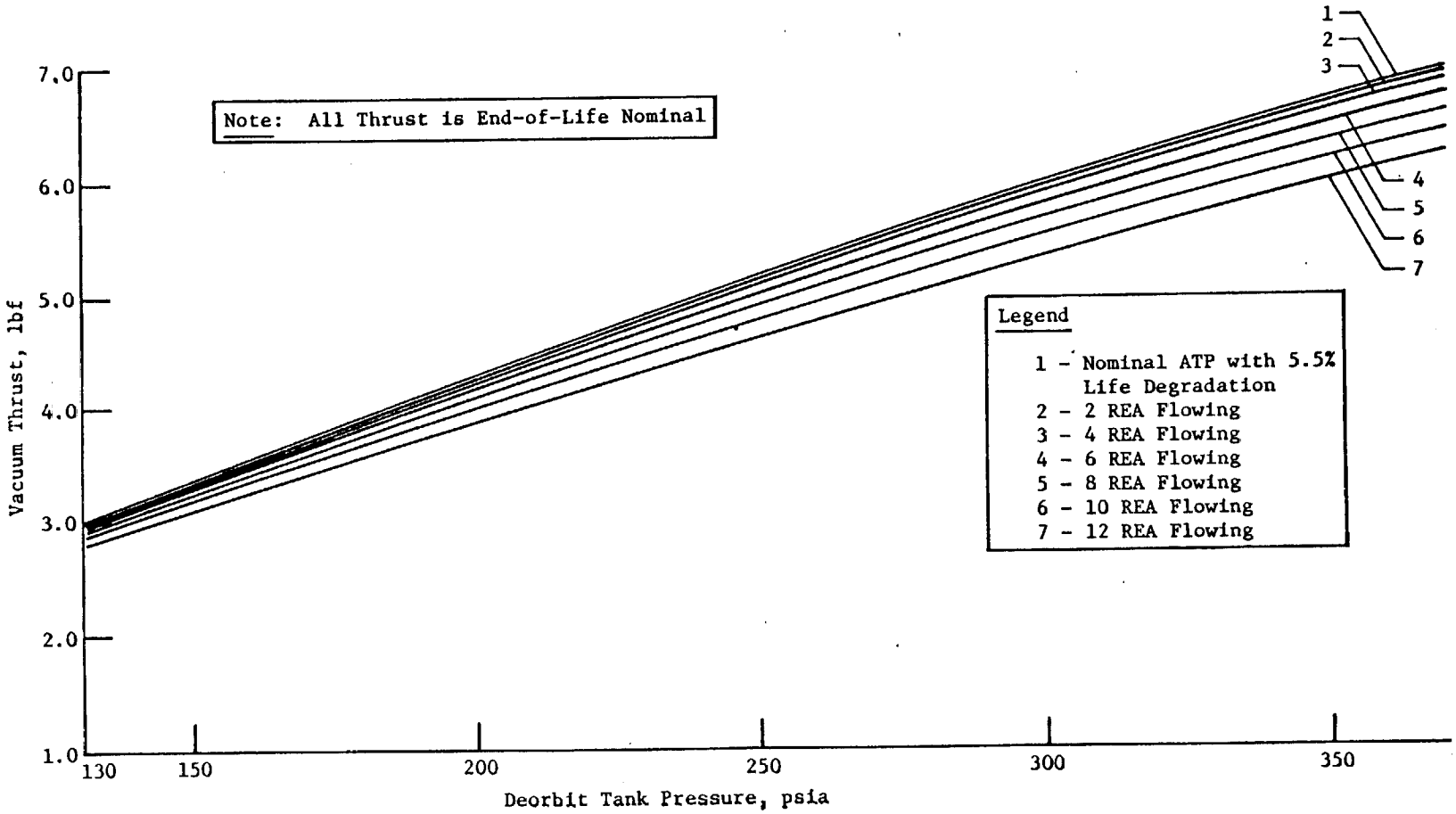

Figure IX-6 Vacuum Thrust versus Tank Pressure

where

$$a_x = \frac{P_{co} \times 0.04173858}{\Delta t} - 0.03748 \text{ for VL1 and}$$

$$a_x = \frac{P_{co} \times 0.0419141}{\Delta t} - 0.06604 \text{ for VL2.}$$

P_{co} is velocity pulse counts (increments).

The duty cycle factor accounts for the cg offset and thrust tolerances. The VL1 duty cycle should have been 0.9404 at the start of deorbit burn and 0.9233 at the end. VL2 respective duty cycles were 0.958 and 0.959. If each engine had the same thrust level at all pressures, the cg offset duty cycle would be 0.956.

The duty cycle change from start to completion of deorbit burn was assumed to change linearly. Engine valve commands were not used to establish the duty cycle because of the large tolerance on off-impulse obtained during a 20-msec off period. For example, from valve commands, an indicated 0.80 duty cycle would actually be between 0.80 and 0.90 in terms of off impulse. Using the equation and flight velocity data, the comparison of predicted to actual was made and plotted in Figure IX-7.

It can be concluded that thrust levels were higher than expected, and for VL2 the end of deorbit burn thrust level was slightly above PD specification limits. From acceptance test data, VL1 engines were nominal and VL2 were averaged 1% higher than nominal. The flight data indicate a 5% difference rather than 1%.

The many parameters that could affect the calculated thrust may account for the difference. Those parameters and estimated tolerances are:

Parameter	Tolerance Effect on Thrust
1) Tank Pressure	±1.5%
2) Line Pressure Prop	±1.5%
3) Duty Cycle	±2.0%
4) Vehicle Acceleration	0.6%
5) Engine Pressure Prop	+4.0, -5.5
6) Engine Acceptance Test	±1.0

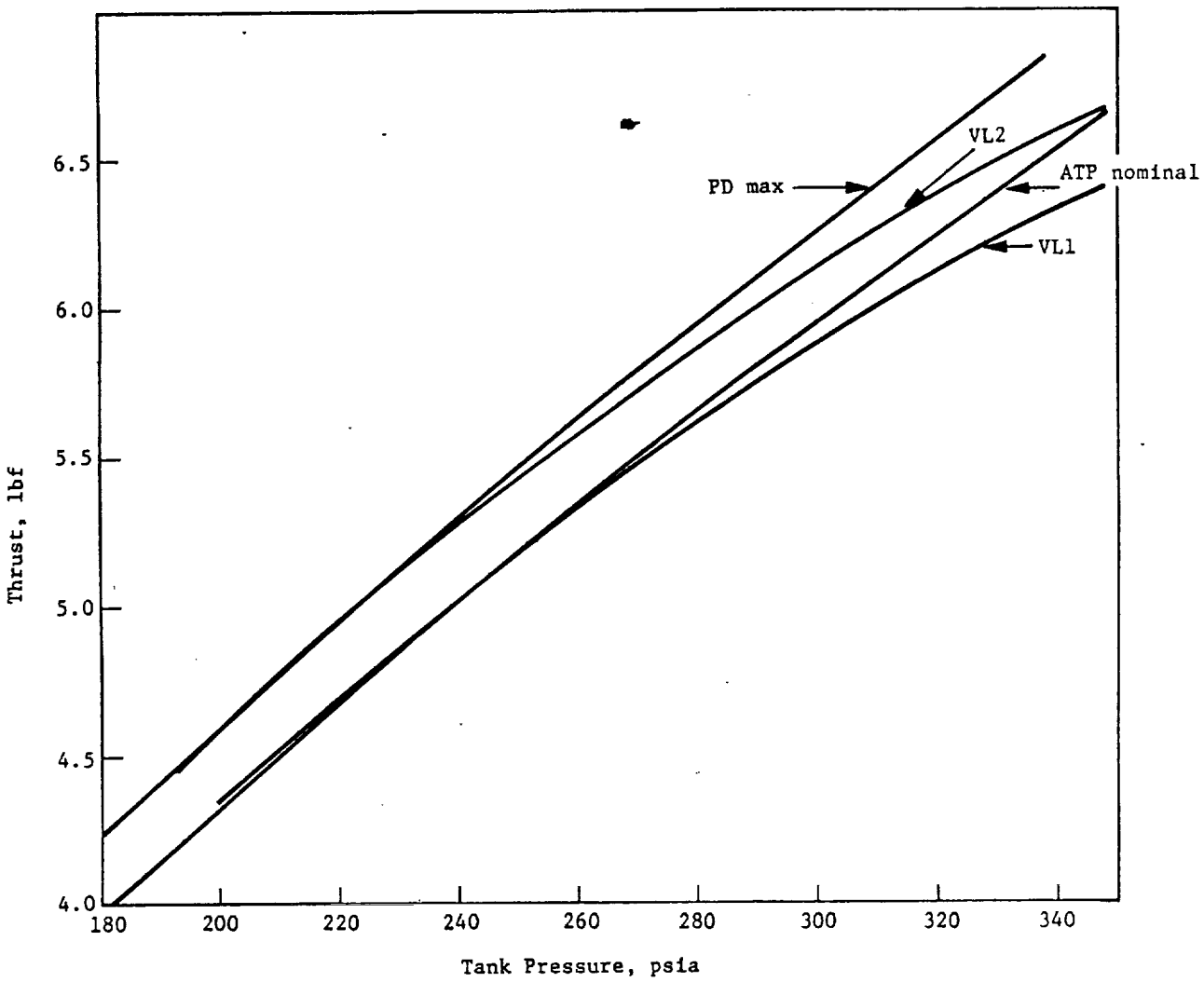

Figure IX-7 Deorbit Thrust Levels

The engine pressure loss effect of -5.5% was assumed for preflight predictions because of noted changes during engine qualification and system verification tests. However, the PTC engines (2) did not show this trend nor did the development engine.

An explanation for an increase in thrust level with storage time is valve seat creep due to preload and time. The expected valve seat creep was between 0.0006 and 0.0009 in. This represents a 10 to 15% change in valve stroke, which translates into a 4 to 5% increase in thrust.

Because of the large number of potential variables, care must be taken when evaluating the data. It can be stated, however, that all engines fired when commanded without valve failure. Vehicle attitude rates verify that no measurable valve leakage occurred.

C. TERMINAL DESCENT PERFORMANCE

Telemetry data available for TD propulsion system performance evaluation were tank pressures and temperatures, throttle valve commands and positions, roll engine commands, and vehicle velocity change increments.

The approach to verify performance was to use telemetry pressure and valve position data to predict delivered thrust. Predicted thrust and acceptance test specific impulse were then used to predict propellant consumption and vehicle weight versus time. Final verification was a comparison of the predicted thrust to actual vehicle acceleration.

Initial conditions were:

		VL1	VL2
1)	Tank Pressure	529 psia	529 psia
2)	Tank Temperature		
	T1	75.9°F	73.6°F
	T2	77.7°F	73.4°F
3)	Vehicle Weight	1498 lb	1496.2 lb
4)	Propellant Load	185.0 lb	185.0 lb

Figures IX-8 and IX-9 show the average of the two tank pressures as a function of GCSC time for VL1 and VL2, respectively. Bleed-in is not shown on the time scale. Tank pressure before bleed-in was 529 psia. Propellant consumed in roll control was calculated from engine pulse counts to be 0.5 lb on each vehicle.

Tables IX-3 and IX-4 show the valve positions at given GCSC time intervals. The values shown are the average for each specific interval. The largest difference between command and achieved valve position (interval) was 0.5%, which indicates low valve hysteresis at all positions. The engine start time could be detected from the pressure surge at the throttle valve and was at GCSC time of 12004.80 sec ± 0.050 ms for Vehicle 1 and 11855.8 ± 0.050 ms for VL2. Because the data sample rate was only 10 Hz, valve response could not be determined. Tables IX-3 and IX-4 also show the predicted line pressure loss and thrust levels. Figures IX-8, IX-9, IX-10 and IX-11 were used to predict the thrust levels shown. Figure IX-12 is the acceptance test specific impulse and was used in conjunction with the thrust data of Tables IX-3 and IX-4 (except at 20 mb) to determine propellant consumed from

$$W_{P_{1-2}} = \sum_{\bar{t}_1}^{\bar{t}_2} \frac{F}{I_{sp}} \Delta t.$$

Tables IX-5 and IX-6 show the propellant used and vehicle weight at the middle of each selected time interval. Also shown is the propellant margin. The margins compare to the expected nominal (75 mean design atmosphere without wind) of 33.0 lb without roll control. Comparison of propellant used to some predicted case is a very tenuous comparison at best. The predicted case assumed the '75 mean atmosphere with no wind. The actual flight proved to be through an atmosphere like this mean with relatively weak winds (although not zero), which is why these comparisons were reasonably good.

The vehicle weights shown in Tables IX-5 and IX-6 and the actual vehicle velocity increments were used to calculate force on the lander as a function of time. The acceleraiton determination equaiton was the same as used for deorbit. Force was determined by

$$F = \frac{\text{weight} \times a_x}{g_c}$$

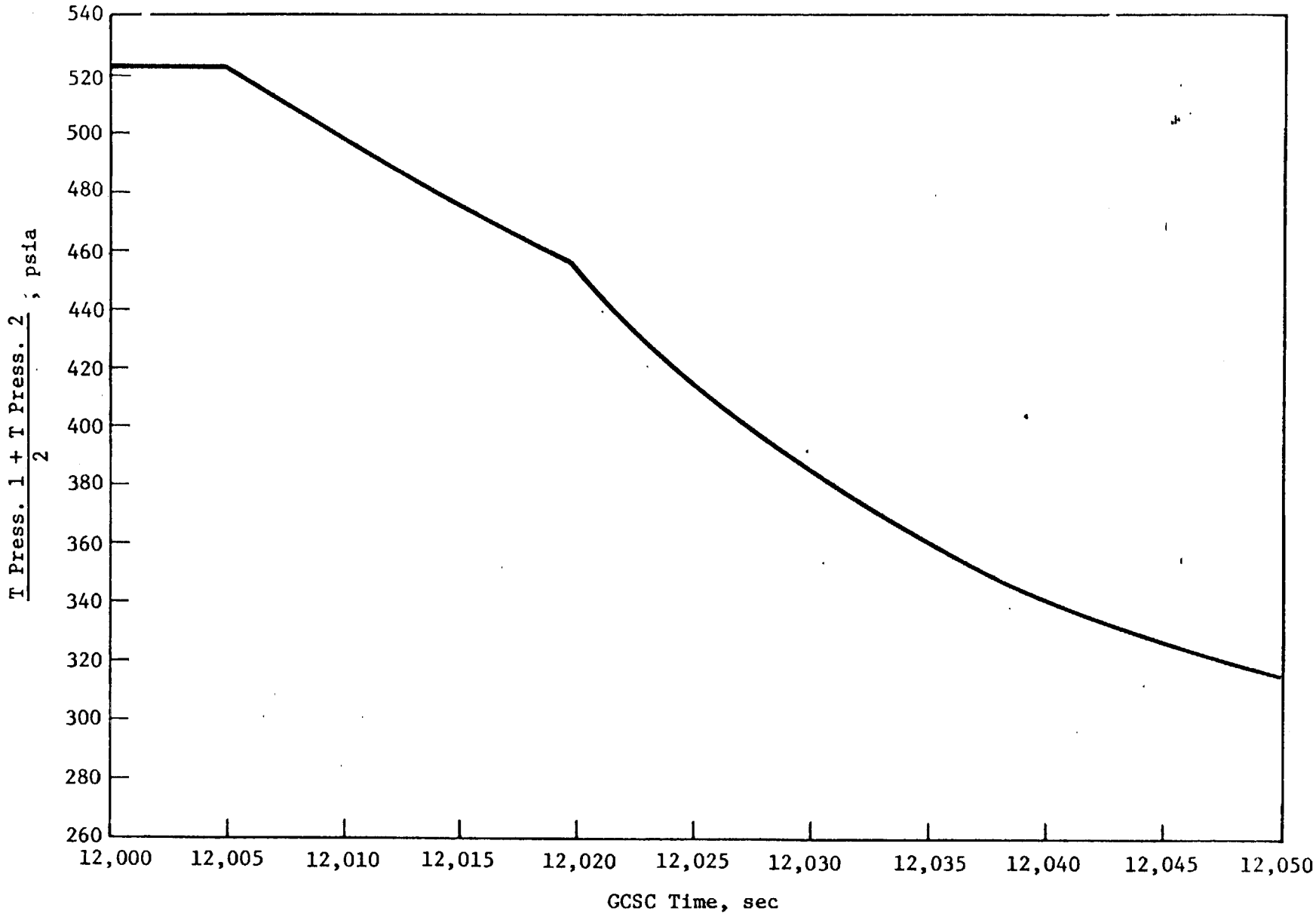

Figure IX-8 TD Tank Pressure

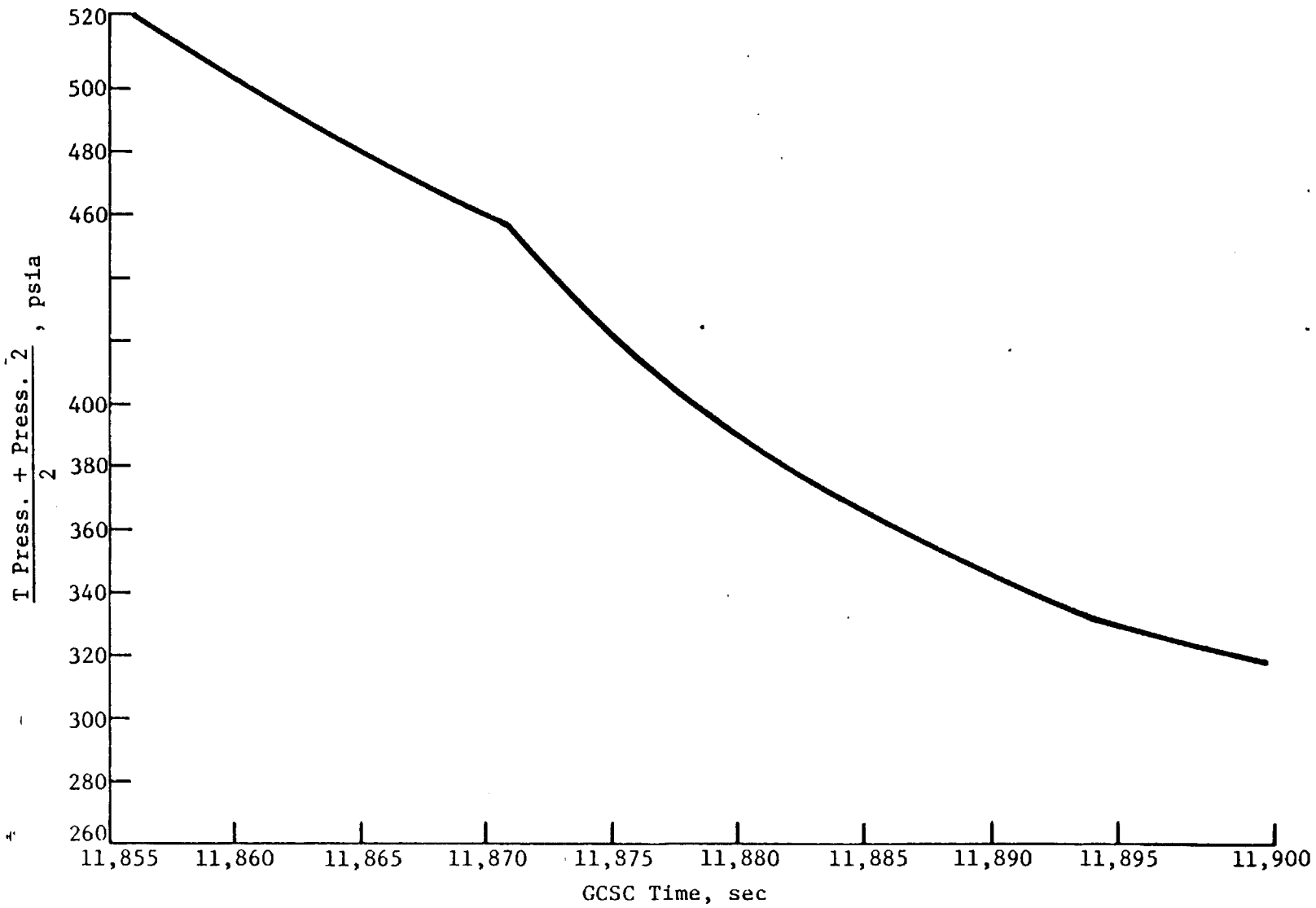

Figure IX-9 VL2 TD Tank Pressure

Table IX-3 VL1 TD Engine Thrust (Prediction)

GCSC Time	VLV-1-%	VLV-2-%	VLV-3-%	P Tank	ΔP Line	P Inlet	F_1 (Pred)	F_2 (Pred)	F_3 (Pred)
	%	%	%	psia	psid	psia	lbf-8 mb	lbf-8 mb	lbf-8 mb
12004.9-12006.9	11.74	7.50	11.48	518.5	3	515.3	147.1	123	146.1
12006.9-12008.4	10.76	7.34	11.92	510	3	507	149.5	133.5	156.1
12008.4-12010.5	11.04	7.16	11.54	500	3	497	149	131.25	151.25
12010.5-12012.5	11.31	6.86	11.50	490.6	3	487.6	148.5	131.0	148.9
12012.5-12014.5	11.45	6.92	11.50	481.8	3	478.8	148.5	128.5	148.5
12014.5-12017.5	11.54	6.76	11.39	471.2	3	468.2	147.7	126.5	147.5
12017.5-12019.5	11.56	6.68	11.48	461	3	458	145.5	123.5	145.5
12019.5-12020.0	73.52	52.89	73.29	455	11	444	481	318.5	480.5
12020.0-12023.0	52.10	42.89	53.54	440	7.6	432.4	336	291.5	343
12023.0-12026.0	52.24	42.85	53.59	418	7.5	410.5	326	282	330.5
12026.0-12029.0	52.56	43.25	54.04	399.3	7.1	392.2	318	275.5	324.5
12029.0-12032.0	52.78	43.24	54.14	382.8	6.8	376.0	309.5	268.5	314
12032.0-12035.0	52.61	43.05	53.90	367.5	6.5	361.0	300.5	260	305.5
12035.0-12038.0	52.77	42.98	53.97	353.8	6.2	347.6	292.5	253	297.5
12038.0-12041.0	53.13	43.19	54.31	341.8	5.9	335.9	287.5	248.5	292.5
12041.0-12042.4	52.74	42.58	53.40	334.3	5.7	328.6	283.5	243.5	287
12042.4-12043.4	22.39	15.73	22.74	331.0	2.0	329.0	165.5	139.5	166.5
12043.4-12045.4	28.29	20.43	27.78	327.5	2.0	325.5	187.5	156.5	183.5
12045.4-12047.5	28.29	20.72	27.99	323.0	2.0	321.0	184.0	156.0	183.5
12047.5-12049.5	28.37	20.49	27.97	319.3	2.0	317.3	183.5	155.5	182.5
12049.5-12050.5	30.17	16.00	24.39	315.9	2.0	313.9	188.5	138.0	168.5

Table IX-4 VL2 TD Engine Thrust (Prediction)

GCSC Time	VLV-1-%	VLV-2-%	VLV-3-%	P Tank	ΔP Line	P Inlet	F_1 (Pred)	F_2 (Pred)	F_3 (Pred)
	%	%	%	psia	psid	psia	lbf-8 mb	lbf-8 mb	lbf-8 mb
11855.8-11857.9	11.81	7.83	11.29	515.0	3.0	512.0			
11857.9-11860.9	11.88	7.05	10.93	506.0	3.0	503.0	154.5	130.5	149.5
11860.9-11863.9	12.00	6.71	11.18	491.8	3.0	488.8	152.5	128.5	148.5
11863.9-11866.9	11.72	6.83	11.37	477.8	3.0	474.8	150.5	126.5	147.5
11866.9-11870.4	12.00	6.78	11.61	466.1	3.0	463.1	148.5	123.5	147.5
11870.4-11870.7	80.29	67.06	80.26	456.7	11.0	445.7	406.5	423.5	496.5
11870.7-11873.7	54.1	42.6	53.7	442.8	7.6	435.2	347.5	290.5	345.5
11873.7-11876.7	54.1	42.8	53.4	419.4	7.5	411.9	334.5	283.5	332.5
11876.7-11879.7	54.5	42.6	54.2	400.8	7.1	393.7	328.5	273.5	327.5
11879.7-11882.7	54.2	42.4	53.6	383.2	6.8	376.4	316.5	264.5	313.5
11882.7-11885.7	54.7	42.5	54.1	368.2	6.8	361.7	308.5	258.5	306.5
11885.7-11888.	54.0	42.1	53.5	355.2	6.3	348.9	298.5	250.5	297.5
11888.7-11891.7	54.0	42.0	53.6	342.5	5.9	336.6	293.5	244.5	292.5
11891.7-11893.0	53.4	41.0	52.6	335.5	5.7	329.8	286.5	238.0	283.5
11893.0-11893.3	11.94	6.78	11.81	332.0	2.0	330.0	125.5	105.5	125.5
11893.3-11896.3	28.36	19.95	27.96	329.6	2.0	327.6	188.5	155.5	186.5
11896.3-11900.3	28.89	20.42	28.77	322.6	2.0	320.6	187.5	156.0	187.5
11900.3-11900.8	25.24	18.12	33.39	318.0	2.0	316.0	172.5	142.5	196.5

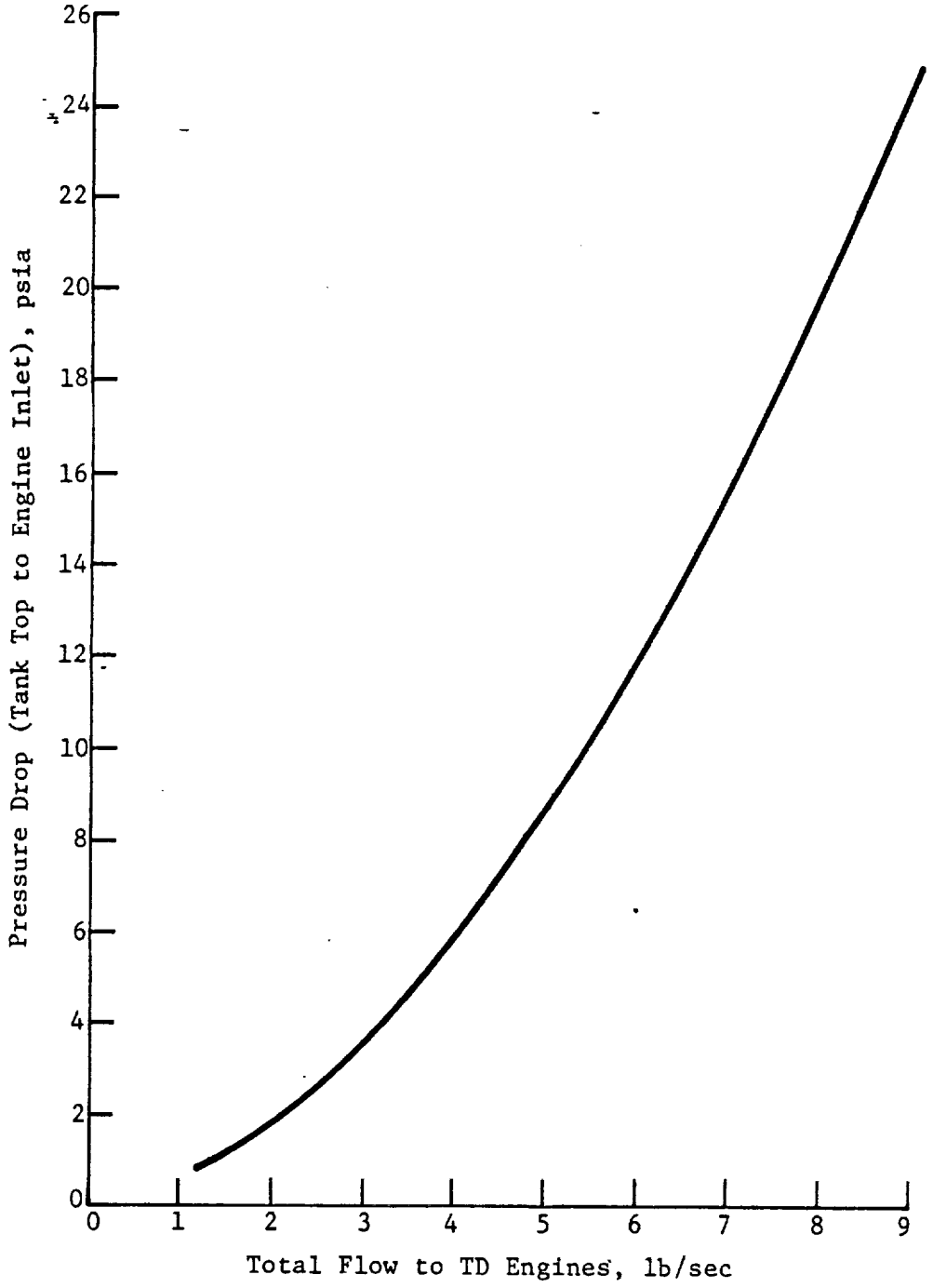

Figure IX-10 Terminal System Line Pressure Drop

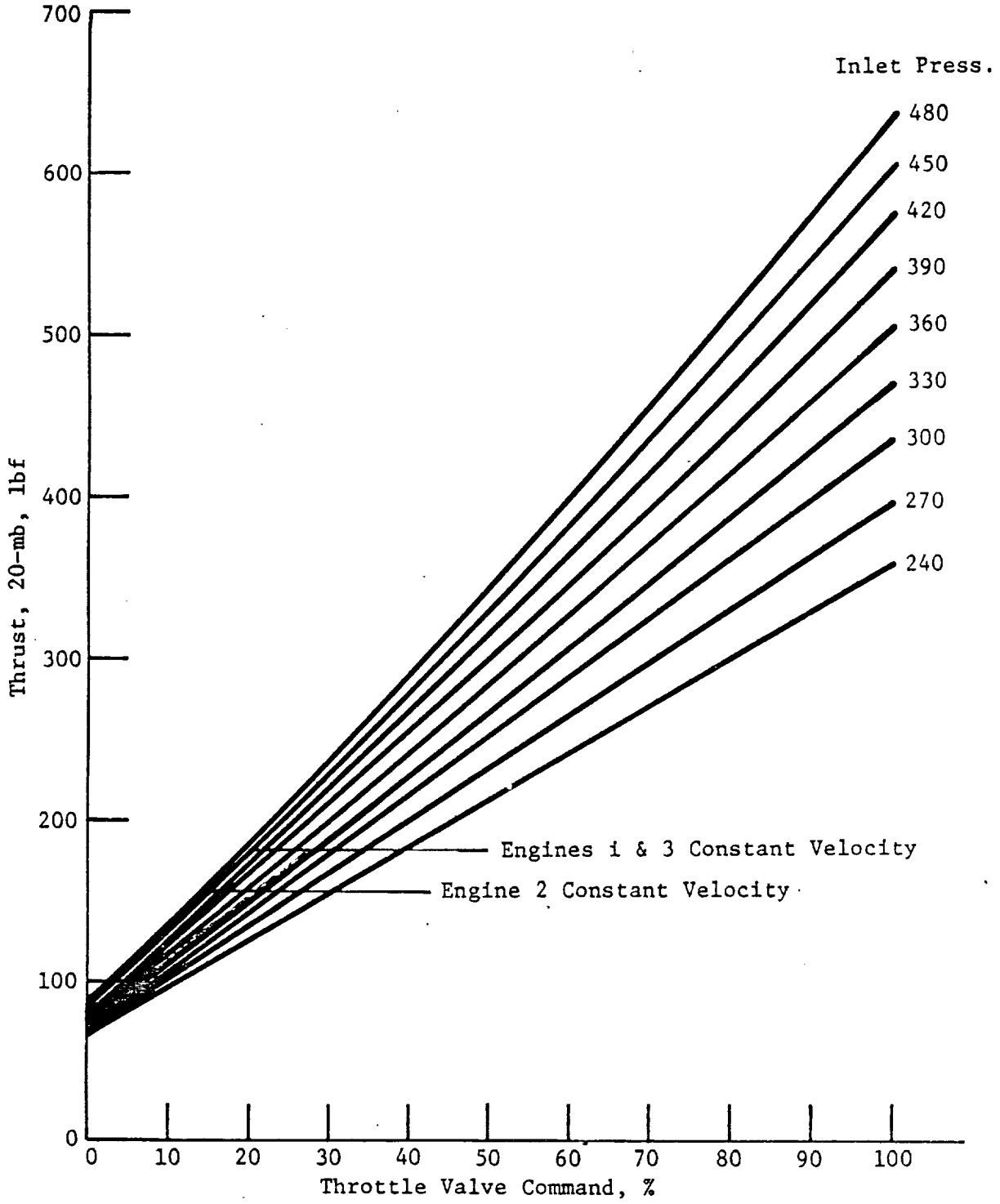

Figure IX-11 Terminal Descent Engine ATP, 20-mb Thrust

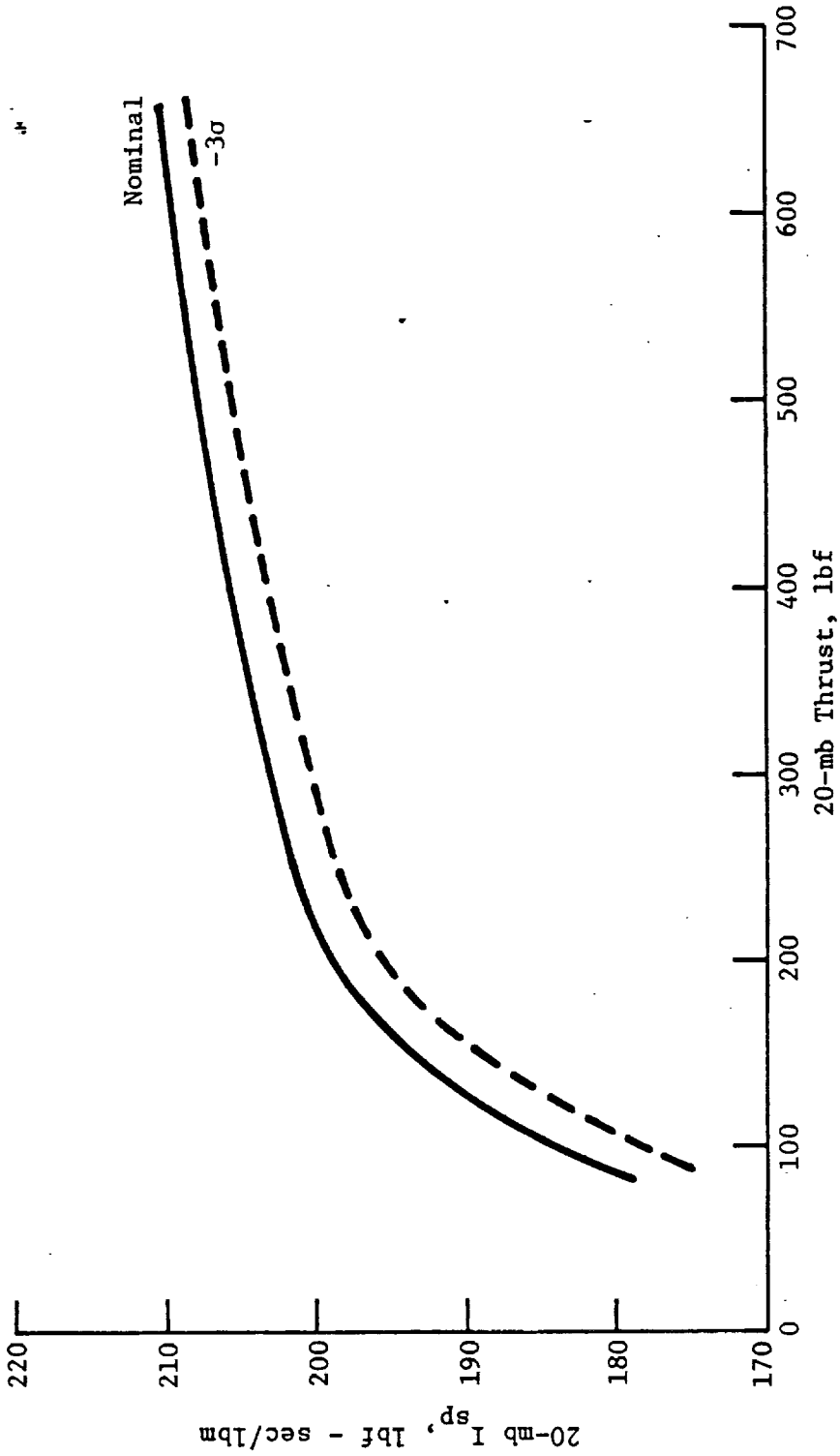

Figure IX-12 TD REA Specific Impulse

Figure IX-12

Table IX-5 VL1 TD Propellant Used

Time	W_p	Vehicle Weight
Initial		1498
12005.9	2.55	1495.5
12007.6	6.84	1491.1
12009.5	10.54	1487.5
12011.5	14.85	1483.2
12013.5	19.12	1478.9
12016.0	24.42	1473.6
12018.5	29.66	1468.3
12019.8	32.94	1465.1
12021.5	41.18	1456.8
12024.5	55.04	1443.0
12027.5	68.52	1429.5
12030.5	81.64	1416.4
12033.5	94.42	1403.6
12036.5	106.89	1391.1
12039.5	119.08	1378.9
12041.7	128.03	1370.0
12042.9	132.11	1365.9
12044.5	135.87	1362.1
12048.5	141.16	1356.8
12048.5	146.39	1351.6
12050.0	150.15	1347.9
12050.54	151.37	1346.7

Roll Control = 0.5
Trapped = 4.8 lb
Total = 156.87
Loaded = 185.00
Margin = 28.13

Table IX-6 VL2 TD Propellant Used

Time	W_p	Vehicle Weight
Initial		1496.2
11859.4	8.26	1487.9
11862.4	14.75	1481.4
11865.4	21.18	1474.97
11868.65	28.07	1468.1
11870.55	32.79	1463.4
11872.20	40.93	1455.2
11875.2	54.94	1441.2
11878.2	68.57	1427.6
11881.2	81.80	1414.4
11884.2	94.63	1401.5
11887.2	107.12	1389.0
11890.2	119.31	1376.9
11892.35	127.89	1368.3
11893.15	130.70	1365.5
11894.8	134.91	1361.3
11898.3	144.08	1352.1
11900.55	149.96	1346.2
11900.94	151.46	1344.7

Roll Control = 0.5
Trapped = 4.8
Total = 156.76
Loaded = 185.00
Margin = 28.24

The comparison of the predicted thrust in Tables IX-3 and IX-4 and the calculated force is shown on Figures IX-13 and IX-14. The excellent agreement verifies that the TD engines performed as expected by providing nominal thrust and specific impulse.

Finally, the tank pressure was plotted as a function of propellant consumed and is shown in Figure IX-15. The polytropic expansion coefficient of 1.295 compares to a value of 1.33 obtained in system verification tests at Denver. The difference can be expected for two reasons: (1) smaller GN_2 mass in the flight tanks (12.5 lb flight to 14.0 lb SV) and (2) longer burn in flight (45.6 sec flight and 37 sec SV). Assuming the heat transfer rates were equal and accounting for additional work done in flight (151.4 lb expelled in SV tests), the calculated γ would be 1.307.

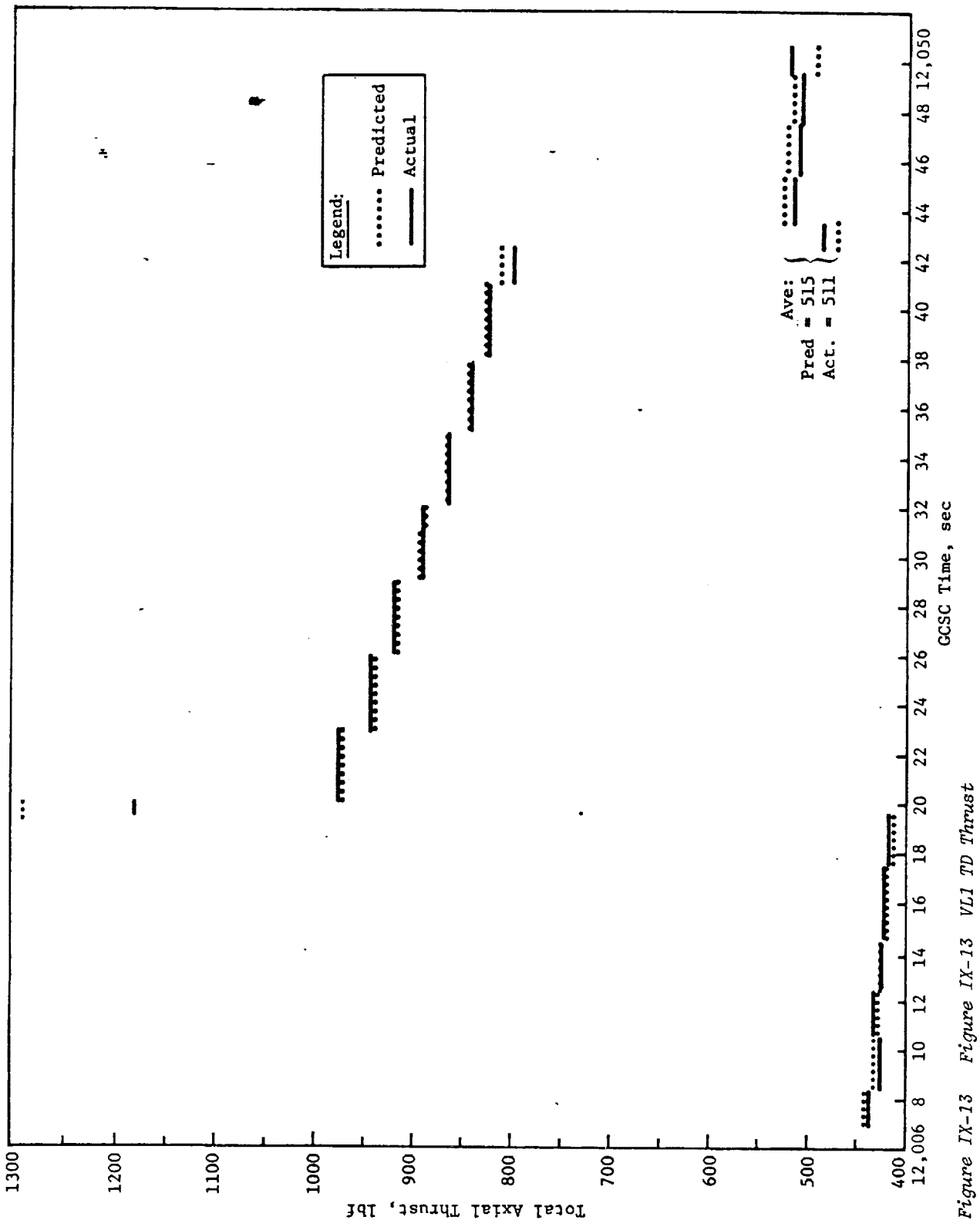

Figure IX-13 VL1 TD Thrust

Figure IX-13

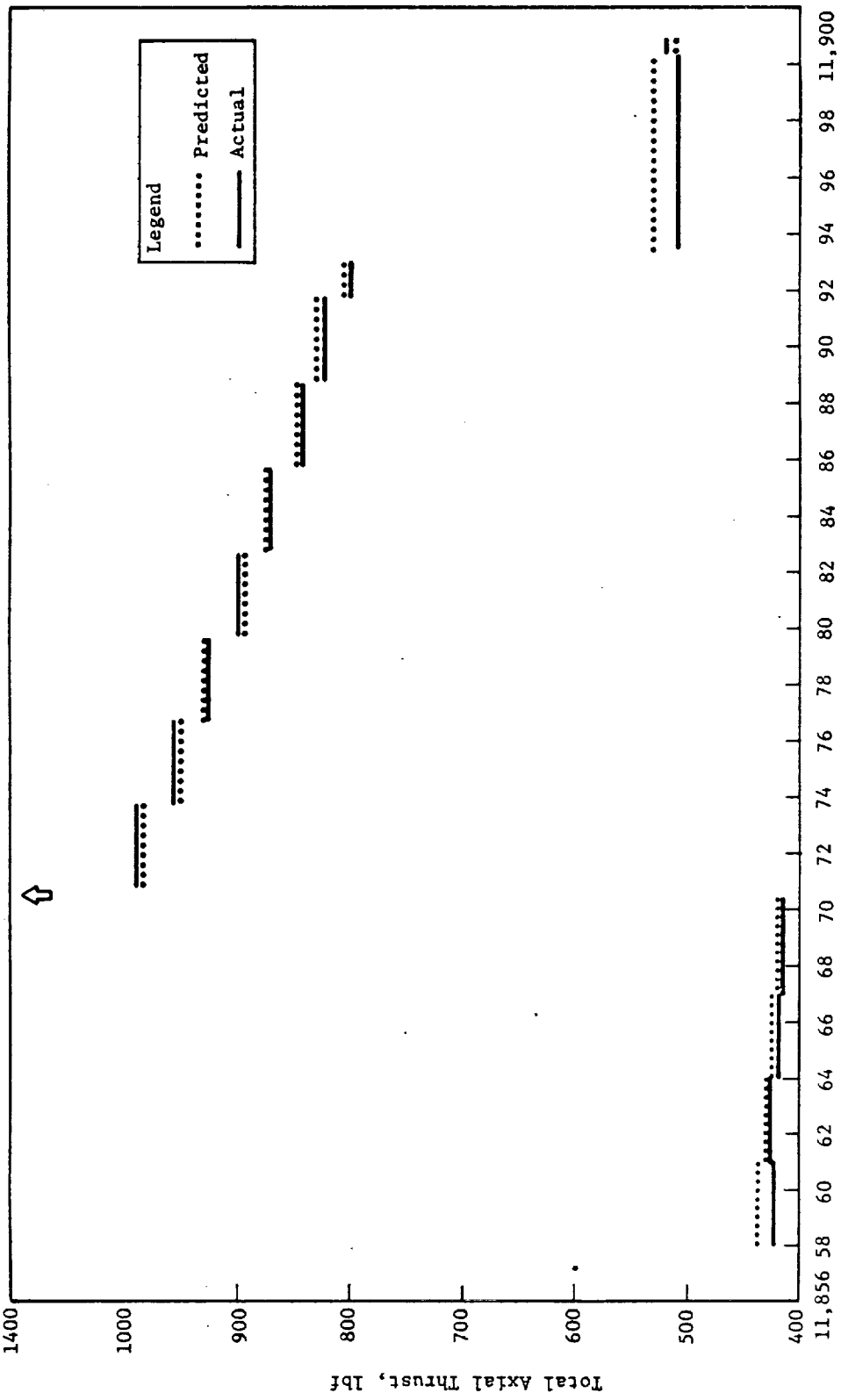

Figure IX-14 VL2 TD Thrust

Figure IX-14

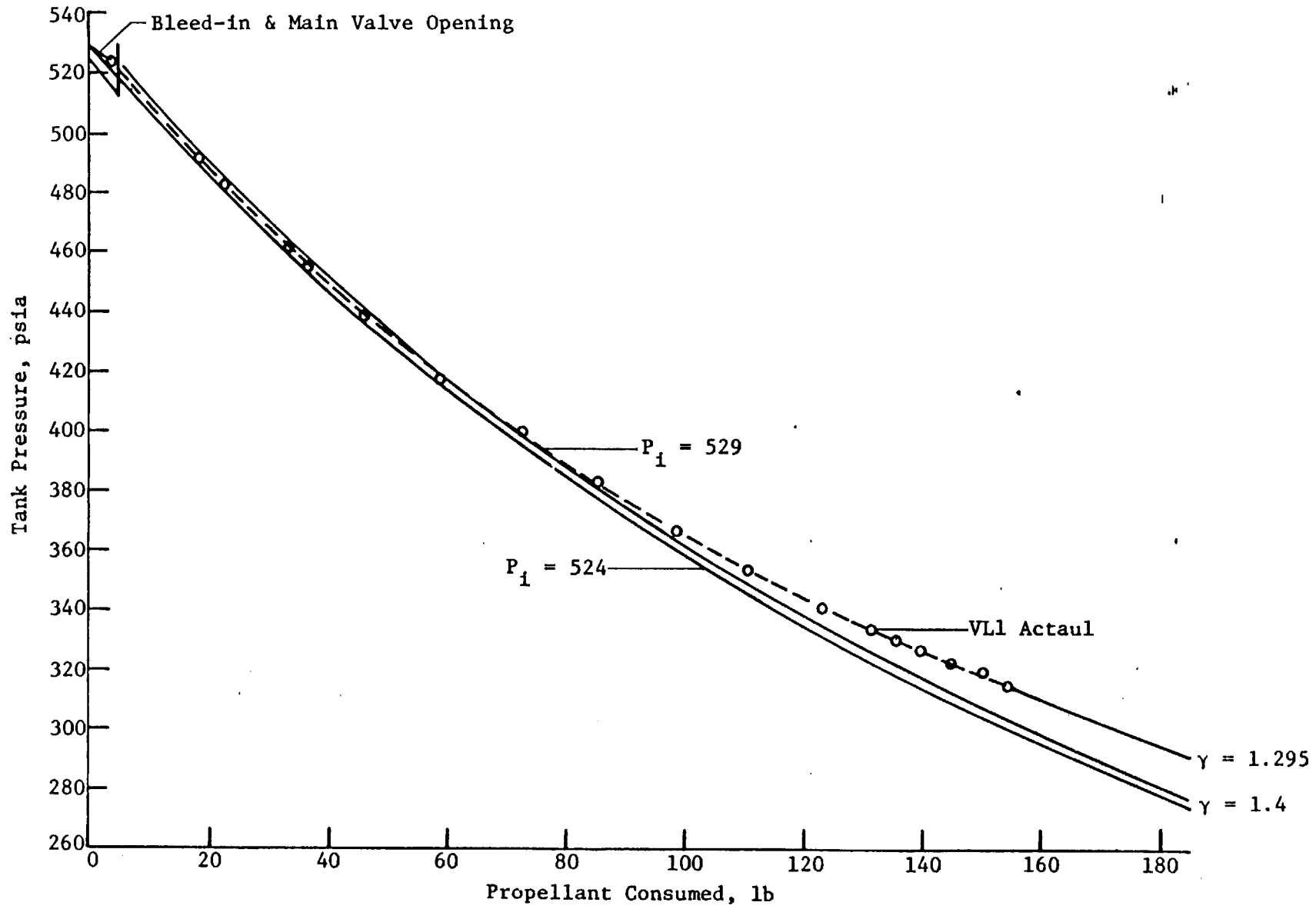

Figure IX-15 TD Tank Pressure versus Propellant Consumed

X. ENTRY TRAJECTORY PERFORMANCE

There are certain aspects of performance related to the trajectory that have an important bearing on software parameters and descent sequencing times. These aspects will be examined in this section.

A. 0.05-g ALTITUDE ACCURACY

The altitude estimate in the navigator is updated to a predetermined estimate of 0.05-g detection. The purpose of this update is to minimize the possibility of premature mortar fire under certain conditions. The difference between the altitude update and the LTARP estimate at 0.05 g should be less than 44,000 ft to assure that this does not occur. The following altitudes were obtained for VL1 and VL2.

	Altitude above LS at 0.05 g, ft	Update Altitude, ft	Error, ft
VL1	263,319	259,636	3,683
VL2	263,878	257,666	6,212

The reason that the error should be less than 44,000 ft is as follows. Referring to Figure X-1, postulate that RA blackout occurs (the following section explains that neither VL1 and VL2 experienced blackout of any kind) and that it started before the 0.05-g event where we could first start using RA data and continued until 7000 fps. Further, assume that we switched to a bad RA at the instant of emergence from blackout and were unable to acquire a lock with it for the entire 30-sec RA switch time, then we took the maximum time of 6 sec to lock up the good RA. This leaves a minimum of 6 sec (25 + 17 - 30 - 6) to update the altitude estimate to the system acceptable error of 550 ft. The navigator is error-rate limited to 11,000 fps down to an error of 11,000 ft, after which the error is reduced exponentially with a time constant of 1 sec. Therefore, the time to reduce the error to 550 ft is:

$$t_{550} = \frac{\text{error} - 11000}{11000} - \ln \frac{550}{11000}$$

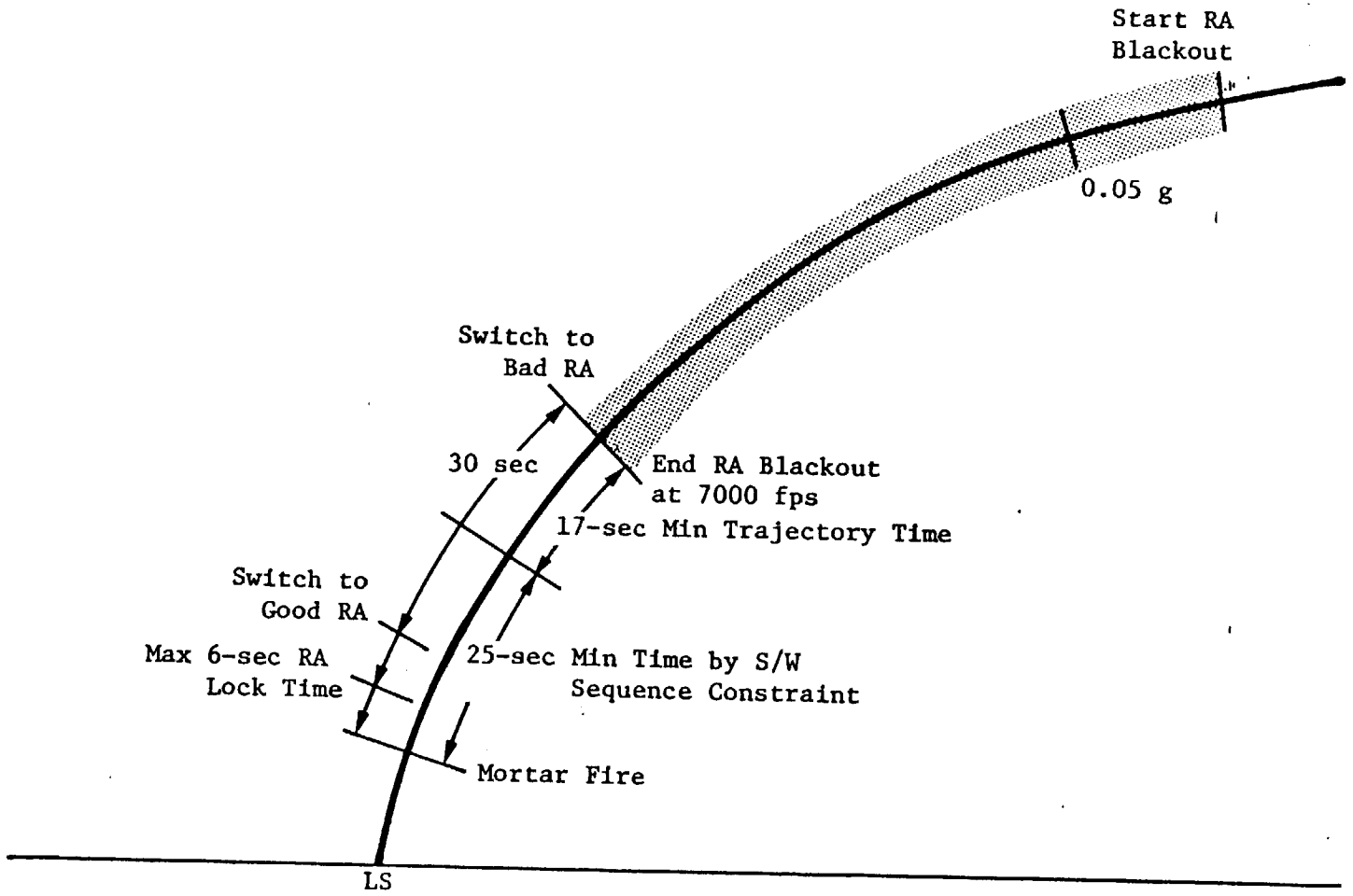

Figure X-1 Critical Trajectory Events Profile

Letting this time be 6 sec, the maximum value that the initial error can have is 44,000 ft, to reduce it to 550 ft within 6 sec. As can be seen from the data, both errors were much less than this.

B. BLACKOUT ALTITUDE RANGE

As explained in the previous section, RA blackout could have serious performance implications given certain trajectory characteristics together with a bad RA. As it turned out, neither VL1 or VL2 experienced any form of either RA or TM blackout.

VCS 3737 was incorporated in the software as a means of guarding against the premature mortar fire phenomenon explained in Section A. Because one of the prime prerequisites for the phenomenon is to have blackout occur along with just the right combination of a host of other circumstances, it is recommended that the reasons for VCS 3737 be critically examined for future missions of this type. Software often changes, and constraints incorporated to solve one problem may have unthought-of consequences in relation to some other, and, if the constraint is not needed, it should be removed.

C. 1.1-km/sec ACCURACY

The error in detecting 1.1 km/sec using the entry navigator velocity estimates should be less than 0.1 km/sec for proper stagnation temperature probe deployment. The following relative velocities obtained from the LTARP runs for VL1 and VL2 were observed at this event.

	Velocity at Probe Deployment, km/sec	Error, km/sec
VL1	1.10198	+0.00198
VL2	1.09993	-0.00007

These errors are in the worst case almost two orders of magnitude better than the requirement.

D. MORTAR FIRE ACCURACY

The subsystem requirement here is to be within ±550 ft of the desired altitude of 19000 ft. The mortar fire altitudes for VL1 and VL2 obtained from the respective LTARP runs and RA data were (altitude of the first fire event):

	Mortar Fire LTARP ft	Altitude from RA Data, ft	Desired, ft
VL1	19316	19273	19000
VL2	19128	19224	19000

The 316 or 273 ft of error for VL1 can be explained as follows. Section VII.A explains that VL1 had a navigator velocity error of -101 ft, which translates one-for-one into a negative navigator altitude bias. Also, the RA terrain bias error of 150 ft that was assumed to exist at this altitude probably did not exist because of the extremely strong return signal received by the RA. This explains 251 ft of the 316 ft of error from LTARP and the 273 ft of error from the best estimate of true altitude obtained from the RA at this time. The difference between the LTARP and and RA numbers was probably caused by a local terrain variation at mortar fire (recall that LTARP measures altitude from the landing site altitude), or more likely was caused simply by an error in estimating altitude by LTARP.

Again, for VL2, the error can be explained by the navigator velocity error of -56 ft and the nonexistent RA terrain bias error of 150 ft, which explains 206 ft of error. This explains almost all of the error as derived from the best estimate given by the RA. For VL2, the difference between LTARP and the RA altitude at mortar fire was probably due to a 100-ft depression that the vehicle was over at mortar fire or, again, just an LTARP error.

For either lander, the mortar fire altitude was well within requirements, especially when considering the entry flight path angle and atmosphere the landers were in.

E. ENGINE START ALTITUDE ACCURACY

The subsystem requirement for this event is to be within ±300 ft of 4798 ft at engine start. The engine start altitudes for VL1 and VL2 obtained from the respective LTARP runs and RA data were (altitude of the first pyro fire event):

	Engine Start Altitude		
	LTARP, ft	From RA Data, ft	Desired, ft
VL1	4787	4801	4798
VL2	4718	4804	4798

The accuracy here is markedly improved from mortar fire as one would expect because the navigator velocity errors have been converged and the RA terrain bias was never compensated for in the first place in the desired engine start altitude, and so it was not done incorrectly.

XI. LANDED ORIENTATION

The vehicle landed orientation was calculated using the IRU sensor data accumulated over a 300-sec period after landing. This data was also used to point the high-gain antenna toward Earth after it was deployed for direct communications with the lander.

Mars Gravity -

VLC1	VLC2
12.20099 ft/sec^2	12.24428 ft/sec^2

Vehicle Tilt -

	VLC1	VLC2
About Yaw	1°47'10"	-7°37'22"
About Pitch	2°23'50"	-3°1'0"
Total	2°59'25"	8°12'16"

The VLC1 vehicle is tilted down to the northwest at an angle of 2°59'25" and 75°0'24" from north. The VLC2 vehicle is tilted down to the northwest at an angle of 8°12'16" and 39°16'59" from north.

Mars Rate as Determined Using IRU Gyro Outputs -

VLC1	VLC2
14.63283 deg/hr	14.58283 deg/hr

Landed Latitude -

VLC1	VLC2
22°40'53.5" North	47°42'24.3" North

Azimuth of +Z Axis CW from North and Leg 1 Orientation CW from North -

1) Azimuth of +Z axis CW from north

VLC1	VLC2
141°37'38"	29°4'38"

2) Leg 1 orientation CW from north

VLC1	VLC2
321°37'38"	209°4'38"

Targeted Leg 1 Orientation CW from North

320°00'00"	210°00'00"